# Contribution of resident macrophages to the fetal liver hematopoietic stem cell niche

**Dissertation**

zur

**Erlangung des Doktorgrades (Dr. rer. nat.)**

der

**Mathematisch-Naturwissenschaftlichen Fakultät**

der

**Rheinischen Friedrich-Wilhelms-Universität Bonn**

vorgelegt von

## Amir Hossein Kayvanjoo

aus

**Tehran, Iran**

**Bonn 2022**

Angefertigt mit Genehmigung der Mathematisch-Naturwissenschaftlichen Fakultät
der Rheinischen Friedrich-Wilhelms-Universität Bonn

# Acknowledgment

Starting my Ph.D. and my dissertation project was a journey that definitely could not be done alone, and I am delighted to be able to express my gratitude to the people that helped me accomplish this milestone and close this chapter in my life.

First and foremost, I am incredibly grateful to Prof. Elvira Mass for offering me this opportunity. She started this journey with me and supported me until the very end despite all the ups and downs. She gave me a chance not only to expand my dry-lab skills but also to learn wet-lab methods, starting from handling a pipette! I am very proud for the knowledge I grasped and the results I have achieved despite starting as a novice, and they would have been almost impossible if she was not there as a supervisor.

I want to extend my sincere thanks to the rest of the lab members, especially Nora Balzer, my dear friend and colleague whom I could always rely on as a helping hand in the experiments and as a morale booster in an indefinite dosage. I hereby express my gratitude to the Schultze lab and Beyer lab for providing the sequencing facility. Special thanks to Colins for his kind help in single-cell sequencing and for providing the protocol. Many thanks also to Niko, Jonas, Patrick, and Kevin for always being ready to help. I also appreciate the help and support I received from Schlizer lab.

Many thanks should also go to my dissertation committee members: Prof. Waldemar Kolanus, Prof. Jan Hasenauer, and Prof. Stefanie Kürten, for evaluating my dissertation. I am also highly thankful to the ImmunoSensation cluster for providing the funding opportunity for my project and their support during my work.

Finally, I would like to express my sincere gratitude to my dear parents, my cousin Banafsheh who has always been there for me and supported me, my friends Ati, Andre, Mona, Reyhaneh, Peter and Vajihe. They provided me with happy distractions to rest my mind and encouraged and supported me during stressful times.

# Abstract

Tissue-resident macrophages are a heterogeneous population of phagocytes found in almost all tissues of the body. Recent studies indicate that most resident macrophages originate from yolk sac progenitors and are maintained by local proliferation independent of hematopoietic stem cells (HSC). It is known that HSC can quickly respond to organismal demands. During embryogenesis, the fetal liver supports the HSC with a unique microenvironment called the "HSC niche" that helps their expansion and maintenance. One of the most important aspects of a niche is cell-cell interactions that can happen either directly or through signaling. In the fetal liver, hepatic macrophages are known to participate in the maturation of erythroblasts. However, whether resident macrophages can also contribute to the fetal liver HSC niche remains enigmatic. Furthermore, the macrophages heterogeneity across different organs is essential for tissue-specific niches and cellular interactions during tissue development as well as tissue homeostasis. However, their heterogeneity within one organ, such as the fetal liver, especially during development, has not been addressed in detail.

In this dissertation, using single-cell RNA-sequencing, it was shown that hepatic macrophages are heterogeneous and have different subpopulations that can have different functions. This heterogeneity was further confirmed through multi-color flow-cytometry and unsupervised clustering of cells using computational methods. Investigating the ontogeny of the identified clusters using three fate-mapping models revealed that all macrophage clusters originated from the yolk sac and are not HSC derived.

Further, immunofluorescent-labeled sections from the fetal liver could show that while many of the macrophages serve as a platform for erythroblasts maturation in the fetal liver, yet some of them also interact with HSC. To test the functionality of hepatic macrophages in HSC, conditional mouse models were developed that lead to the depletion of macrophages in the fetal liver. The results indicated that hepatic macrophages are responsible for erythroblast maturation, as enucleation of red blood cells is not efficient when macrophages are lacking. Further, it was shown that macrophages are part of the HSC niche since stem cells have a differentiation bias towards the myeloid linage in knock-out embryos. These results were further confirmed by performing a bulk RNA- sequencing using HSC from embryos of mouse models.

All in all, the findings of this dissertation support the hypothesis that hepatic macrophages play a crucial role in the development and maintenance of fetal liver hematopoiesis and provide evidences for their heterogeneity within the fetal liver.

**Table of Contents**

# 1. Introduction

## 1.1. Hematopoiesis

The hematopoietic system provides an organism from the embryonic stages until adulthood with a continuous supply of mature blood cells. This system is established during embryonic development, and its' developmental program begins in the yolk sac (YS) and continues to the region defined as the para-aortic splanchnopleura (P-Sp)/aorta-gonad-mesonephros (AGM) and later on to the spleen, fetal liver (FL), and finally the bone morrow (BM) (Figure 1) (Russell 1979, Godin, Garcia-Porrero et al. 1993, Medvinsky, Samoylina et al. 1993, Wang and Wagers 2011). Despite some differences, the fetal and adult hematopoietic systems are generally comparable and share similarities, such as developing multiple lineages from the hematopoietic stem cells (HSC) (Lemischka, Raulet et al. 1986, Jordan, McKearn et al. 1990).

HSC are the source of all the circulating erythroid and immune cells in the bloodstream, including the red blood cells (RBCs), platelets, granulocytes, monocytes, and lymphocytes in the adult. HSC are relatively unique; in addition to their ability to replenish themselves (self-renewal) , they continuously differentiate into different cell types (Wilson, Laurenti et al. 2008, Busch, Klapproth et al. 2015). These specific properties make HSC transplantable into a recipient allowing a complete reconstitution of the blood cells (Sawai, Babovic et al. 2016).

Since most of the initial studies on hematopoiesis were initially focused on adult organisms, it was initially assumed that HSC are the source of all the immune cells, including the tissue-resident macrophages. Hence, it was widely accepted that the yolk sack (YS) produces HSC in the adult organism and during embryogenesis (Weissman, Papaioannou et al. 1977). However, in 1975 and 1976, two studies using the chimeras of quail-chicken showed that HSC were originating intra-embryonically (Dieterlen-Lievre 1975, Dieterlen-Lievre, Beaupain et al. 1976). Later on, different studies could show that HSC in mammals, including the mice, were intra-embryonically derived. In mice, the emergence of HSC starts at embryonic day (E) 10.5 from the hemogenic endothelium (HE) in the AGM region of the embryo (Muller, Medvinsky et al. 1994, Cumano, Ferraz et al. 2001, Kumaravelu, Hook et al. 2002).

It has been shown that hematopoiesis happens in successive waves (Orkin 1995, Zhu and Emerson 2002), and recent studies recent indicate the existence of additional multipotent progenitors (MPP) with HSC characteristics (Beaudin, Boyer et al. 2016, Yvernogeau, Gautier et al. 2019).

In the mouse, the hematopoiesis can be divided into three waves. The first wave is known as primitive hematopoiesis and happens at around E7.5 (Palis, Robertson et al. 1999, Palis, Chan et al. 2001, Bertrand, Jalil et al. 2005, Chen, Li et al. 2011, McGrath, Frame et al. 2015). The second wave is characterized by erythro-myeloid precursors (EMP) differentiation into blood cells and occurs at around E8.25. EMP originate from HE of the YS vasculature and are highly proliferative (Gritz and Hirschi 2016). The third wave is marked by the generation of the HSC in AGM and is known as the definitive hematopoiesis. This wave happens at around E10.5 (Figure 2). (Muller, Medvinsky et al. 1994, Medvinsky and Dzierzak 1996, Palis, Robertson et al. 1999, Palis, Chan et al. 2001, Chen, Li et al. 2011, Ivanovs, Rybtsov et al. 2011, Boiers, Carrelha et al. 2013, Nakano, Liu et al. 2013, McGrath, Frame et al. 2015).
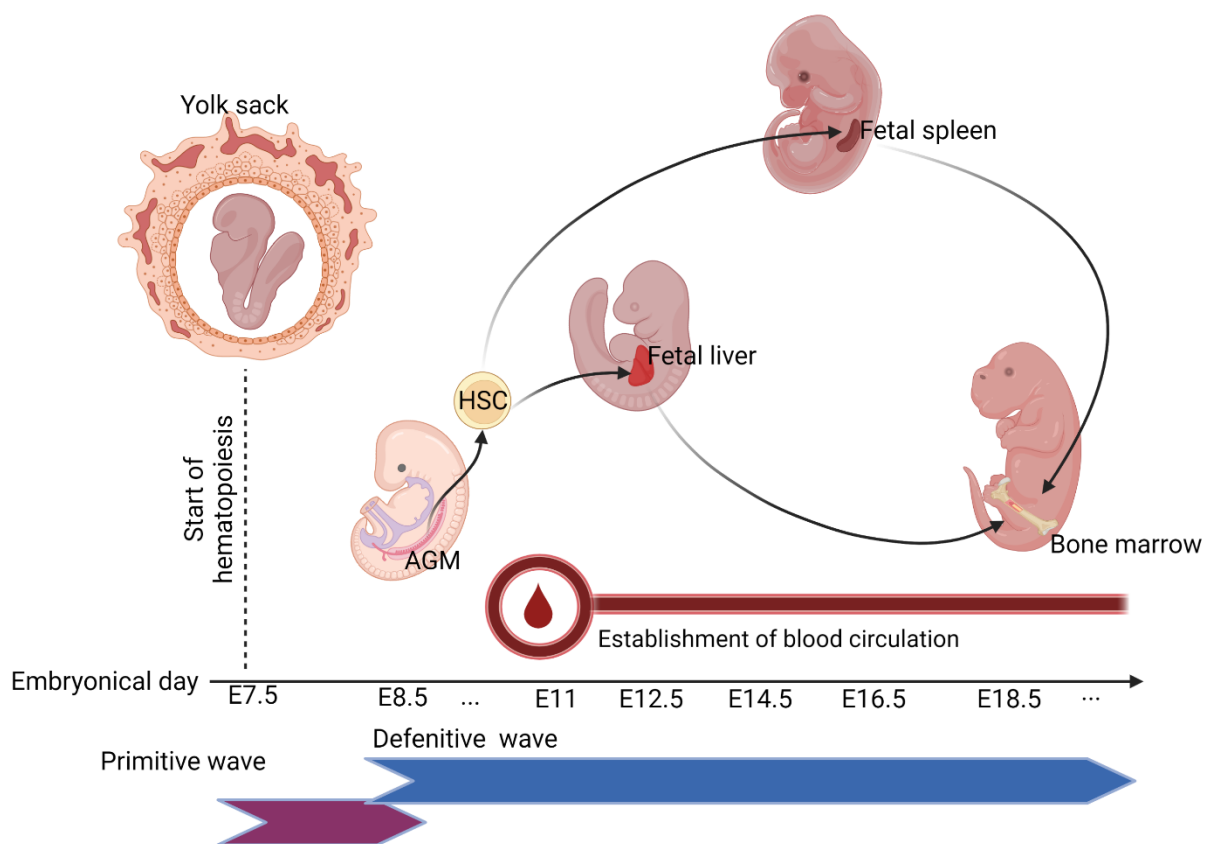


**Figure 1. The timeline of hematopoiesis in the mouse embryo.**

The different locations of hematopoiesis. The yolk sac is the initial location of hematopoiesis, known as a primitive wave. It produces the first primitive precursors around embryonic day (E) 7.5. At around E10.5, the HSC emerges in the aorta-gonad-mesonephros (AGM) region, which migrates to the fetal liver, fetal spleen and finally to the bone marrow and contributes to adult hematopoiesis. (Figure was adapted from Hayashi, Sezaki et al. (2019) and recreated using biorender.com)

### 1.1.1. Primitive hematopoiesis

In the mouse, primitive hematopoiesis occurs at around E7.5 in the extra-embryonic mesoderm layer of the YS within distinct clusters of cells called blood islands (Russell 1979, Palis 2016). This wave is transient and is replaced by definitive hematopoiesis rapidly.

The primary function of this wave is to produce transient hematopoietic cells to support the embryo with the necessary cells required for further development. The primitive hematopoiesis can give rise to the primitive erythroid progenitors, embryonic macrophages (Mφ), and primitive megakaryocytes necessary for oxygenation, defense and vascular maintenance, respectively (Kingsley, Malik et al. 2004, Bertrand, Jalil et al. 2005, Palis 2014).

Blood islands are composed of primitive hematopoietic cells in the center and sparse endothelial cells in the periphery (Hoeffel and Ginhoux 2018). The YS blood islands can generate restricted myeloid progenitors that can only give rise to the Mφ lineage; hence, they are uni-potent. In addition to that, these cells can give rise to bi-potent progenitors capable of differentiating into erythrocytes and megakaryocytes (Tober, Koniski et al. 2007, Hoeffel and Ginhoux 2018), suggesting that primitive hematopoiesis is limited to these three lineages.

The produced erythrocytes from the bi-potent progenitors within the blood islands are known as embryonic or primitive erythrocytes. These cells are different from the erythrocytes that are produced during the definitive hematopoiesis in the fetal liver (FL) and bone marrow (BM) as they are large, nucleated, and can produce the embryonic forms of globin (Barker 1968, Brotherton, Chui et al. 1979, Russell 1979).

## 1.1.2. The definitive hematopoiesis

Shortly following the formation of primitive cells (around 24hr later), at around E8.25, the second wave of hematopoiesis occurs in different sites of the mouse embryo. The YS is the first tissue to produce hematopoietic cells during mouse embryogenesis by producing multipotent EMP (Palis, Robertson et al. 1999); therefore, this wave is considered as HSC-independent hematopoiesis.

EMP are generated via an endothelial-to-hematopoietic transition in the YS. They proliferate and differentiate in the YS into erythroid and myeloid cells. EMP can be found in the bloodstream and the FL of the mouse embryo by E10.5. Despite the lack of HSC activity within EMP, e.g., they lack B-lymphoid potential, these progenitors give rise to the first definitive cells, including erythrocytes, megakaryocytes, Mφ, which are tissue-resident (Gomez Perdiguero, Klapproth et al. 2015) and other myeloid lineages (Palis, Robertson et al. 1999, McGrath, Frame et al. 2015) (Figure 2).
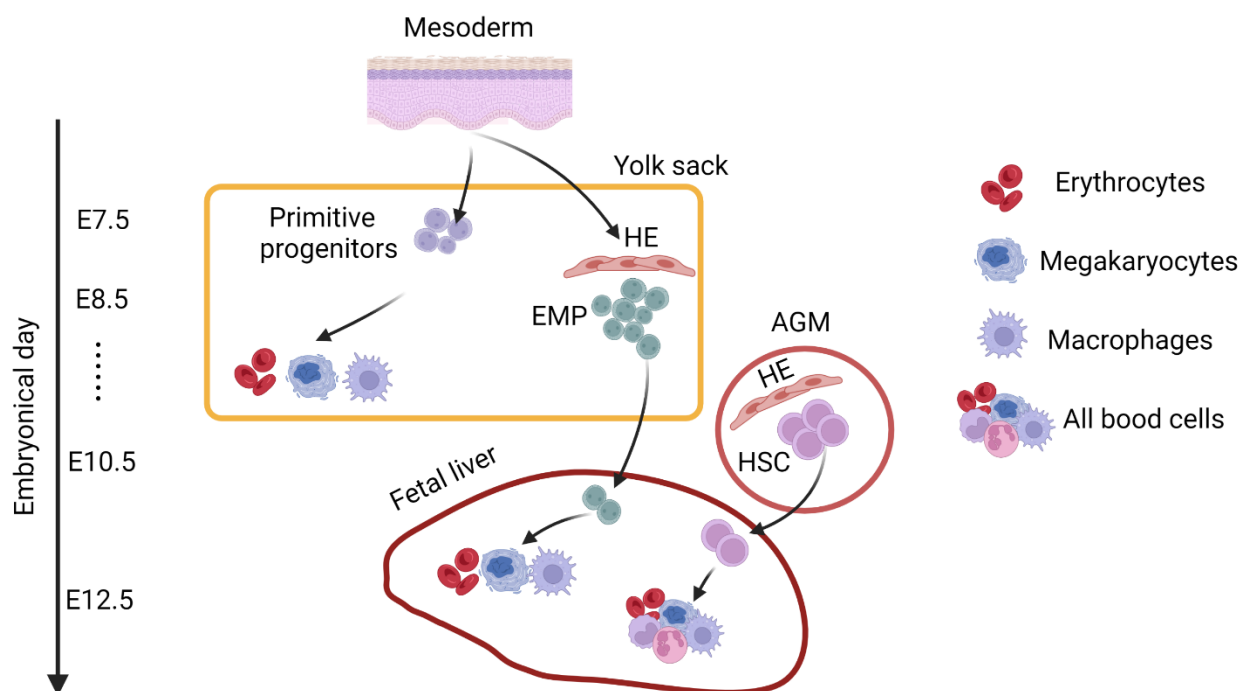


**Figure 2. A schematic model of hematopoietic ontogeny.**

The first primitive wave originates from the yolk sack's mesoderm and gives rise to primitive erythroid, megakaryocyte, and Mφ. The second wave is started upon the generation of erythromyeloid progenitor (EMP), which originates from the yolk sack's hemogenic endothelium (HE) region. The EMP give rise to definitive erythroid, megakaryocyte, and Mφ, which become tissue-resident. Finally, the third wave of hematopoiesis originates from the HE part of the aorta-gonad-mesonephros (AGM) and gives rise to all the blood cells. (Figure adapted from Palis (2016) and recreated using biorender.com)

4

Following the second wave, the third wave of hematopoiesis occurs between E9.5-E11 in the mouse embryo. In this wave HSC emerge from the HE region AGM (Cumano, Dieterlen-Lievre et al. 1996, Medvinsky and Dzierzak 1996). The AGM is an embryonic tissue derived from the mesodermal germ layer that contains the dorsal aorta, the genital ridge (which gives rise to the gonads), and the mesonephros (which gives rise to the kidneys), and that extends from the anterior limbs to the posterior limbs of the E9.5 to E12.5 mouse embryo (Rugh 1968, Kaufman 1992). The generated HSC migrate to the FL and undergo a maturation process (Taoudi, Gonneau et al. 2008, Kieusseian, Brunet de la Grange et al. 2012). Within the FL, HSC expands and differentiate into all myeloid and lymphoid cell types in addition to erythrocytes. HSC are defined by their ability to offer long-term multi-lineage hematopoietic reconstitution (LTR) upon transplantation into lethally irradiated mice and further secondary recipients (Morrison, Hemmati et al. 1995). The HSC can be identified using their expressed markers; Lineage$^-$CD45$^+$Sca1$^+$c-Kit$^+$ (LSK). HSC are classified into two main groups based on their reconstitution ability in the long and short term. These two groups are known as long-term HSC (LT-HSC) and are LSK CD150$^+$CD48$^-$ and short-term HSC (ST-HSC), which are LSK CD150$^-$CD48$^-$ (Kim, He et al. 2006). The HSC further give rise to other progenitors, namely multipotent progenitors (MPP), lympho-myeloid-primed progenitors (LMPP), common lymphoid progenitors (CLP) and common myeloid progenitors (CMP) (Figure 3) (Ramond, Berthault et al. 2014).

HSC activity can be first detected in the BM at E17.5; it has been shown that they can be found in the fetal spleen at around E15.5 although they lack significant expansion (Christensen, Wright et al. 2004, Bertrand, Desanti et al. 2006). The role of MPP is highlighted during adulthood as they have been shown to be responsible for replenishment of cell lineages while, the activity of HSC during adulthood in the BM has been described to be primarily quiescent, and their expansion happens only intending to maintain the HSC pool number (Charbord, Tavian et al. 1996, Sun, Ramos et al. 2014, Busch, Klapproth et al. 2015, Pei, Feyerabend et al. 2017, Rodriguez-Fraticelli, Wolock et al. 2018).
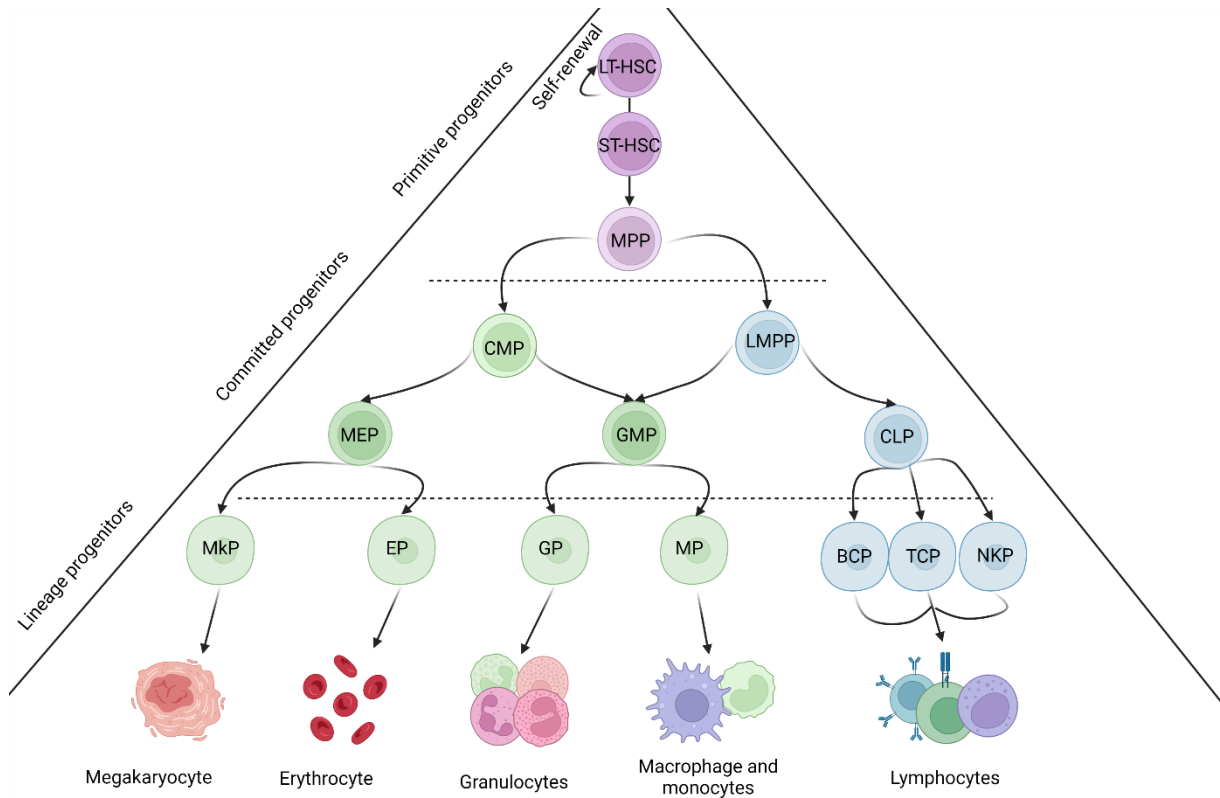
**Figure 3. Schematic model of hematopoiesis by HSC.**

HSC can be classified into two main groups known as long-term HSC (LT-HSC), which has a self-renewal ability, and short-term HSC (ST-HSC), which will give rise to other progenitors. LT-HSC, long-term hematopoietic stem cell; ST-HSC, short-term hematopoietic stem cell; LMPP, lymphoid-primed multipotent progenitor; MPP, multipotent progenitor; CMP, common myeloid progenitor; CLP, common lymphoid progenitor; GMP, granulocyte-macrophage progenitor; MEP, megakaryocyte–erythrocyte progenitor; BCP, B cell progenitor; TCP, T cell progenitor; NKP, NK cell progenitor; MP, macrophage progenitor; GP, granulocyte progenitor; EP, erythrocyte progenitor; MkP, megakaryocyte progenitor. (Figure adapted from Ratliff, Templeton et al. (2014) and recreated by biorender.com)

## 1.2.  Mφ development, ontogeny and heterogeneity

Mφ are immune cells that belong to the mononuclear phagocyte system (MPS), a family of professional phagocytes which includes dendritic cells and monocytes. They play an essential role in both tissue homeostasis and inflammation. They respond to inflammatory events in the body, trigger an innate immune response, and are known for phagocytosing pathogens, apoptotic cells, and debris. Furthermore, they can contribute to the pathophysiology of several diseases, including cancer and various inflammatory disorders.  They are also crucial for antigen presentation and cytokine production to modulate other immune cells' functions (Huber and Stingl 1981).

According to the MPS, it has been widely accepted that Mφ are differentiated cells that lack proliferative potential and are constantly repopulated by circulating monocytes (van Furth and Cohn 1968). However, later studies on Mφ ontogeny using congenic parabiotic mice that share the same circulation could show that this view is not entirely accurate. Congenic parabionts have mixed cell types, including mixed HSC and mixed lymphocytes and monocytes in the blood (Merad, Manz et al. 2002). Therefore, if Mφ were derived from monocytes, it is assumed that they should have the same level of chimerism as circulating monocytes. However, it was shown that even after a year of parabiosis, the tissue-resident Mφ of the skin (Langerhans cells) and the brain-resident Mφ (microglia) were not mixed in the tissues (Merad, Manz et al. 2002, Ajami, Bennett et al. 2007, Ginhoux, Greter et al. 2010)  suggesting that Mφ could be maintained independently of circulating precursors in adult mice.

It has now been shown through different studies that Mφ are derived from three ontogenies (see the review: Wu and Hirschi (2020)). Firstly, during the first wave of hematopoiesis, Mφ are detectable at E.9 and are originating from the YS of the embryo (Naito, Yamamura et al. 1989, Takahashi, Yamamura et al. 1989), although it is thought that the earlier primitive wave produces them. Yolk sac-derived Mφ continue to proliferate and colonize the rest of the embryo. By E12.5, they are replenished by Mφ generated from later waves (Schulz, Gomez Perdiguero et al. 2012, McGrath, Frame et al. 2015, Palis 2016).

The second ontogeny group of Mφ originate from EMP at around E8.25 (Hoeffel, Chen et al. 2015). EMP have erythroid and myeloid potential, but not lymphoid. As soon as the blood circulation is established, EMP migrate into the FL and produce the first enucleated erythrocytes in addition to bi-potent granulocyte/macrophage progenitors and mast cells (Palis, Robertson et al. 1999, Bertrand, Jalil et al. 2005, McGrath, Frame et al. 2015).

Since the EMP lack long-term potential in adults upon transplantation, the EMP wave of hematopoiesis is also called "transient definitive wave" (Hoeffel and Ginhoux 2018). The results from several previous studies could suggest that EMP give rise to fetal-derived tissue-resident Mφ (Guilliams, De Kleer et al. 2013, Hoeffel, Chen et al. 2015) except for brain microglia as these cells directly originate from primitive hematopoiesis from YS progenitors (Kierdorf, Erny et al. 2013). Fetal HSC-derived monocytes may also contribute to tissue-resident Mφ; however, their overall contribution is unclear. The generation of Mφ from EMP is through a constants programming of these cells that has been described as the core Mφ program. The EMP cells that follow the Mφ fate undergo this reprogramming and turn into pre-macrophages (pMacs) (Mass, Ballesteros et al. 2016). These cells simultaneously colonize the whole embryo at around E9.5 in a chemokine-receptor-dependent manner through the expression of *Cx3cr1*. Once the pMac are within a tissue, they start to have a specific expression of transcriptional regulators and genes, making them tissue-specific Mφ. For example, the tissue-resident Mφ in the liver, the Kupffer cells express *Id1* and *Id3* transcriptional regulators while the tissue-resident Mφ in the lung, the alveolar Mφ express *Pparg* (Gautier, Chow et al. 2012, Mass, Ballesteros et al. 2016).

Finally, the third and the last identified ontogeny of Mφ belongs to the HSC. Definitive HSC hematopoiesis starts at around E9.5, mainly in the intra-embryonic AGM region (Medvinsky and Dzierzak 1996), and they migrate to the FL where they expand, and by around E16.5, they start migrating to the fetal BM (Dzierzak and Speck 2008, Coskun, Chao et al. 2014). Mφ originating from HSC replace the EMP-derived Mφ in almost all adult tissues except the brain and, to some extent, the skin (Hoeffel, Wang et al. 2012, Sheng, Ruedl et al. 2015). However, it has been shown that both YS and HSC- derived Mφ can coexist in some tissues such as the heart and liver (Yap, Cabrera-Fuentes et al. 2019, Bleriot, Chakarov et al. 2020).

Recent studies have provided fate-mapping tools that can be helpful in shading light into the ontogeny of Mφ that are arising from HSC and monocytes. For example, the *Ms4a3^{Cre}* fate-mapping model is efficient in tracing monocytes and the Cxcr4CreERT2 has been proven successful in labeling GMP and HSC, respectively, thereby distinguishing HSC-derived monocytes from yolk-sac derived macrophages (Liu, Gu et al. 2019, Werner, Mass et al. 2020).

Tissue Mφ have a broad role and function. They can participate in the maintenance, homeostasis, remodeling and repair of tissues. The different functions of Mφ can be reflected in their heterogeneity and tissue specification. For example, it has been shown that alveolar Mφ have a high expression of scavenger and pattern recognition receptors (McCusker and Hoidal 1989, Palecanda, Paulauskis et al. 1999) as they are involved in infiltration and cleaning the lungs from microorganisms and particles. Microglia were found to play a role in modulating neuron outgrowth and positioning during brain development in mice (Squarzoni, Oller et al.

2014). In spleen, Mφ have been found to be specialized in recycling iron and catabolizing haem (Haldar, Kohyama et al. 2014, Soares and Hamza 2016).

One of the best-described roles of Mφ is their participation in the process of erythropoiesis and maturation of erythrocytes. Erythropoiesis is the process by which erythroid progenitors proliferate and differentiate into enucleated erythrocytes through different stages (Gregory and Eaves 1978). The different stages of erythrocytes maturation can be identified through their surface expression of CD71 and Ter119 (Chen, Liu et al. 2009). During embryogenesis, definitive erythropoiesis occurs in the FL within a specialized structure called erythroblastic island (Bessis 1958). These islands consist of an Mφ, so-called a central Mφ, which is surrounded by multiple erythroblasts. Mφ were proposed to promote erythropoiesis by directly transferring iron to erythroid progenitors (Bessis and Breton-Gorius 1962). During the final stage of erythroid differentiation, the erythroblast expels its nucleus as part of its maturation. Mφ has a critical role during this process since it will phagocytose the expelled nucleus, supporting the erythropoiesis process (Seki and Shirasawa 1965, Skutelsky and Danon 1972).

Mφ are quite diverse, and their intrinsic heterogeneity can be traced back to their distinct origins and maturation, which is compounded by interactions with neighboring cells and diverse microorganisms. Mφ heterogeneity is mostly inter-tissues, but their heterogeneity has been observed in a single organ such as the mouse spleen, which contains phenotypically diverse Mφ (Kraal 1992, Mebius and Kraal 2005). The red pulp of the spleen contains a subset of Mφ that are F4/80$^+$, and their primary is clearance of erythrocytes by responding to heme through induction of Spi-C, which is a specific transcription factor (Haldar, Kohyama et al. 2014). These Mφ have a role in heme catabolism and iron storage and reutilization. The white pulp of the spleen contains a subset of Mφ that are F4/80$^-$ but they express CD68 in abundance. These Mφ play an essential role in the clearance of apoptotic cells, especially the B cells (den Haan and Kraal 2012). The inter-tissue heterogeneity of Mφ also has been investigated in the adult liver, and according to a study, some evidence hint toward two distinct Mφ populations in the adult liver, known as Kupffer cell 1 (KC1) and Kupffer cell 2 (KC2) that are embryonically derived (Bleriot, Barreby et al. 2021). The KC1 makes the majority of the macrophages in the adult liver, and they are CD206$^{lo}$ESAM$^-$ while the KC2 population is CD206$^{hi}$ESAM$^+$, and unlike KC1, they are involved in metabolic processes such as fatty acid metabolism. These two populations express core Mφ signature genes such as *Clec4f* and *Csf1r* while expressing different genes and proteins.

In summary, more studies reveal that macrophages are more heterogeneous than initially anticipated within a tissue; however, their heterogeneity within the FL is still not fully understood.

## 1.3. HSC niche - a microenvironment for expansion of HSC

The developing FL is made of different cell types, including hepatic and hematopoietic lineages. During embryogenesis, the FL originates from the liver bud (Zong and Friedman 2014). Liver buds are generated at around E9.5 after the hepatic endoderm cells, known as hepatoblasts, undergo a delamination process from the epithelium and invade the adjacent cranial mesenchyme known as septum transversum mesenchyme (STM). At around E10–15 the liver buds proliferate and become vascularized, and this is around the time that it is colonized by HSC to become the major fetal hematopoietic organ. The FL supports the HSC with a unique microenvironment that helps their expansion and maintenance. The hypothesis that HSC and other stem cells are regulated by their surrounding environment was proposed in 1978 by Schofield (Schofield 1978). According to this proposal, the stem cells are maintained by the surrounding cells so-called their "niche".

The initial niche term referred to the local BM microenvironment that provides crucial factors for HSC self-renewal and differentiation. The BM niche was first described as a place that controls the quiescence and cell cycle of HSC and regulates the fate of HSC daughter cells (Scadden 2014). In vitro co-culture assays using osteoblast cells and HSC could show that osteoblasts produce different growth factors such as G-CSF (granulocyte-colony stimulating factor; CSF3) essential for HSC differentiation (Taichman, Reilly et al. 2000). Furthermore, it has been proven that egress of the HSC from the BM can be regulated by the local neurotransmitters, from the sympathetic nervous system (SNS) perivascular nerves, which are tightly associated with the BM vasculature (Katayama, Battista et al. 2006, Mendez-Ferrer, Lucas et al. 2008). Most HSCs reside close to BM sinusoidal endothelial cells (Kiel, Yilmaz et al. 2005, Kunisaki, Bruns et al. 2013). An in-vitro study has shown that the expression of Notch ligands by endothelial cells (EC) can stimulate the HSC proliferation and prevents HSC exhaustion (Kobayashi, Butler et al. 2010), and the deletion of a Notch ligand, Jag1, from EC resulted in lower HSC numbers (Poulos, Guo et al. 2013). The proliferation effect of the EC could also be seen in-vivo, and the Notch signaling in EC could expand HSC (Kusumbe, Ramasamy et al. 2016).

One of the most critical aspects of the FL niche for HSC is cell-cell interactions that can happen either directly or through signaling. Stromal regulation of hematopoiesis has been suggested by previous studies in which hematopoietic progenitors were co-cultured with either FL fibroblast or epithelial-stromal cell lines (Tsai, Emerson et al. 1986, Hata, Nanno et al. 1993). Moreover, it has been shown that angiopoietin-like 2 and 3 (angptl2, 3) from the FL stromal cells help expand HSC (Zhang, Kaba et al. 2006) and hepatoblasts that can expand LT-HSC around 20-fold (Chou, Flygare et al. 2013). EC, which are another type of stromal cells has

been reported to express membrane-bound stem cell factor (SCF) and play a role in HSC expansion (Neo, Booth et al. 2018). It has been shown that two subtypes of EC, arterial EC and sinusoidal EC, contribute to the HSC niche and the majority of HSCs are directly touching at least one EC (Lu, Liu et al. 2021).

Furthermore, EC can provide distinct signaling molecules that contribute to important signaling pathways such as Wnt and Notch signaling. The interaction between HSC and hepatic stellate cells/perivascular mesenchymal cells (PMC) has been observed within the FL. Similar to the interaction of EC and HSC, it has been shown that the majority of FL HSC are in close proximity to PMC (Dong, Russell et al. 2021). These PMC express N-cadherin and are also enriched with the expression of niche factors, such as CXCL12 and KITL.

Up to this date, researchers could shed light on the interaction between HSC and the hepatic cells in the FL; however, it is very likely that different FL populations such as Mφ play distinct roles in the maintenance and expansion of HSC through cellular networks which require further investigations.

## 1.4. Aims of the thesis

Despite the proven different roles of Mφ and their heterogeneity across different tissues, several aspects of these powerful phagocytic cells have not been addressed. This thesis aimed to shed light on the following topics.

1-     Investigating the role of Mφ in supporting HSC during embryogenesis in the FL
2-     Heterogeneity and diversity of Mφ within the FL
3-     Addressing the ontogeny of possible different Mφ groups in the FL

# 2. Material

## Key resources tables

**Table 1. List of antibodies for investigating the Mφ heterogeneity in the FL**

| Heterogeneity Panel | | | | | |
|---|---|---|---|---|---|
| **Primary Abs** | | | | | |
| **Antigen** | **Conjugate** | **Clone** | **Dilution** | **Source** | **Cat. #** |
| Ly-6C | Biotin | HK1.4 | 1:400 | BioLegend | 128004 |
| Ly-6G | BUV395 | 1A8 | 1:200 | BD | 563978 |
| Vcam-1 | BUV563 | 429 | 1:200 | BD | 741246 |
| Ter119 | BUV615 | TER-119 | 1:400 | BD | 751534 |
| CD11b | BUV737 | M1/70 | 1:200 | BD | 612800 |
| CD115 | BUV661 | AFS98 | 1:400 | BD | 750949 |
| CD45 | BUV805 | 30-F11 | 1:400 | BD | 748370 |
| CD33 | Super Bright 436 | 9A11-CD33 | 1:400 | Thermo Fisher Scientific | 62-0331-82 |
| F4/80 | BV510 | T45-2342 | 1:100 | BD | 743280 |
| CD169 | BV605 | 3D6.112 | 1:200 | BioLegend | 142413 |
| CD192 (CCR2) | BV650 | 475301 | 1:200 | BD | 747968 |
| CD182 (CXCR2) | BV711 | V48-2310 | 1:400 | BD | 747812 |
| TIM-4 | BV786 | 21H12 | 1:200 | BD | 742778 |
| CD63 | PerCP/Cy5.5 | NVG-2 | 1:100 | BioLegend | 143912 |
| CD369 (Clec7a) | PE | bg1fpj | 1:100 | Thermo Fisher Scientific | 12-5859-82 |
| CX3CR1 | PE/Dazzle™ 594 | SA011F11 | 1:200 | BioLegend | 149013 |
| CD204 | PE/Cy7 | M204PA | 1:400 | Thermo Fisher Scientific | 25-2046-82 |
| Clec4f | AF647 | 3E3F9 | 1:100 | BioLegend | 156804 |
| CD206 (MMR) | AF700 | C068C2 | 1:100 | BioLegend | 141734 |
| CD16/32 (Fcg R III/II) | - | 93 | 1:100 | BioLegend | 101302 |
| **Secondary Abs** | | | | | |
| **Antigen** | Conjugate | Clone | Dilution | Source | **Cat. #** |
| Streptavidin | BUV496 | - | 1:400 | BD | 612775 |

**Table 2. List of antibodies for quantification of HSC and progenitors in the FL**

| Antigen | Conjugate | Clone | Dilution | Source | Cat. # |
|---|---|---|---|---|---|
| **HSC flow-cytometry Panel** | | | | | |
| **Primary Abs** | | | | | |
| CD11b | Biotin | M1/70 | 1:800 | BioLegend | 101204 |
| NKp46 | Biotin | 29A1.4 | 1:200 | BioLegend | 137616 |
| CD3 | Biotin | 145-2C11 | 1:200 | BioLegend | 100304 |
| CD19 | Biotin | 6D5 | 1:400 | BioLegend | 115504 |
| Gr1 | Biotin | RB6-8C5 | 1:400 | BioLegend | 108404 |
| Ter119 | Biotin | TER-119 | 1:200 | BioLegend | 116204 |
| Kit (CD117) | BV711 | 2B8 | 1:200 | BioLegend | 105835 |
| Sca1 | BV510 | D7 | 1:100 | BioLegend | 108129 |
| CD48 | AF647 | HM48-1 | 1:200 | BioLegend | 103416 |
| CD150 | PE-Cy7 | TC15-12F12.2 | 1:400 | BioLegend | 115914 |
| CD16/32 | APC-Cy7 | 93 | 1:100 | BioLegend | 101328 |
| CD34 | BV421 | MEC14.7 | 1:100 | BioLegend | 119321 |
| CD135 | PE | A2F10 | 1:100 | BioLegend | 135306 |
| CD127 | PerCP/Cy5.5 | A7R34 | 1:100 | BioLegend | 135022 |
| **Secondary Abs** | | | | | |
| Streptavidin | FITC | - | 1:200 | BD | 405201 |

**Table 3. List of antibodies for quantification of Mφ and myeloid cells in the FL**

| Myeloid cells flow-cytometry Panel (Fetal liver) | | | | | |
|---|---|---|---|---|---|
| **Primary Abs** | | | | | |
| **Antigen** | **Conjugate** | **Clone** | **Dilution** | **Source** | **Cat. #** |
| CD45 | BUV805 | 30-F11 | 1:400 | BD | 748370 |
| CD11b | PECy7 | M1/70 | 1:800 | BioLegend | 101216 |
| Tim4 | AF647 | RMT4-54 | 1:400 | BioLegend | 130008 |
| F4/80 | BV421 | BM8 | 1:400 | BioLegend | 123132 |
| Ly6C | BV510 | HK1.4 | 1:200 | BioLegend | 128033 |
| Ly6G | PerCP/Cy5.5 | 1A8 | 1:400 | BioLegend | 127616 |
| Cx3cr1 | PE-Dazzle594 | SA011F11 | 1:400 | BioLegend | 149014 |
| CD71 | FITC | RI7217 | 1:100 | BioLegend | 113806 |
| CD206 | BV711 | C068C2 | 1:200 | BioLegend | 141727 |
| CD169 | BV605 | 3D6.112 | 1:200 | BioLegend | 142413 |
| Vcam1 | Biotin | MVCAM.A | 1:400 | BioLegend | 105703 |
| Ter119 | BV421 | TER-119 | 1:300 | BioLegend | 116234 |
| **Secondary Abs** | | | | | |
| Streptavidin | BV785 | - | 1:200 | BD | 405249 |

**Table 4. List of antibodies for sorting Mφ from the FL and Mφ quantification in the fetal brain and lung**

| Sorting and quantification panel | | | | | |
|---|---|---|---|---|---|
| **Primary Abs** | | | | | |
| **Antigen** | **Conjugate** | **Clone** | **Dilution** | **Source** | **Cat. #** |
| CD45 | BUV805 | 30-F11 | 1:400 | BD | 748370 |
| CD11b | PECy7 | M1/70 | 1:800 | BioLegend | 101216 |
| F4/80 | BV421 | BM8 | 1:400 | BioLegend | 123132 |

**Table 5. List of antibodies for sorting HSC from the FL**

| HSC FACS Panel | | | | | |
|---|---|---|---|---|---|
| **Primary Abs** | | | | | |
| **Antigen** | **Conjugate** | **Clone** | **Dilution** | **Source** | **Cat. #** |
| CD11b | Biotin | M1/70 | 1:800 | BioLegend | 101204 |
| NKp46 | Biotin | 29A1.4 | 1:200 | BioLegend | 137616 |
| CD3 | Biotin | 145-2C11 | 1:200 | BioLegend | 100304 |
| CD19 | Biotin | 6D5 | 1:400 | BioLegend | 115504 |
| Gr1 | Biotin | RB6-8C5 | 1:400 | BioLegend | 108404 |
| Ter119 | Biotin | TER-119 | 1:200 | BioLegend | 116204 |
| Kit (CD117) | APC-Cy7 | 2B8 | 1:200 | BioLegend | 105835 |
| Sca1 | BV510 | D7 | 1:100 | BioLegend | 108129 |
| CD48 | AF647 | HM48-1 | 1:200 | BioLegend | 103416 |
| CD150 | PE-Cy7 | TC15-12F12.2 | 1:400 | BioLegend | 115914 |
| **Secondary Abs** | | | | | |
| Streptavidin | FITC | - | 1:400 | BioLegend | 405201 |

**Table 6. List of immunofluorescence antibodies**

| Immunofluorescence staining panel | | | | | |
|---|---|---|---|---|---|
| **Antibody** | **Conjugate** | **Titration** | **Provider** | **Cat. #** | **Type** |
| CD31 | - | 1:300 | Thermo Fisher Scientific | MA3105 | Primary antibody |
| Iba1 | - | 1:300 | Abcam | 178847 | Primary antibody |
| F4/80 | BV421 | 1:300 | BioLegend | 123132 | Primary antibody |
| Tim4 | AF647 | 1:300 | BioLegend | 130008 | Primary antibody |
| Ter119 | PE | 1:300 | BioLegend | 116207 | Primary antibody |
| c-Kit (CD117) | BV711 | 1:300 | BioLegend | 105835 | Primary antibody |
| CD150 (SLAM) | AF647 | 1:50 | BioLegend | 115918 | Primary antibody |
| Goat anti-Rabbit IgG (H+L) | AF488 | 1:300 | Thermo Fischer Scientific | A11008 | Secondary antibody |
| Goat anti-Rat IgG (H+L) | AF555 | 1:300 | Thermo Fischer Scientific | A21434 | Secondary antibody |

**Table 7. List of chemicals and solutions**

| Chemicals and solutions | | |
|---|---|---|
| **Item** | **Company** | **Cat. #** |
| BSA (Bovine Serum Albumin) | Sigma-Aldrich | A9647-500G |
| DAPI (4´,6-Diamidino-2-Phenylindole, Dilactate) | BioLegend | 422801 |
| EDTA (Ethylenediaminetetraacetic acid) | Sigma-Aldrich | E9884-500G |
| Entellan® mounting medium | Merck Millipore | 1079610100 |
| PBS (10x) without Ca$^{++}$, Mg$^{++}$ | Biozym | 882131 |
| QIAzol Lysis Reagent | Qiagen | 79306 |
| Rat serum | Bio-Rad | C13SD |
| Sakura Finetek ™ Tissue-Tek O.C.T. Compound | Fisher Scientific | 12351753 |
| DRAQ7 | BioLegend | 424001 |
| Taq-Polymerase Mastermix | VWR | K1082 |
| Nuclease-free water | GE Healthcare | SH30538.01 |
| Sodium hydroxide | Merck | 1.06498.1000 |
| TRIS-Hydrochloride | AppliChem Panreac | 50012105 |
| DNA ladder | New England Biolabs | N3231S |
| Paraformaldehyde | Thermo Fisher Scientific | 11586711 |
| Dulbecco's Phosphate-Buffered Saline | PAN-Biotech | P04-53500 |
| Sucrose | Fisher Scientific | 10638403 |
| Methanol | Fisher Scientific | 10164663 |
| Dimethylsulfoxide | Millipore Sigma | D8418-50ML |
| Triton X100 | Fisher Scientific | BP151-100 |
| Bovine Serum Albumin | Sigma-Aldrich | A9647-500G |
| Sodium Azide | Carl Roth | K305.1 |
| Normal Goat Serum | VWR | ICNA 08642921 |
| Ethylenediaminetetraacetic acid | Sigma-Aldrich | E9884-500G |
| DNase | Sigma-Aldrich | DN25-1G |
| CollagenaseD | Sigma-Aldrich | 11088882001 |
| Fetal calf serum | Bio&Sell | FBS. S 0615HI |
| Roswell Park Memorial Institute medium (Seahorse XF RPMI medium) | Agilent Technologies | 103576-100 |
| Propidium iodide | Thermo Fisher Scientific | BMS500PI |
| MethoCult | StemCell Technologies | 03434 |

| | | |
|---|---|---|
| Weise buffer tablet | Merck | 109468 |
| May-Grünwald solution | Merck | 101424 |
| Giemsa solution | Merck | 109204 |
| Benzyl-alcohol | - | - |
| Benzyl-benzoate | - | - |

**Table 8. List of main buffers**

| Buffers | |
|---|---|
| **Buffer** | **Components** |
| FACS buffer | BSA 0.5%<br>EDTA 2mM<br>Diluted in 1x PBS |
| 1X PBS | 10X PBS<br>Diluted with bidest water (1:10) |

**Table 9. List of main laboratory equipment**

| Laboratory equipment | | |
|---|---|---|
| **Item** | **Cat. #/Description** | **Company** |
| FACSAriaTM III | Cell Sorter | BD Biosciences |
| FACSymphony | Flow cytometer | BD Biosciences |
| Guava easyCyte | Flow Cytometer | Luminex |
| Leica M80 | Microscope | Leica |
| LSM 880 | Confocal Microscope | Zeiss |
| 5810R Centrifuge | Centrifuge | Eppendorf |
| Universal 16A centrifuge | Centrifuge | Hettich |
| AXIO Lab.A1 | Microscope | Zeiss |

# 3. Methods

## 3.1. Experimental mouse models

### 3.1.1. Breeding and plug-check

All mice were maintained on a C57BL/6 background and housed in SPF conditions. Animal procedures were performed in adherence to our project licenses 2018.A056 issued by the "Landesamt für Natur, Umwelt und Verbraucherschutz" (LANUV).

*Tnfrsf11a$^{Cre}$; Pu.1$^{flox/+}$* mice were crossed to *Pu.1$^{flox/flox}$* to generate Mφ-depleted embryos. *Tnfrsf11a$^{Cre}$; Id1$^{flox/flox}$; Id3$^{flox/flox}$* mice were crossed to *Id1$^{flox/flox}$; Id3$^{flox/flox}$* to generate liver-resident Mφ-depleted embryos. *Rank$^{Cre}$Rosa26$^{eYFP}$*, *Ms4a3$^{Cre}$Rosa26$^{eYFP}$* and *Cxcr4$^{Cre}$Rosa26$^{eYFP}$* mice were crossed to an R26*Rosa26$^{eYFP}$* to generate fate-mapper embryos.

The mice were mated overnight. Breeding always took place in a male´s cage, and possible mating was investigated through plug-checking the next day (between 8:00 am and 9:00 am). Upon observation of a plug, the day of vaginal plug formation was estimated as E0.5. The pregnancy of mice was observed for three different dates; E14.5, E16.5, and E18.5. Depending on the experiment, the embryos were harvested at one of the mentioned time points.

### 3.1.2. Genotyping

A small part of embryonic/adult tissues (ear tag or tail) were dissolved in 200µl of 50 mM NaOH for 20-30 min at 95 °C. 20µl of 1M TRIS HCl with a pH of 8 was added. Afterward, 1µl of supernatant was taken for the subsequent master mix solution with a total volume of 10µl per sample that consists of 0.5µl for each of the forward and reverse primers, 5µl DreamTaq ™ Green PCR Master-Mix and H$_2$O for the rest of the volume.

After the PCR program was done, samples were applied onto a 1.5% agarose gel in 1x TBE buffer and separated via electrophoresis at 120V for 30 min. The DNA was stained using Sybr safe/green and visualized via UV light. The genotyping of *Rank$^{Cre}$Rosa26$^{eYFP}$*, *Ms4a3$^{Cre}$Rosa26$^{eYFP}$* and *Cxcr4$^{Cre}$Rosa26$^{eYFP}$* embryos were done by checking the YFP expression by flow-cytometry by dissolving and mechanically disturbing a small piece of embryonic tissue.

**Table 10. List of primers for genotyping**

| Gene | Primer | Sequence |
|---|---|---|
| *Id3*<sup>f/f</sup> | Forward<br>Reverse | 5´ATT CTT GAC GCC AGT GAG TC 3´<br>5´CCC ACA GCT CTG AGG TCA T 3´ |
| *Id1*<sup>f/f</sup> | Forward | 5´TGG GCT GGG AAG TAT TCA AG 3´ |
| | Reverse | 5´CAC AGG CAA GCC CTG ATA TT 3´ |
| *Rank*<sup>Cre</sup> | Forward | 5´ TGA AGG GTG ACA TCA TCG TGG T 3´ |
| | Reverse | 5´ ACT TCT CCA TGG TAG CCT CCT CC 3´ |
| | Reverse(mut) | 5´ AAT AGG GGT GGG GTG ATA 3´ |
| *Pu.1*<sup>f/f</sup> | Forward | 5'-CTT CACTGC CCATTC ATT GGC TCA TCA-3' |
| | Reverse | 5'-GCT GGG GAC AAG GTT TGATAA GGG AA-3' |
| | Reverse(mut) | 5'-CAA CCG GAT CTA GACTCG AGG A-3' |

Note: The gene labels *Id3*<sup>f/f</sup>, *Id1*<sup>f/f</sup>, *Pu.1*<sup>f/f</sup> use non-mathematical superscript notation rendered as [f/f] and *Rank*<sup>Cre</sup> as [Cre].

**Table 11. PCR program for genotyping.**

| Step | Temperature | Time |
|---|---|---|
| Initial denaturation | 95°C | 3 min |
| Denaturation | 95°C | 30 sec |
| Primer annealing | 60°C | 30sec |
| Elongation | 72°C | 30sec |
| Final extension | 72°C | 5 min |

Denaturation, primer annealing and elongation is to repeat for 35 cycles.

## 3.2. Immunostaining

### 3.2.1. Preparation of tissues and cryosectioning

Pregnant mice were sacrificed through cervical dislocation. Embryos at E14.5 were harvested and stored in the cold 1x Dulbecco's Phosphate-Buffered Saline (DPBS w/o Ca and Mg, PAN-Biotech) and dissected under a Leica M80 microscope. A small piece of every embryo's tail was collected in a 1.5 ml safe-lock tube (Eppendorf tube) for genotyping. FLs were harvested and divided into four lobes. Three lobes were fixed in 1% paraformaldehyde (PFA) overnight at 4°C for IF staining, and one lobe was used for the CFU assay. Fixed lobes were washed three times for 10 minutes with DPBS, incubated in 30% sucrose, and stored in a fridge inside DPBS.

### 3.2.2. Tissue dehydration

The pieces of FL were dehydrated using increasing methanol (Fisher Scientific) gradient diluted in DPBS. They were incubated on a shaker for 30 min in Eppendorf tubes in 1 ml methanol of every concentration at room temperature (RT). Different methanol grades were used at 50%, 80%, and 100%. The samples were bleached by shaking in 20 % dimethylsulfoxide (DMSO, Sigma) for 30 min. Dehydration continued with descending 80% and 50% methanol concentration, followed by 30 min incubation in DPBS. Tissues were incubated in a blocking buffer (DPBS with 0.3% Triton X100 (Sigma), 0.2% Bovine Serum Albumin (BSA, Thermo Scientific), 5% DMSO, 0.1% Sodium Azide (Carl Roth), 5% Normal Goat Serum (NGS, VWR)) shaking overnight at 4 °C to block unspecific binding sites.

### 3.2.3. Antibody staining

The staining was done first using the primary antibodies (AB). Samples were incubated with AB overnight at 4 °C in 200µl 0.4% PBT (DPBS with 0.4% Triton x100) and handled in dark conditions. Afterward, the samples were washed three times for 10 min in washing buffer (DPBS with 0.2% Triton x100, 3% NaCl (Grüssing) at RT. The same procedure was repeated using the secondary ABs and, if needed, using the directly conjugated AB a third time.

### 3.2.4. Tissue clearing

FL lobes were washed three times for 10 min in washing buffer and incubated using an increasing methanol gradient. Methanol was diluted with water. Tissues were transferred in 1 ml 50% methanol in 10 ml Duran glasses for 30 min on a shaker at RT. Afterward, the liver pieces were transferred in 70%, 95%, and three times in 100% methanol for 30 min each. Tissues were cleared in benzyl-alcohol benzyl-benzoate (BABB 1:2 proportion). FL lobes were placed for 30 min in 50% BABB, followed by incubation in 100% BABB for 30 mins. After clearing, the tissue became transparent.

### 3.2.5. Embedding

The tissues were placed in a cavity slide (Brand) filled with 120µl of 100% BABB. A round cover glass was carefully placed on the tissue using fine forceps. The cover glass was attached to the slide by using a slight amount of pressure. The excessing BABB was absorbed using tissue paper. After a few minutes, the glass borders were sealed using nail polish and dried in the fridge.

### 3.2.6. Microscopy and image analysis

Samples were 3D visualized using LSM 880 Zeiss confocal microscope with 63x (oil) objective. With the ZenBlack (Zeiss) software, a 3x3 tile scan was performed, and a Z-stack section of the region of interest was done. Images were stitched and exported as OMETIFF files using ZenBlue (Zeiss). Mφ quantification and HSC distance measuring were done using the microscopy image analysis software Imaris (v.7.4.2, Bitplane). Only F4/80$^+$ Mφ were counted for quantification. Quantification was done manually by marking F4/80$^+$ cells using the "Spot" function in Imaris. Distance between HSC and Mφ was measured using the "Measurement Points" function in Imaris. Measuring points were set in the estimated center of the cells. The software automatically calculated the distance between two points.

## 3.3. Colony-forming unit assay

CFU was performed according to the "Mouse Colony-Forming Unit (CFU) Assays Using MethoCult™" GF M3434 protocol (StemCell Technologies) (STEMCELL).

### 3.3.1. Preparation of cell suspension

One FL lobe was used for the CFU assay. The lobe was collected in 150µl fluorescence cell sorting (FACS) buffer (1x DPBS with 2% 100mM Ethylenediaminetetraacetic acid (EDTA, Sigma-Aldrich), 0,5% BSA) in a 48 well plate. 150µl digestion enzyme (0.6µl DNase (Sigma-Aldrich), 0.6µl CollagenaseD (Sigma-Aldrich), 9µl fetal calf serum (FCS, Bio&Sell), 139.8µl 1x DPBS) was added. Then samples were mechanically disrupted with a small scissor and incubated for 30 min at 37 °C. Following the digestion, the tissue was transferred on a 70 µm strainer placed on a 6 well plate filled with 2 ml FACS buffer. If necessary, the remaining tissue was carefully minced using a plunger. The whole volume was transferred in a FACS tube and centrifuged in an Eppendorf Centrifuge 5810R (5 mins, 400g, 4°C). The supernatant was discarded, and the pellet was resuspended in 1 ml sterile Roswell Park Memorial Institute medium (RPMI, supplemented with 10% FCS, 1% Penicillin-Streptomycin, 1% D-Glutamate, 1% Pyruvate). The suspension was diluted at 1:5 to determine the cell number using a cell counter (Guava easyCyte by Luminex). Propidium iodide (PI, Invitrogen) was used to stain dead cells to exclude them from counting. $3x10^5$ cells were taken from the suspension and filled up to 1 ml with RPMI to achieve a $3x10^5$ cells/ml concentration.

1.5 ml MethoCult aliquots (StemCell Technologies) were thawed at RT and vortexed vigorously. 150µl of the cell suspension was added to the MethoCult, vortexed, and let rest until all bubbles vanished. 1 ml MethoCult mixed with the cell suspension was slowly taken up using a microliter pipette. The tip was placed precisely below the surface to prevent bubbles from adhering to the pipette's tip. The whole volume was transferred to a 35 mm cell culture dish (VWR). The cell culture dish was cautiously tilted until it was covered with medium. Occurring bubbles were carefully removed using a 20µl pipette. Two 35 mm cell culture dishes with the medium were placed in a 94x16 cell culture dish (Greiner bio-one). Another 35 mm dish filled with 3 ml aqua bidest was added to the dish closed with a lid to ensure sufficient humidity. The plates were not moved for a minimum of 4 days resting in the incubator (37°C, 4% $CO_2$).

After 12 days of cell culture, colonies were picked with 10µl FACS buffer and stored in 1.5 ml Eppendorf tubes filled with another 10µl cooled FACS buffer. Six samples were transferred on a slide using a funnel assembly which contained a layer of filter paper and was attached to the front of a slide. Slides were centrifuged using a universal 16A centrifuge (Hettich) at ca. 1000 rounds per min (RPM) for 5 mins. The filter paper absorbed Excessing buffer. The remaining buffer was air-dried for at least 30 mins. Cells were fixed using 800µl ice-cold methanol per slide. Methanol-fixed cells were manually stained using a May-Grünwald-Giemsa staining solution.

### 3.3.2. May-Grünwald-Giemsa cell staining

The staining was performed using chambers filled with May-Grünwald and Giemsa staining solutions. Weise buffer was prepared using a buffer tablet (Merck). First, the slides were placed for six min in a staining chamber filled with May-Grünwald solution (15 mL May-Grünwald solution (Merck), 10 mL Weise buffer, 75 mL deionized water) followed by two rinsing steps in Weise buffer for one min each. Afterward, the slides were stained in Giemsa solution (5 mL Giemsa solution (Merck), 95 mL Weise buffer) for 20 mins, followed by two washing steps in Weise buffer for 1 min. Using an AXIO Lab.A1 (Zeiss) verified if the staining was successful. If not, the steps were repeated until all cells were stained. After 30 min of air-drying, samples were embedded with entellan (Merck). Since the entellan was fully polymerized, representative pictures were taken using the AXIO imager microscope with a 40x objective.

### 3.3.3. Colony identification

Colonies were first identified by their phenotype after 12 days of cell culture. Therefore, their size, shape, and density were analyzed based on representative pictures shown in the CFU assay protocol by STEMCELL Technologies. Secondly, the identification has been validated by the May-Grünwald-Giemsa staining of the colonies.

## 3.4. Flow-cytometry of the samples

### 3.4.1. Samples preparation and measurement

Pregnant mice were sacrificed through cervical dislocation at one of the E14.5, E16.5, and E18.5 time points. The FL, brain, and lung were harvested from the embryos, and they were treated with a 300µL digestive enzyme mix containing 0.1% DNase, 0.1% collagenase and 3% fetal bovine serum (FBS) in PBS buffer in one well, incubating for 15-20 min at 37°C.

The samples were homogenized through several pipetting and were transferred to a well of 6 well plate that contains 3 ml of FACS buffer via a 100µm strainer. If necessary, the tissues were mechanically disturbed using a plunger. The filtered cell suspensions were transferred into the FACS tubes and centrifuged at 400 g for 5 min at 4 °C. The supernatants were removed, and the pellets were resuspended in 50µL blocking solution (2% rat serum) for 10 min incubation on ice. The volume of each sample was measured using a pipette, and it was topped up to 300 µm (x6).

Depending on the purpose of the experiment, 50μL of each sample was mixed with 50μL of the biotin-labeled antibody mix, and they were incubated for 25-30 min on ice. Afterward, the samples were washed by adding 100μL FACS to the suspension and centrifuge at 400 g for 5 min at 4 °C. The supernatants were removed, and the pellets were resuspended if necessary, using 50μL the directly conjugated antibody mix, and they were incubated again for 25-30 min on ice. At the end of incubation, the samples were rewashed by adding 100μL FACS to the suspension and centrifuge at 400 g for 5 min at 4 °C (Table 1, Table 2,  Table 3, and Table 4).

Finally, the pellets were resuspended cells in 100μL FACS buffer. The cells were stained with Hoechst or DRAQ7 as live/dead staining before flow-cytometry. The final dilution of live/dead staining was 1:10000 for Hoechst or 1:1000 when using DRAQ7. Cells were recorded using a FACSymphony™ (BD Biosciences) cytometer. The whole volume of stained samples belonging to the *Tnfrsf11a^{Cre}; Pu.1^{flox/+}* and *Tnfrsf11a^{Cre}; Id1^{flox/flox}; Id3^{flox/flox}* embryos were measured. However, for any other samples, e.g., the fate-mapping embryos and wild-type embryos for analyzing the heterogeneity, only 1-1.5 million total cells were recorded.

### 3.4.2.  Analysis of flow-cytometry data for quantification of cells

Flow-cytometry data analysis was performed using FlowJo™ Software v.10.8.1 Becton, Dickinson and Company. The total recorded cells were multiplied by six to get an approximate total cell number for the whole tissue. The population of interest was analyzed using three different gating strategies to quantify different cell types. The quantification of HSC and progenitors was done using Figure 4 gating strategy, the quantification of myeloid cells in the FL and the erythrocytes differentiation was done using Figure 5 gating strategy, and the quantification of Mφ in the control organ, the fetal brain and the fetal lung, was done using Figure 6 gating strategy. The count of each cell type was recorded and plotted using R and the ggplot2 (v. 3.3.5) and ggpubr (v. 0.4.0) (Wickham, Chang et al. 2016, Kassambara and Kassambara 2020).
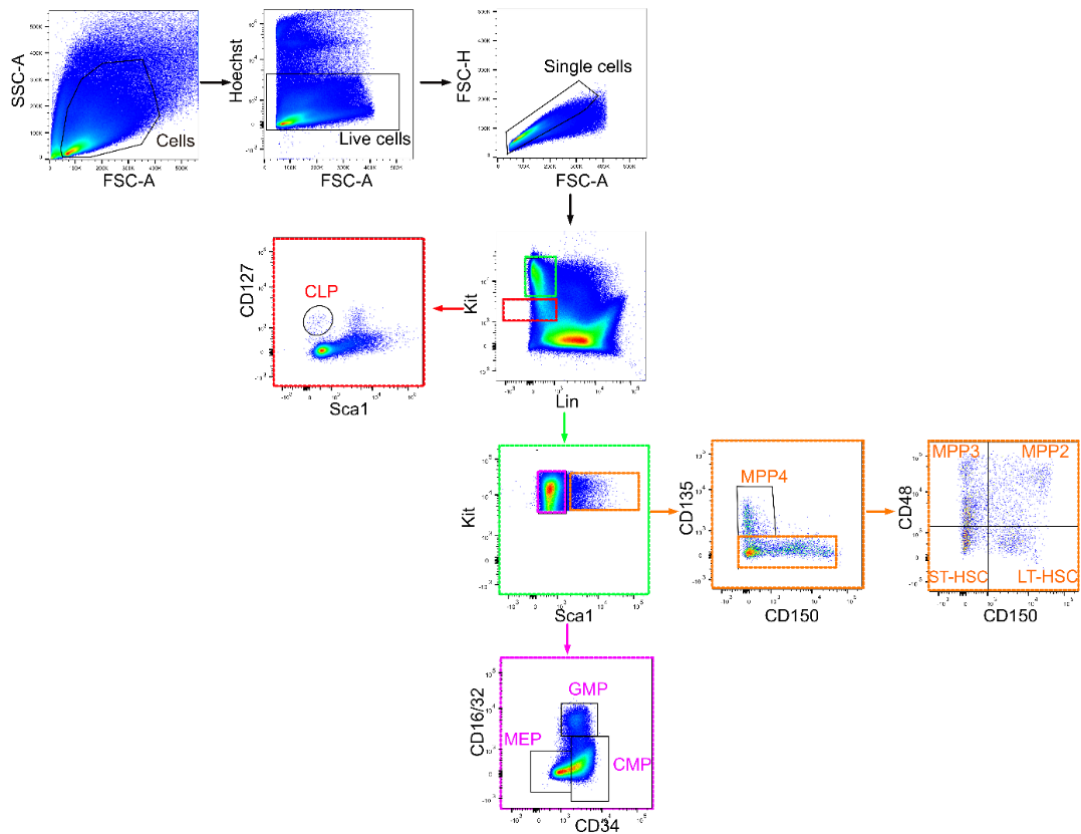
**Figure 4. Gating strategy for quantification of HSC and progenitors in the FL**
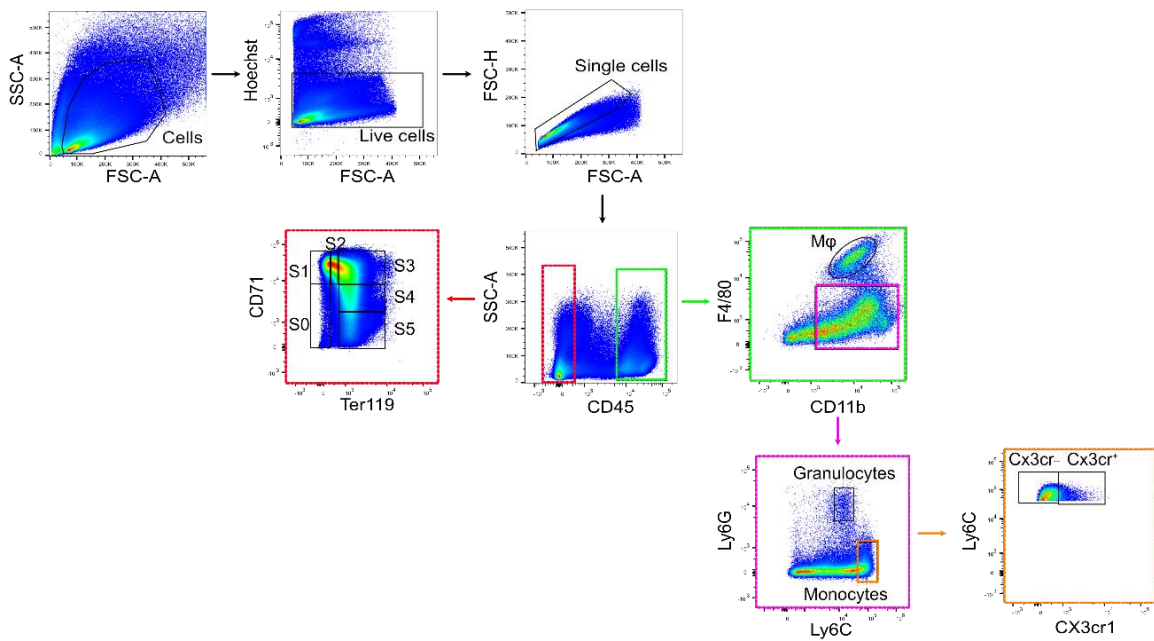


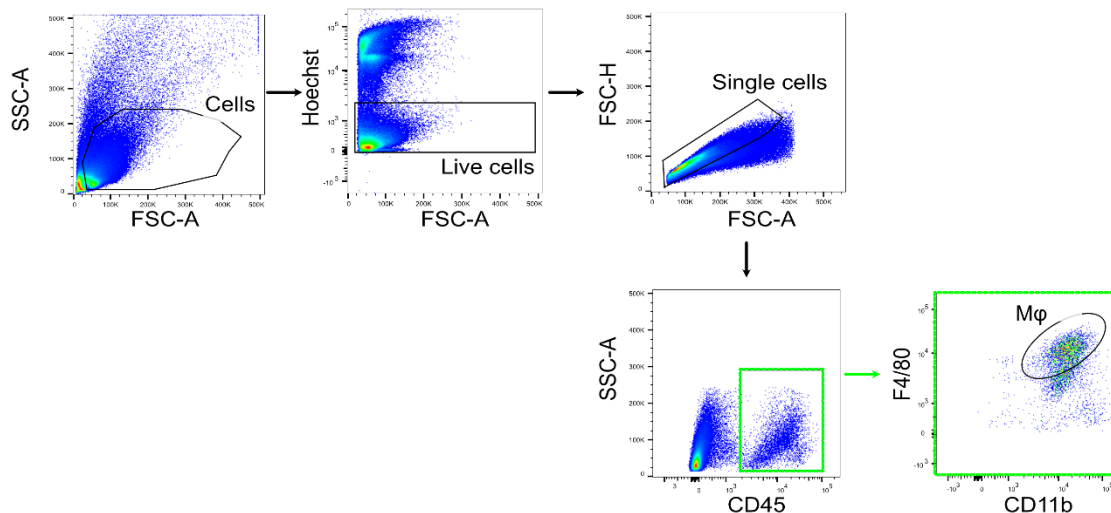**Figure 5. Gating strategy for quantification of myeloid cells in the FL**

**Figure 6. Gating strategy for quantification of Mφ in the fetal brain and lung**

### 3.4.3. Analysis of flow-cytometry data for heterogeneity of Mφ

The CD11b$^+$ F4/80$^+$ cells were gated (see Figure 7) and downsampled using downsample plug-in (v.3.3.1) in Flowjo. The downsampled population was imported and analyzed in R (https://www.r-project.org/ v. 4.0.5). The importing and processing of data was done using the CATALYST package (v. 1.18.1) (Crowell H 2022), which was installed through the Bioconductor package (v 3.14). The visualization of data was done using the UMAP algorithm (McInnes, Healy et al. 2018), and the clustering of data was done using FlowSOM (Van Gassen, Callebaut et al. 2015) clustering and ConsensusClusterPlus metaclustering (Wilkerson and Hayes 2010). CATALYST package uses a simple wrapper to combine the FlowSOM and ConsensusClusterPlus clustering. Using FlowSOM, the wrapper first performs high-resolution clustering and later on using ConsensusClusterPlus metaclustering a lower resolution of clustering using the previous clusters are provided. In the first step of the wrapper, the data is initially clustered into the multiplication of two dimensions: Xdim x Ydim, which would provide n groups. In the second step, the wrapper will metacluster populations into a minimum of 2 through a maximum of k clusters. The resulted clusters were manually inspected for expression of different markers and clusters of interests were subset and merged if necessary to form final clusters that would represent the Mφ and their heterogeneity. The YFP signal in fate-mapping sample was inspected using the same method in final clusters.
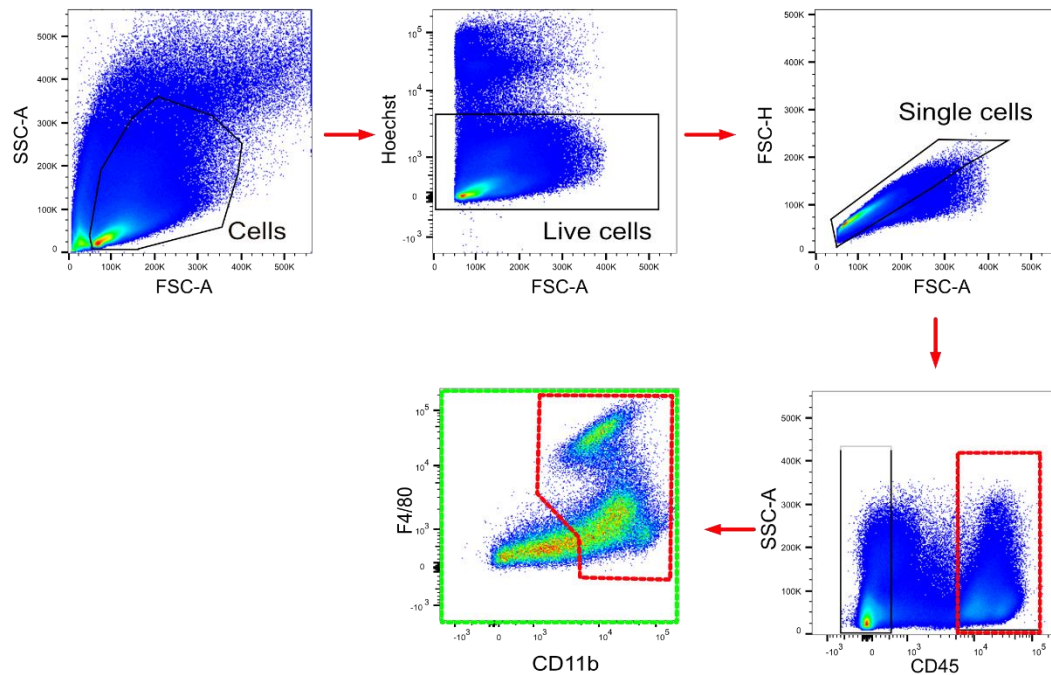
**Figure 7. Gating strategy for down-sampling of data for flow-cytometry analysis**

## 3.5. Bulk RNA sequencing

### 3.5.1. Cell isolation and sorting

Pregnant mice were sacrificed through cervical dislocation at E14.5 and the FL were harvested from the embryos. They were treated with a 300µL digestive enzyme mix containing 0.1% DNase, 0.1% collagenase and 3% fetal bovine serum (FBS) in PBS buffer in one well, incubating for 15-20 min at 37°C. The samples were homogenized through several pipetting and were transferred to a well of 6 well plate that contains 3 ml of FACS buffer via a 100µm strainer. If necessary, the tissues were mechanically disturbed using a plunger. The filtered cell suspensions were transferred into the FACS tubes and centrifuged at 400 g for 5 min at 4 °C. The supernatants were removed, and the pellets were resuspended in 50µL blocking solution (2% rat serum) for 10 min incubation on ice.

100µL of the antibody mix (Table 5. List of antibodies for sorting HSC from the FL was directly added, and they were incubated for 25-30 min on ice. Afterward, the samples were washed by adding 100µL FACS to the suspension and centrifuge at 400 g for 5 min at 4 °C. At the end of incubation, the samples were washed by adding 100µL FACS to the suspension and centrifuge at 400 g for 5 min at 4 °C.

Finally, the pellets were resuspended cells in 100µL FACS buffer. The cells were stained with dapi as live/dead staining in a final dilution 1:10000 before flow-cytometry analysis using

BD FACS ARIA III™. ~700-1200 The HSC were sorted according to the gating strategy into eppi tubes containing 500µL of Qiazol lysis buffer.
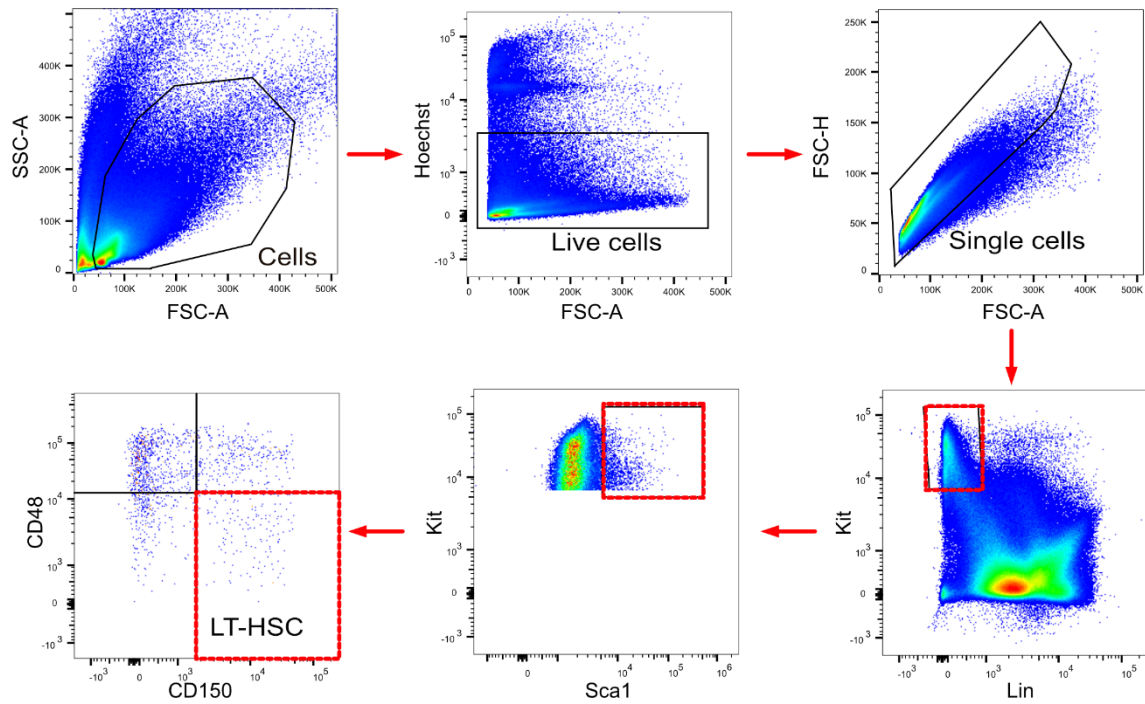


**Figure 8. Gating strategy for sorting of LT-HSC from the FL.**

### 3.5.2. Library preparation and sequencing

Total RNA was extracted using the miRNeasy micro kit (Qiagen) and quantified via RNA assay on a tape station 4200 system (Agilent). 5ng total RNA was used as an input for library generation via SmartSeq 2 (SS2) RNA library production protocol as Picelli, Faridani et al. (2014) described. Pre-amplification PCR was performed with 16 cycles for samples. Libraries were quantified using the Qubit HS dsDNA assay (Invitrogen), and fragment size distribution was analyzed via D1000 assay on a tapestation 4200 system (Agilent).

SS2 libraries sequenced single-end with 75 cycles on a NextSeq2000 system using P3 chemistry (Illumina). Samples were demultiplexed and fastq files generated using bcl2fastq2 v2.20 before alignment and quantification using Kallisto v0.44.0 based on the Gencode (mm10, GRCm38) vM16 (Ensembl 91) reference genomes.

### 3.5.3. Bulk-RNA quantification and analysis

Sequencing results from the experiments were pseudoaligned using the Kallisto tool set. The counts were imported into R and analyzed using the DEseq2 package (Love, Huber et al. 2014). The counts were transformed using the variance Stabilizing Transformation (VST) function of the DEseq2 pipeline. The KO samples were compared to the Ctrl during the analysis, and genes were ranked on the differential expression. The ranked gene list was used for Gene Set Enrichment Analysis (GSEA) using the clusterProfiler package (Yu, Wang et al. 2012).

## 3.6.  Single-cell RNA sequencing

### 3.6.1. Cell isolation and sorting

Pregnant mice were sacrificed through cervical dislocation at E14.5, and the FLs were harvested from the embryos. They were treated with a 300µL digestive enzyme mix containing 0.1% DNase, 0.1% collagenase and 3% fetal bovine serum (FBS) in PBS buffer in one well, incubating for 15-20 min at 37°C. The samples were homogenized through several pipetting and were transferred to a well of 6 well plate that contains 3 ml of FACS buffer via a 100µm strainer. If necessary, the tissues were mechanically disturbed using a plunger. The filtered cell suspensions were transferred into the FACS tubes and centrifuged at 400 g for 5 min at 4 °C. The supernatants were removed, and the pellets were resuspended in 50µL blocking solution (2% rat serum) for 10 min incubation on ice.

100µL of the antibody mix (Table 4) was directly added, and they were incubated for 25-30 min on ice. Afterward, the samples were washed by adding 100µL FACS to the suspension and centrifuge at 400 g for 5 min at 4 °C. At the end of incubation, the samples were washed by adding 100µL FACS to the suspension and centrifuge at 400 g for 5 min at 4 °C.

Finally, the pellets were resuspended cells in 100µL FACS buffer. The cells were stained with dapi as live/dead staining in a final dilution 1:10000 before flow-cytometry analysis using BD FACS ARIA III[TM]. The CD11b^{+} F/80^{+} cells were sorted according to the gating strategy (Figure 9) into eppi tubes containing 100µL of FACS buffer. The cells were used for loading the arrays in the next steps for Single-cell RNA sequencing.
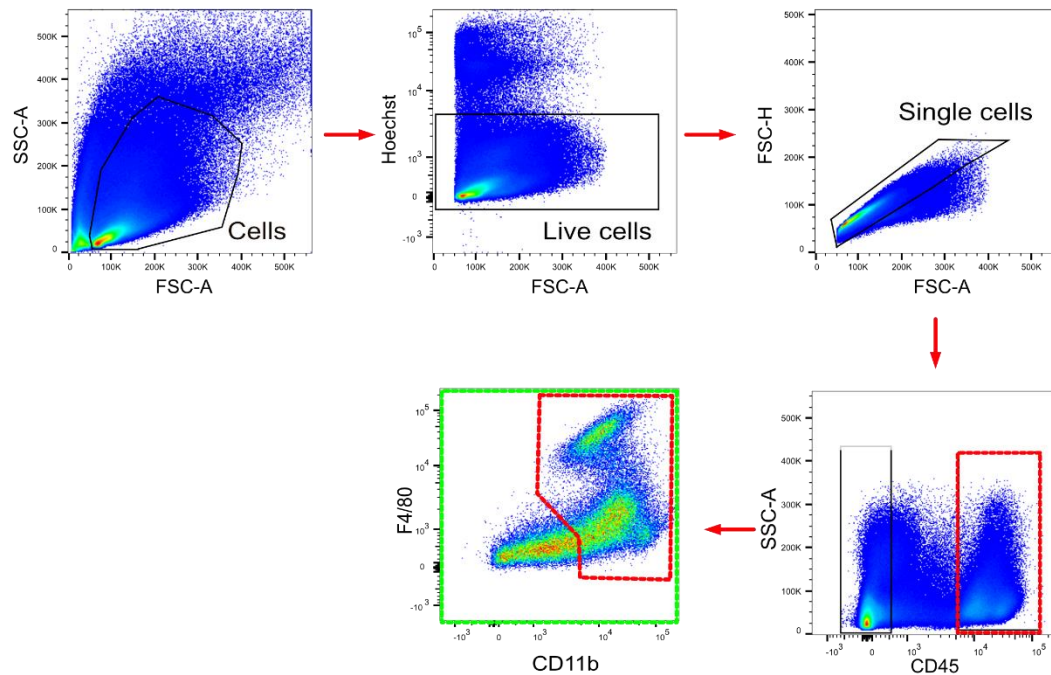
**Figure 9. Gating strategy for sorting Mφ from the FL**

### 3.6.2. Preparation of Seq-Well arrays

Seq-Well arrays were prepared as described by Gierahn et al. (Gierahn, Wadsworth et al. 2017). Briefly, Sylgard base and crosslinker were mixed at a 10:1 ratio for 10 minutes to produce a PDMS master mix and placed under vacuum for 15 to 30 minutes to remove air bubbles. Next, the PDMS was poured into a master mold and incubated for 2h at 70°C. The arrays were then removed from the molds, cleaned and functionalized. The functionalization process adds chemical moieties to the surface of the arrays, which facilitate their sealing with a semi-permeable polycarbonate membrane and the interchange of lysis and RNA hybridization buffers. First, the arrays were rinsed with 100% absolute EtOH, dried at room temperature, plasma treated for 7 min and successively submerged in APTES (0.05% APTES in 95% EtOH), acetone and PDITC buffers (0.2% PDITC, 10% pyridine, 90% DMF). Upon further washes with acetone, the arrays were spun and dried at 70°C for 2h. The arrays were then incubated at room temperature for 20 min followed by incubation with 0.2% chitosan solution (pH=6.3) at 37°C for 1.5 h. After chitosan incubation, the arrays were incubated overnight in PGA buffer (20 µg/mL polyglutamic acid, 2 M NaCl, 100 mM sodium carbonate (pH=10)) at room temperature under vacuum pressure. Finally, the arrays were removed from the vacuum and were rotated for 3 h at room temperature and subsequently stored at 4°C for at least 24 h before use.

### 3.6.3. Preparation of Seq-Well libraries

Seq-Well libraries were generated as described by Gierahn et al and Hughes et .al (Gierahn, Wadsworth et al. 2017, Hughes, Wadsworth et al. 2020). Briefly, the PGA buffer was replaced with Bead Loading Buffer (BLB: 100 mM Sodium Carbonate with 10% BSA), air bubbles were removed from the wells under vacuum, and 110,000 barcoded mRNA-capture beads were loaded. Afterwards, the BLB buffer was replaced with an RPMI 1640 media containing 10% FCS (RPMI-10) and it was incubated for 10 mins. The RPMI-10 media was aspirated, and 30,000 CD11b$^+$ F4/80$^+$ cells in RPMI-10 were loaded. After cell loading, the arrays were briefly rocked for 10 min in the XYZ plane to help distribute the cells loaded. The loaded arrays with beads and cells were washed five times with PBS. After washing with PBS, the arrays were soaked with RPMI 1640 medium without FCS and sealed using polycarbonate membranes treated with air plasma under mild vacuum (Diener electronic) for 7 min. Afterward, the sealed arrays were placed in Agilent clamps and incubated at 37°C for 30 min in a cell culture incubator. After the incubation, the arrays were removed from the clamps and incubated in 5 mL of pre-lysis buffer (5M guanidine thiocyanate, 1mM EDTA) until the top glass slide was loosened and removed. The pre-lysis buffer was aspirated, and the arrays were covered with 5 mL complete lysis buffer (5M guanidine thiocyanate, 1mM EDTA, 0.5% Sarkosyl and 1% β-mercaptoethanol in H$_2$O) for 20 min on the rotator. After the 20 min of cell lysis, the lysis buffer was aspirated, and the arrays were covered with 5 mL hybridization buffer (2M NaCl, 3mM MgCl$_2$ and 0.5% Tween-20 in PBS) and rotated on ice in the XYZ plane for 40 min followed by 3 min of washing with the wash buffer. Next, the mRNA capture beads were washed from the arrays and collected using the wash buffer (2M NaCl, 3mM MgCl2 and 20mM Tris-HCl pH 8.0 in H$_2$O) into 1.5 mL eppendorf tubes using a combination of bead removal method 1 (Hughes, Wadsworth et al. 2020) and the Lifter slip method (Gierahn, Wadsworth et al. 2017). The beads are spun down at 2000xg to aspirate the wash buffer and then washed once with 1X Maxima RT Buffer at 2000xg for 1 min. The mRNAs on the beads are then reverse-transcribed on the pellet using 200μl Maxima Reverse Transcriptase reaction mix (5X Maxima RT buffer, 4% Ficoll PM-400, 1mM dNTPs, 1U/μL RNase inhibitor, 2.5 μM template switch oligonucleotide (TSO) primer and 10U/μL Maxima Reverse Transcriptase in H$_2$O) for 30 min at room temperature with end-over-end rotation followed by 90 min incubation at 52°C with end-over-end rotation. The reaction was stopped by washing the beads with TE buffer (10mM Tris-HCl pH 8.0 and 1mM EDTA in H$_2$O) supplemented with 0.01% Tween-20 (TE-TW) and TE buffer supplemented with 0.5% SDS (TE-SDS). After a washing step in 10mM Tris-HCl pH 8.0, excess primers were digested in an exonuclease reaction (ExoI buffer and 1U/μL ExoI in H2O) for 50 min at 37°C with end-over-end rotation and washed in TE-TW and TE-SDS. A second strand synthesis was performed on the exonuclease treated libraries by first aspirating the TE-

TW buffer and resuspending the libraries in freshly prepared 500 µL 0.1 M NaOH. This was then rotated end-over-end for 5 min at room temperature spun down at 800xg for 1 min to remove the supernatant. The bead pellets were washed once with 500 µL TE-TW followed by a wash in 500 µL 1X TE buffer with each wash followed by centrifugation at 800xg for 1 min. After the 1X TE wash, the pellet was resuspended in 200 µL of second strand synthesis mix (Maxima RT buffer, 30% PEG8000, 10mM dNTPs, 1mM dN-SMRT oligo, Klenow Exo$^-$ Enzyme) for 1 hour at room temperature with end-over-end rotation. The reaction was stopped by washing the beads twice with 500 µL TE-TW buffer, once with 500 µL TE buffer, once with 500 µL water and finally left in 500 µL water. Resuspended beads in water were counted with a Fuchs-Rosenthal cytometer in a bead counting solution (10% PEG, 2.5 M NaCl). Pools of 3,000 beads in10µl were then added to 40µl PCR reaction master mix (2X KAPA HiFi Hotstart Readymix and 25 µM SMART PCR/IS PCR primer in $H_2O$) for the amplification of reverse-transcribed cDNA libraries (95°C for 3 min, 4 cycles of 98°C for 20 s, 65°C for 45 s, 72°C for 3 min, 12 cycles of 98°C for 20 s, 67°C for 20 s, 72°C for 3 min and final extension of 72°C for 5 min). After PCR, 18,000-24,000 beads (ranging from 6 to 8 PCR reaction tubes) were combined (hereafter referred to as 'pools') and processed. The pools were cleaned with 0.6x volumetric ratio AMPure XP beads (5 min incubation with beads at room temperature, followed by 5 min on the magnet, two washes with 80% EtOH, 3 min dry-out, elution with 100µl $H_2O$ off magnet for 5 min, followed by 2 min on the magnet for collection of the eluent), followed by a 1.0X volumetric ratio AMPure XP beads (5 min incubation with beads at room temperature, followed by 5 min on the magnet, two washes with 80% EtOH, 3 min dry-out, elution with 22µl $H_2O$ off magnet for 5 min, followed by 2 min on the magnet for collection of the eluent). The library integrity and quantification were assessed using a High Sensitivity D5000 assay for the Tapestation 4200 (Agilent).

### 3.6.4. Loading of in-house Tn5

Tn5 kindly produced and provided by Mathias Geyer and colleagues were loaded with linker oligonucleotides. Briefly, single-stranded oligonucleotides were mixed in a 1:1 ratio. For pre-annealing, 2µl of the oligonucleotide solution was mixed with 8µl of $H_2O$ and incubated in a thermocycler (95°C for 3 min, 70°C for 3 min and 45 cycles of temperature reduction (-1°C per 30 s)). The annealed oligonucleotides (0.25 vol.) were added to 0.1 vol. Tn5 solution and supplemented with 0.4 vol. glycerol (100%), 0.12 vol. dialysis buffer and 0.13 vol. $H_2O$. After incubation for 60 min at room temperature, the loaded Tn5 protein was stored at -20°C.

### 3.6.5. Tagmentation

The cDNA libraries (1 ng) were tagmented with home-made single-loaded Tn5 transposase in TAPS-DMF buffer (50mM TAPS-NaOH (pH 8.5), 25mM MgCl2, 50% DMF in H2O) for 10 min at 55°C and the tagmented products were cleaned with the MinElute PCR kit following the manufacturer's instructions. Finally, a master mix was prepared (2X NEBNext High Fidelity PCR Master Mix, 10 µM barcoded index primer, 10 µM P5-SMART-PCR primer) and added to the samples to attach the Illumina indices to the tagmented products in a PCR reaction (72°C for 5 min, 98°C for 30 s, 15 cycles of 98°C for 10 s, 63°C for 30 s, 72°C for 1 min). The pools were cleaned with 0.6 x volumetric ratio AMPure XP beads. The final library quality was assessed using a High Sensitivity DNA5000 assay on a Tapestation 4200 (Agilent), and quantified using the Qubit high-sensitivity dsDNA assay.

### 3.6.6. Sequencing of Libraries

Seq-Well libraries were equimolarly pooled and clustered at 1.4pM concentration with 10% PhiX using High Output v2.5 chemistry on a NextSeq500 system. Sequencing was performed paired-end using custom Drop-Seq Read 1 primer for 21 cycles, 8 cycles for the i7 index and 61 cycles for Read 2. Single-cell data were demultiplexed using bcl2fastq2 (v2.20).

### 3.6.7. Processing of scRNA-seq raw data

Fastq files from Seq-Well were loaded into a snakemake-based data pre-processing pipeline (version 0.31, available at https://github.com/Hoohm/dropSeqPipe) that relies on the Drop-seq tools provided by the McCarroll lab (Macosko, Basu et al. 2015). STAR alignment within the pipeline was performed using the murine GENCODE reference genome and transcriptome mm10 release vM16 (Team 2014).

## 3.7. Analysis of single-cell RNA sequencing

### 3.7.1. Clustering analysis

The Single-cell RNA was analyzed using scanpy package (v.1.8.1) (Wolf, Angerer et al. 2018) in python (v.3.4.1) (Van Rossum and Drake Jr 1995). The cells were pre-processed and filtered by checking for cells that express less than 200 genes and genes that are expressed in less than three cells. After the filtration, cells were processed further and clustered using the Leiden algorithm (Traag, Waltman et al. 2019). The clusters were investigated using their differentially expressed genes (DEG). The DEG lists were identified using Wilcoxon-Signed-Rank Test (Rey and Neuhäuser 2011) by comparing each cluster to the rest of the clusters. Furthermore, different marker lists were overlaid on the clusters in order to identify different cell types and exclude the ones that are not Mφ through subsetting the clusters of interests. The subset clusters were analyzed and processed again and the DEG for the final clustering were extracted using the same statistical method.

### 3.7.2. Psuedotime analysis

A psuedotime analysis using the Partition-based graph abstraction (PAGA) method (Wolf, Hamey et al. 2019) was performed to analyze the trajectory of these groups. The PAGA algorithm reconstructs the lineage relations of a whole adult animal (Plass, Solana et al. 2018) mainly due to its data-driven formulation. It also has been shown that the manifold learning algorithms in PAGA can converge faster. They produce faithful embeddings to the global topology of high-dimensional data, making it a suitable option for deriving interpretable abstractions of the noisy k-nearest neighbors (K-NN)-like graphs used to represent the manifolds within single-cell data. PAGA represents the data as a neighborhood graph of a group of single cells within the formulation of (G)raph= (V, E), where V is each node within the graph and corresponds to a cluster and E is each edge representing each edge a neighborhood relation between the clusters. The edges in the PAGA representation are weighted edges, representing a statistical measure of connectivity between the clusters. The width of each edge visualizes this; edges with more width indicate stronger relations and the other way around.

### 3.7.3. Correlation matrix

In order to make a correlation between the single cell RNA-seq data and the flow-cytometry data, the clusters of interest from both of the datasets were extracted. The expression values of mutual markers between them were kept and normalized for each of the two datasets. The correlation between the two datasets was calculated using spearman's rank correlation coefficient and results were visualized using pretty heatmap package (Kolde and Kolde 2015) in R.

### 3.7.4. Data Integration

The human FL Single-cell RNA-seq data was retrieved from the previous study (Popescu, Botting et al. 2019) and was loaded into scanpy. The human dataset clusters were subset, and only three clusters, Kupffer cell cluster, Mono-Mac cluster, and EI VCAM+ cluster, were selected. These human clusters were integrated and merged with the final clusters from the mouse dataset using BBKNN (batch balanced k nearest neighbors) (Polanski, Young et al. 2020). This is a fast and straightforward method for batch alignment that performs batch correction at the neighborhood graph inference step. Identifying a neighborhood graph is a common step in single-cell analysis that is usually done by identifying each cell's k nearest neighbors in a principal component space. After the data integration, using the ingest function in the scanpy package, the embeddings and annotations of a selected query dataset is overlaid on a reference dataset. This is done by projecting on the query dataset PCA or UMAP fitted on the reference dataset. Using this method, the human dataset was selected as a query, and the six clusters from the mouse data were selected as the reference. This would allow finding the human cells with the most correspondence to identified Mφ populations in the mouse.

# 4. Results

## 4.1. Mφ regulate hematopoiesis during embryogenesis in the fetal liver

### 4.1.1. Development of transgenic mouse models targeting fetal liver Mφ

In order to study the effect of Mφ on hematopoiesis during embryogenesis, two genetic mouse models were investigated. The first mouse model was the Pu.1 model that consists of *Tnfrsf11a$^{Cre}$; Pu.1$^{flox/flox}$* and *Cre-negative Pu.1$^{flox/flox}$* and *Pu.1$^{flox/+}$* littermate controls (hereafter referred to as Pu.1$^{KO}$ and Pu.1$^{Ctrl}$). Pu.1 is a crucial transcription factor for the development of Mφ. Therefore, the hypothesis was that this model would lead to the depletion of all Mφ across all tissues since Tnfrsf11a is expressed in all pMacs, thereby targeting all fetal macrophages (Mass, Ballesteros et al. 2016). The lack of Mφ in the early postnatal white adipose tissue could be confirmed previously (Cox, Crozet et al. 2021); however, a characterization of fetal tissues is lacking so far. The second mouse was the Id1/Id3 model comprises *Tnfrsf11a$^{Cre}$; Id1$^{flox/flox}$; Id3$^{flox/flox}$* and *Cre-negative Id1$^{flox/flox}$; Id3$^{flox/flox}$* littermate controls (hereafter referred to as Id1/Id3$^{KO}$ and Id1/Id3$^{Ctrl}$). Id1 and Id3 are two transcriptional regulators expressed specifically in Kupffer cells (KCs) early during embryogenesis (Mass, Ballesteros et al. 2016). Depletion of Id3 led to a severe reduction, around 3-fold, of KCs at embryonic day (E)14.5, indicating that Id proteins play an essential role in KC development (Mass, Ballesteros et al. 2016). Thus, targeting Id1 and Id3 should lead to a specific reduction or depletion of KCs in the fetal liver.

For both models, three fetal organs belonging the knock-out (KO) and control (Ctrl) embryos were harvested at three embryonic time points: E14.5, E16.5, and E18.5. These organs are the FL, the brain, and the lung. The FL is the main organ of interest studied for the possible changes in hematopoiesis upon depletion of Mφ. The two other organs were studied to analyze the precision of Mφ depletion in other tissues other than FL.

Flow cytometry analysis showed that Mφ were depleted in all three organs in the Pu.1[KO] embryos at E14.5 (Figure 10 A-C, see Figure 5 for gating strategy). The depletion targeted the majority of Mφs, and their population was reduced approximately by 90% compared to the control embryos. Interestingly, Mφ repopulated the FL at later time points (E16.5 and 18.5). At the same time, the same re-population could not be seen in the lung or the brain.
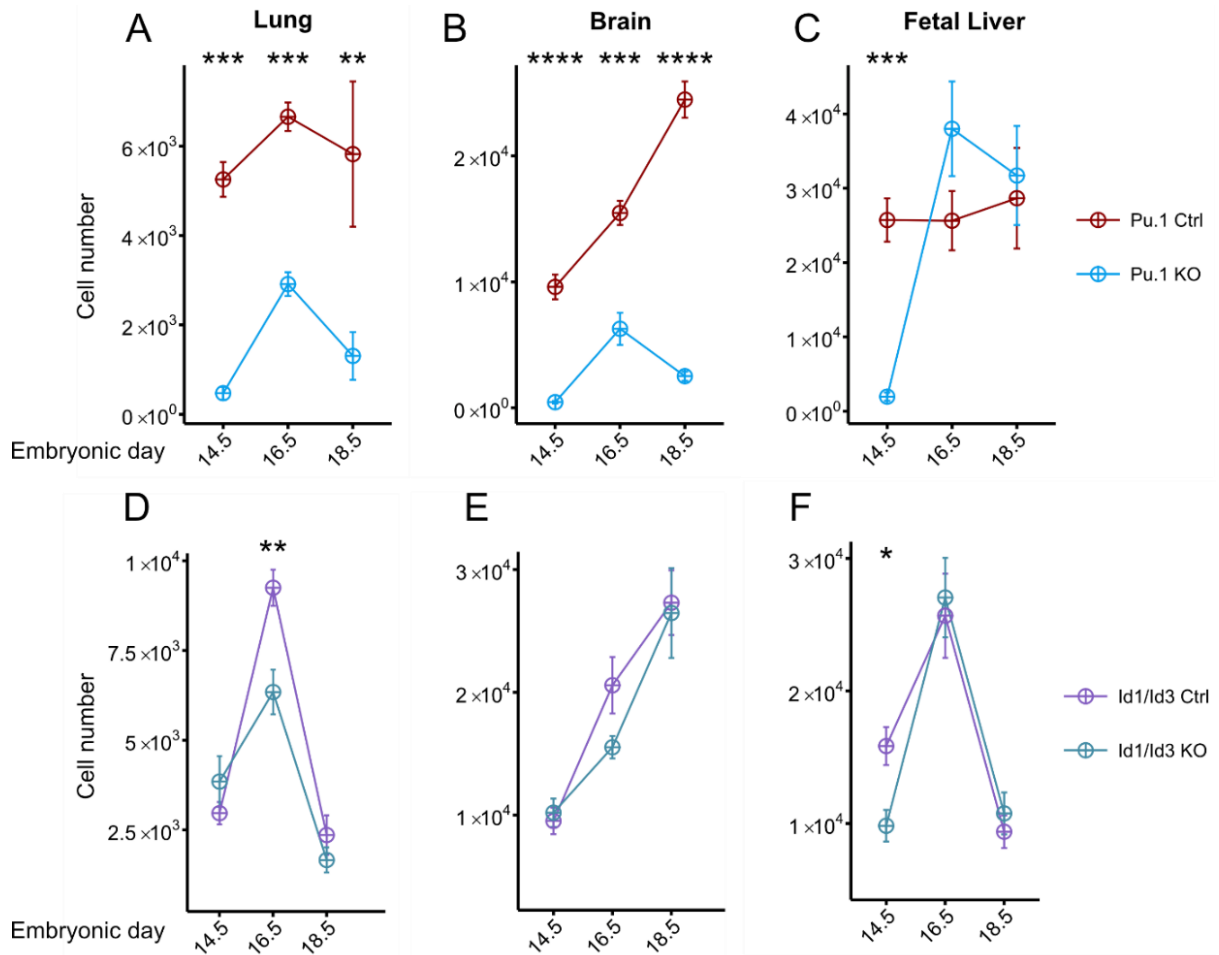


**Figure 10. Flow cytometry analysis of Mφ at different time points during embryogenesis in Pu.1 and Id1/Id3 models.**

**A.** Mφ quantification in the fetal lung in Pu.1 embryos. n= 5 KO, 11 Ctrl at E14.5, 5 KO, 11 Ctrl at E16.5, and 8 KO, 13 Ctrl at E18.5 **B.** Mφ quantification in the fetal brain of Pu.1 embryos. n= KO 6, 15 Ctrl at E14.5, 5 KO, 11 Ctrl at E16.5, and 8 KO, 13 Ctrl at E18.5 **C.** Mφ quantification in the fetal liver in Pu.1 embryos. n= 5 KO, 11 Ctrl at E14.5, 5 KO, 11 Ctrl at E16.5, and 8 KO, 13 Ctrl at E18.5 **D.** Mφ quantification in the fetal lung in Id1/Id3 embryos. n= 8 KO, 17 Ctrl at E14.5, 7 KO, 7 Ctrl at E16.5, and 6 KO, 7 Ctrl at E18.5 **E.** Mφ quantification in the fetal brain of Id1/Id3 embryos. n= 9 KO, 19 Ctrl at E14.5, 7 KO, 7 Ctrl at E16.5, and 6 KO, 7 Ctrl at E18.5 **F.** Mφ quantification in the fetal liver in Id1/Id3 embryos. n= 9 KO, 18 Ctrl at E14.5, 7 KO, 7 Ctrl at E16.5, and 6 KO, 7 Ctrl at E18.5. Data are presented as mean ± SEM. ****$P<0.0001$, ***$P<<0.001$, **$P<0.01$, and *$P<0.05$

For the Id1/Id3 model, at E14.5, the depletion of Mφ was observed in the FL. On the one hand, unlike the Pu.1 model that could deplete around 90% of the Mφ, in the Id1/Id3 model, around 25% of the Mφ were targeted. On the other hand, similar to the Pu.1 model, the Mφ were repopulated at E16.5 and E18.5. The brain and lung analyses show that the Mφ number was not changing among the Id1/Id3[KO] and Id1/Id3[Ctrl] embryos, except in the lung at E16.5. At this specific time point, the Mφ in the Id1/Id3[KO] embryos tend to decrease compared to the Id1/Id3[Ctrl] (Figure 10D-F).

Immunofluorescence staining of FL cryosections at E14.5 using an anti-F4/80 antibody could confirm the depletion of Mφ using imaging. Figure 11 shows representative images from the staining. Figure 11A and B show Ctrl and KO FL sections of the Pu.1 model, and in accordance with flow cytometry results, Mφ are almost entirely depleted in the Pu.1[KO]. In a previous study performed by a bachelor student in the lab, the quantification of the macrophages in the immunofluorescence sections showed a statistically significant decrease in the Mφ number between Pu.1[Ctrl] and Pu.1[KO] (Heider 2021).
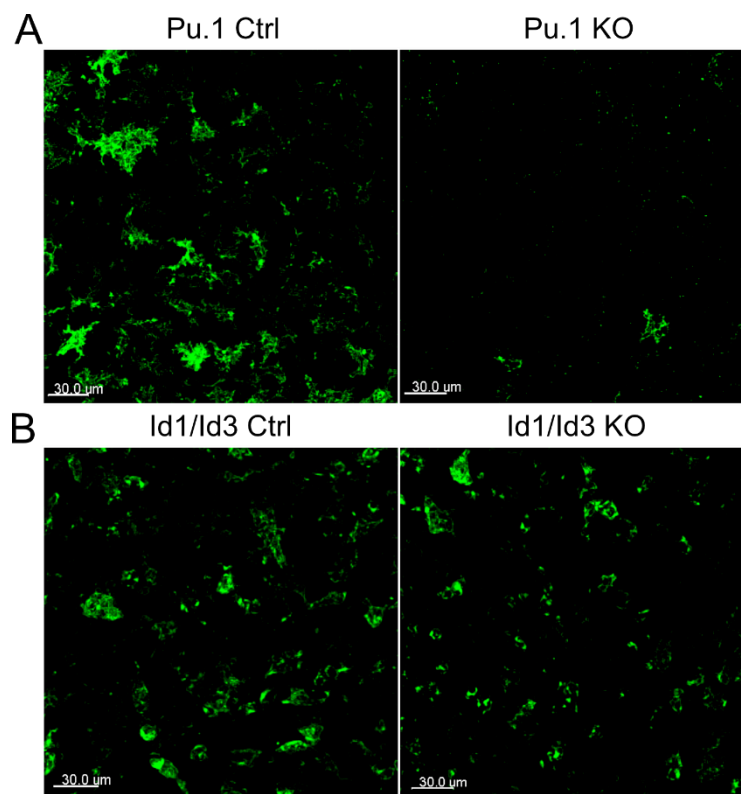


**Figure 11.** The immunofluorescence staining of Mφ on FL cryosections.

**A.** F4/80 staining of Pu.1[Ctrl] FL. **B.** F4/80 staining of Pu.1[KO] FL. **C.** F4/80 staining of Id1/Id3[Ctrl] FL. **D.** F4/80 staining of Id1/Id3[Ctrl] FL.

The depletion of Mϕ in the Id1/Id3 model could also be observed via immunofluorescent staining of Iba1$^+$F4/80$^+$ cells. However, as expected from the flow cytometry results, this depletion was not complete, as shown for the Pu.1 model. The quantification of the Mϕ in a previous study (Heider 2021) showed a 50% decrease in the number upon comparing Id1/Id3$^{KO}$ to the Id1/Id3$^{Ctrl}$ sections (KO n=3, Ctrl n=3). F4/80$^+$ Mϕ were manually quantified in a specific region of interest (ROI) in that study. There was a statistically significant (p = 0.0119) decrease in Mϕ numbers between Pu.1$^{KO}$ and Pu.1$^{Ctrl}$ FLs. The Id1/Id3 did not show a statistically significant change between Id1/Id3$^{KO}$ and Id1/Id3$^{Ctrl}$. However, the Mϕ number decreased from an average of 21 Mϕ per ROI in the Id1/Id3$^{Ctrl}$ to 8 Mϕ/ROI in the Id1/Id3$^{KO}$ (KO n=3, Ctrl n=3).

## 4.1.2. Depletion of Mφ do not affect total cell number across the tissues

Considering the observed results, the subsequent analysis investigated whether Mφ depletion could affect the total cell number of organs or parent gate of a cell type. Hence, the total cell number of harvested organs was compared between the KO and Ctrl embryos. In addition, the cell number of the progenitor of these cells (here referred to as the parent cells) were also compared between the KO and Ctrl embryos. The parent cell numbers that were investigated are: CD45 positive cells (CD45$^+$), Lineage$^-$ (CD11b, NKp46, CD3, CD19, Gr1, Ter119, referred to as L$^-$), Lineage$^-$ Sca1$^+$ Kit$^+$ (LSK), and Lineage$^-$ Kit$^+$ Sca1$^-$ cells (L$^-$, K$^+$, S$^-$). The total cell analysis of the FL showed no significant change between the Pu.1$^{KO}$ and Pu.1$^{Ctrl}$ embryos. The number of cells was relatively stable at E14.5 and E18.5.
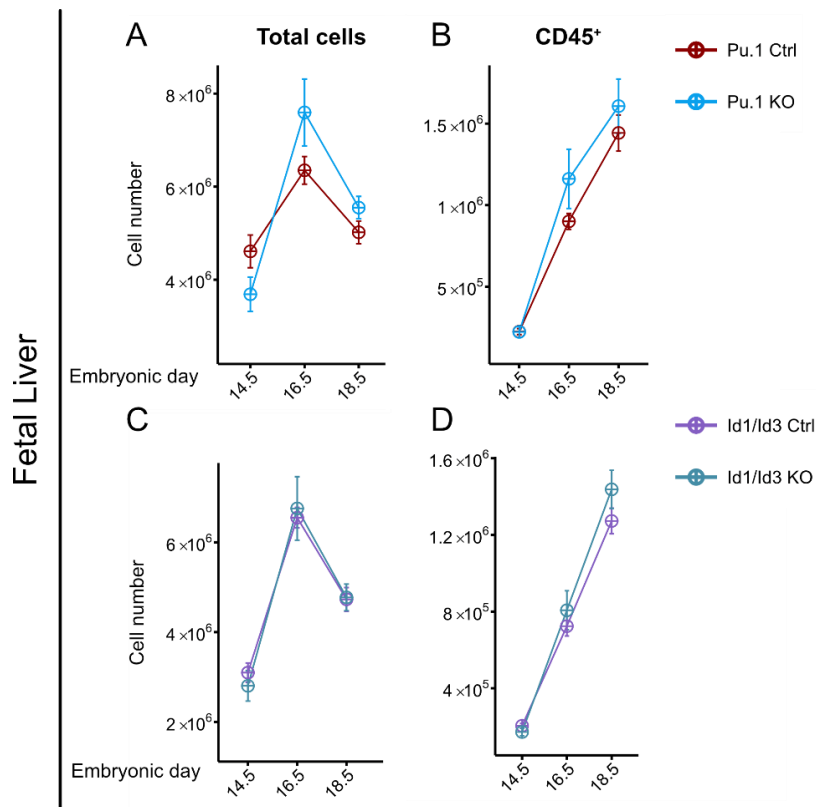


**Figure 12. Flow cytometry analysis of total cells and CD45$^+$ cell number at different time points in the FL during embryogenesis in Pu.1 and Id1/Id3 models.**

**A.** Total cell number in the FL in Pu.1 embryos. n= 5 KO, 11 Ctrl at E14.5, 5 KO, 11 Ctrl at E16.5, and 8 KO, 13 Ctrl at E18.5 **B.** The CD45+ cell number in the FL in Pu.1 embryos n= 5 KO, 11 Ctrl at E14.5, 5 KO, 11 Ctrl at E16.5, and 8 KO, 13 Ctrl at E18.5 **C.** Total cell number in the FL in Id1/Id3 embryos. n= 9 KO, 18 Ctrl at E14.5, 7 KO, 7 Ctrl at E16.5, and 6 KO, 7 Ctrl at E18.5.  **D.** Total CD45+ cell number in the FL in Id1/Id3 embryos. n= 9 KO, 18 Ctrl at E14.5, 7 KO, 7 Ctrl at E16.5, and 6 KO, 7 Ctrl at E18.5. Data are presented as mean ± SEM. ****P<0.0001, ***P<<0.001, **P<0.01, and *P<0.05

A similar result was observed for the Id1/Id3[KO] and Id1/Id3[Ctrl] embryos. The total cell number was not changing across the conditions (Figure 12C). The amount of CD45^{+} cells was not affected by the depletion of the Mφ. All of the Pu.1[KO] and Pu.1[Ctrl] and the Id1/Id3[KO] and Id1/Id3[Ctrl] embryos showed no change in the number CD45^{+} cells (Figure 12B and D).

In the next step, the total cell number of the brain was studied. The results showed no significant change between the KO and Ctrl embryos in both Pu.1 and Id1/Id3 mouse models for the total cell number (Figure 13A and C).
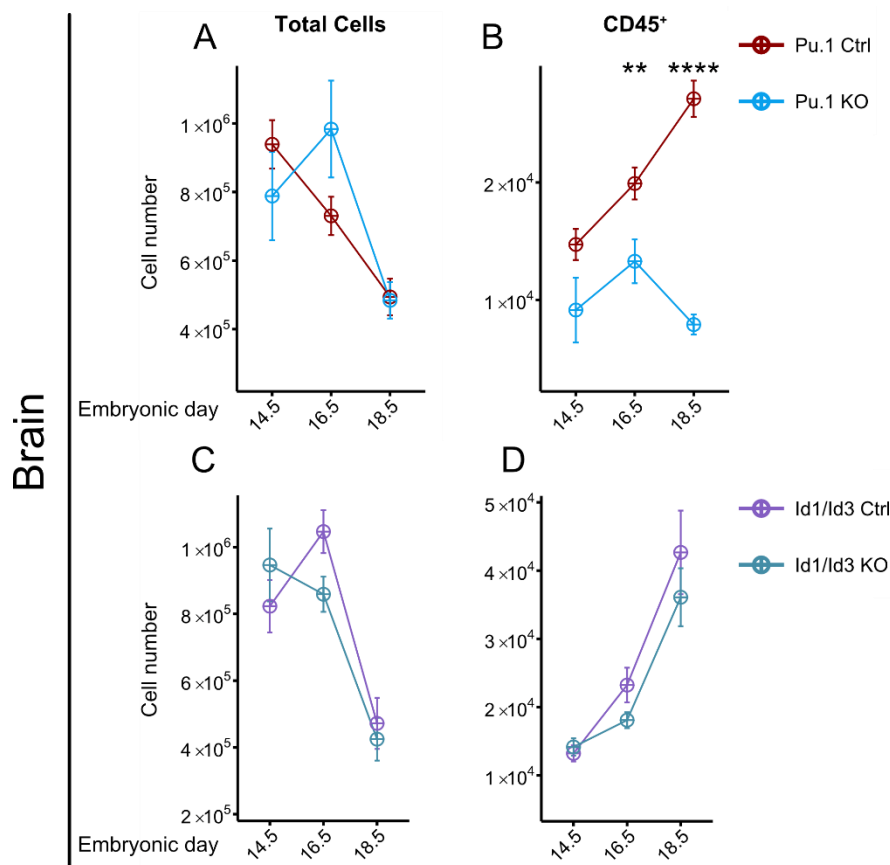


**Figure 13. Flow cytometry analysis of total cells and CD45^{+} cell number at different time points in the fetal brain during embryogenesis in Pu.1 and Id1/Id3 models.**

**A.** Total cell number in the fetal brain in Pu.1 embryos n= KO 6, 15 Ctrl at E14.5, 5 KO, 11 Ctrl at E16.5, and 8 KO, 13 Ctrl at E18.5 **B.** CD45+ cell number in the fetal brain in Pu.1 embryos. n= KO 6, 15 Ctrl at E14.5, 5 KO, 11 Ctrl at E16.5, and 8 KO, 13 Ctrl at E18.5 **C.** Total cell number in the fetal brain in Id1/Id3 embryos. n= 9 KO, 19 Ctrl at E14.5, 7 KO, 7 Ctrl at E16.5, and 6 KO, 7 Ctrl at E18.5 **D.** Total CD45+ cell number in the fetal brain in Id1/Id3 embryos. n= 9 KO, 19 Ctrl at E14.5, 7 KO, 7 Ctrl at E16.5, and 6 KO, 7 Ctrl at E18.5. Data are presented as mean ± SEM. ****$P<0.0001$, ***$P<<0.001$, **$P<0.01$, and *$P<0.05$

The number of total cells in the brain in both models was increased at E16.5, and then a sharp decrease was observed at E18.5. The flow cytometry data from the Pu.1 model showed that CD45^{+} cells started to decrease in Pu.1[KO] embryos at E16.5, and the number of CD45^{+} cells reached the lowest in Pu.1[KO] embryos, while in the Pu.1[Ctrl] embryos, the cell number constantly increased by the time (Figure 13B). Investigating the CD45^{+} cell number in Id1/Id3 mouse model showed no change in the Id1/Id3[KO] and Id1/Id3[Ctrl] embryos in contrast to the Pu.1 model (Figure 13D).

Similar to the brain, the total cell number of the lung was investigated. The results showed no significant change between the Pu.1[KO] and Pu.1[Ctrl] embryos. However, in the Id1/Id3 mouse models at E18.5, the Id1/Id3[KO] embryos had fewer cell numbers than the Id1/Id3[Ctrl] embryos (Figure 14A and C).
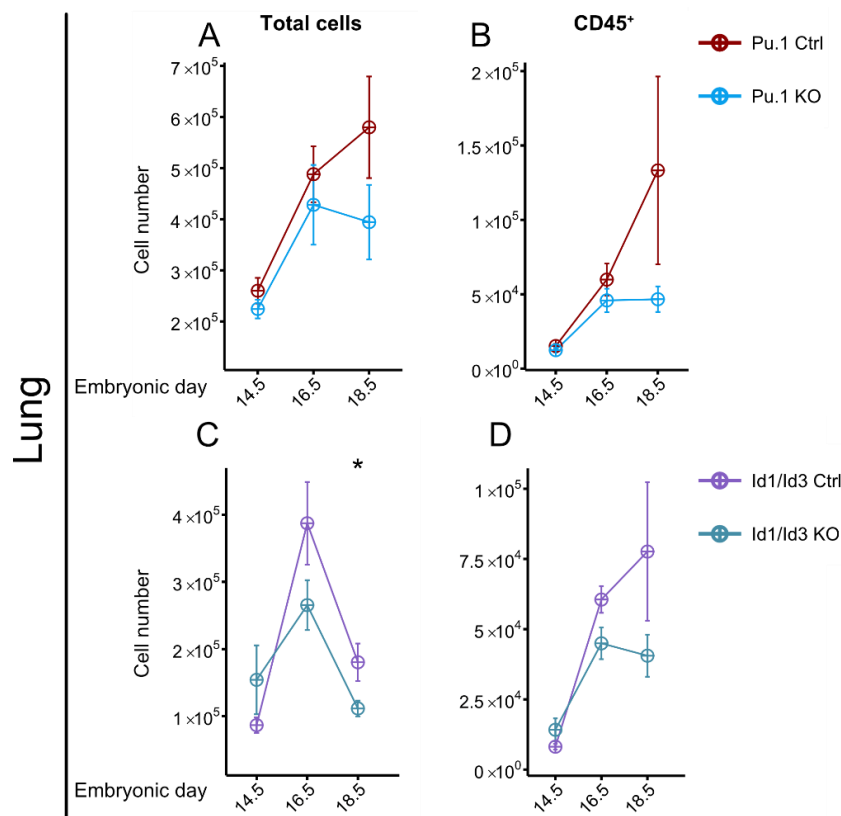


**Figure 14. Flow cytometry analysis of total cells and CD45^{+} cell number at different time points in the fetal brain during embryogenesis in Pu.1 and Id1/Id3 models.**

**A.** Total cell number in the fetal lung in Pu.1 embryos. n= 5 KO, 11 Ctrl at E14.5, 5 KO, 11 Ctrl at E16.5, and 8 KO, 13 Ctrl at E18.5 **B.** CD45+ cell number in the fetal lung in Pu.1 embryos. n= 5 KO, 11 Ctrl at E14.5, 5 KO, 11 Ctrl at E16.5, and 8 KO, 13 Ctrl at E18.5 **C.** Total cell number in the fetal lung in Id1/Id3 embryos n= 8 KO, 17 Ctrl at E14.5, 7 KO, 7 Ctrl at E16.5, and 6 KO, 7 Ctrl at E18.5 **D**. Total CD45+ cell number in fetal lung in Id1/Id3 embryos. n= 8 KO, 17 Ctrl at E14.5, 7 KO, 7 Ctrl at E16.5, and 6 KO, 7 Ctrl at E18.5. Data are presented as mean ± SEM. ****P<0.0001, ***P<<0.001, **P<0.01, and *P<0.05, Wilcoxon test.

The flow cytometry data from the Pu.1 and Id1/Id3 models showed that $CD45^+$ cells increase with time in both KO and Ctrl embryos. However, this increase stops at E18.5 for the KO embryos in both models (Figure 14B and D).

Studying the number of the cells in the $L^-$ $Kit^+$ $Sca1^-$ parent gate showed no changes at E14.5 and E16.5 for Pu.1 model. However, at E18.5, the $Pu.1^{KO}$ embryos displayed more cell numbers than the $Pu.1^{Ctrl}$ embryos (Figure 15A). Furthermore, analysis of the LSK cells revealed no significant changes at any time point comparing the two conditions in Pu.1 model (Figure 15B). In the Id1/Id3 model, analyzing the $L^-$ $Kit^+$ $Sca1^-$ and LSK parent gates showed no significant trend in cell numbers (Figure 15C and D).
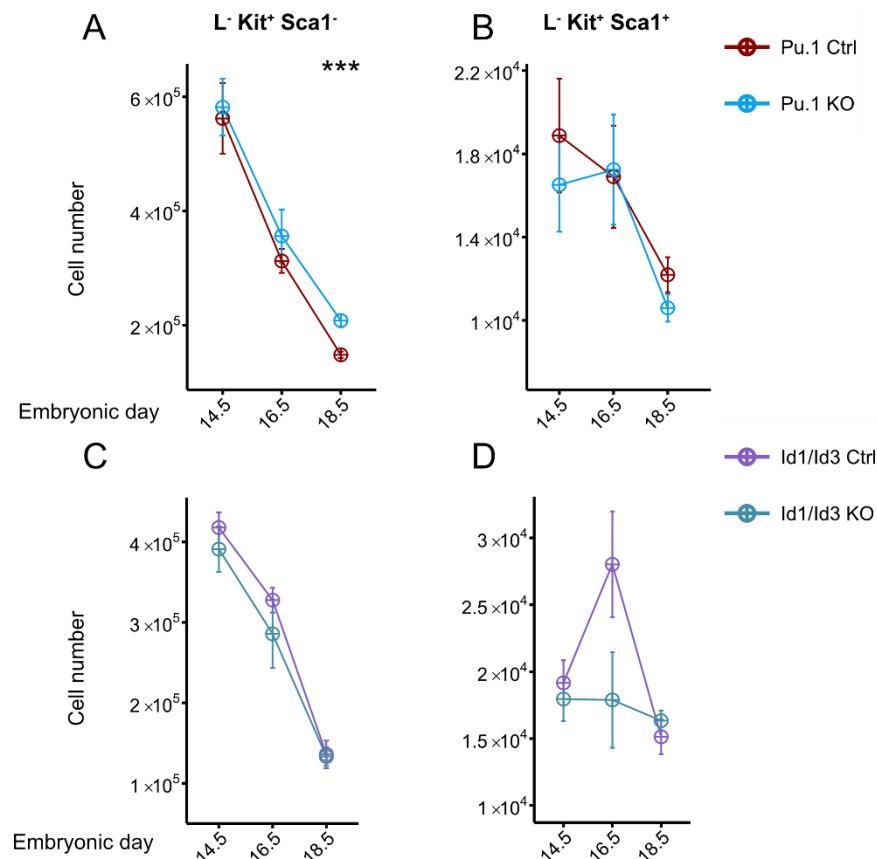


**Figure 15. Flow cytometry analysis of the different parent cell numbers at different time points in the FL during embryogenesis in Pu.1 and Id1/Id3 models.**

**A.** $L^-S^+K^-$ cell number in FL in Pu.1 embryos. n= 5 KO, 6 Ctrl at E14.5, 5 KO, 11 Ctrl at E16.5, and 8 KO, 13 Ctrl at E18.5 **B.** LSK cell number in FL in Pu.1 n= 5 KO, 6 Ctrl at E14.5, 5 KO, 11 Ctrl at E16.5, and 8 KO, 13 Ctrl at E18.5 **C.** $L^-S^+K^-$ cell number in FL in Id1/Id3 embryos. n= 5 KO, 12 Ctrl at E14.5, n=6 KO, 7 Ctrl at E16.5, and n= 6 at E18.5 **D.** Total LSK cell number in FL in Id1/Id3 embryos. n= 5 KO, 12 Ctrl at E14.5, n=6 KO, 7 Ctrl at E16.5, and n= 6 KO, 7 Ctrl at E18.5. Data are presented as mean ± SEM. ****P<0.0001, ***P<<0.001, **P<0.01, and *P<0.05, Wilcoxon test.

### 4.1.3. Depletion of Mφ shifts hematopoiesis towards the myeloid lineage

Upon confirmation of a transient depletion or reduction of Mφ using the Pu.1 or Id1/Id3 mouse models, respectively, possible consequences for the hematopoiesis were investigated in the FL across the different time points. Flow cytometry analyses of the Pu.1 mouse model showed that the number of the long-term and short-term hematopoietic stem cells (LT-HSC and ST-HSC) did not change significantly between the Pu.1$^{KO}$ and Pu.1$^{Ctrl}$ embryos (Figure 16A and B). LT-HSC numbers were decreased at E16.5, followed by a sharp increase at E18.5 in KO and WT embryos, while the ST-HSC constantly decrease over time and reach their least at E18.5.
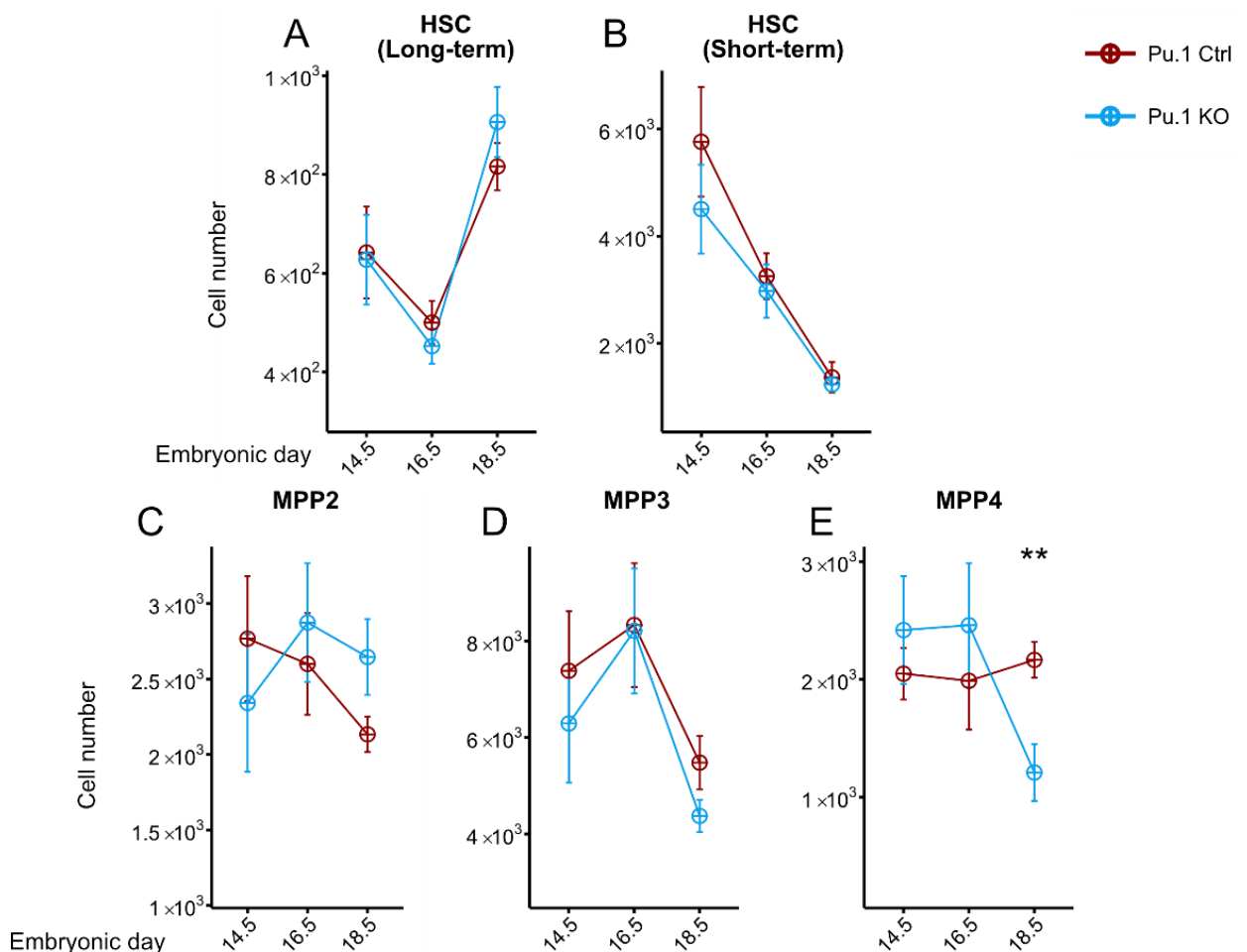


**Figure 16. Analysis of the HSC and progenitor cells in the fetal livers of the Pu.1 model during embryogenesis.**

**A.** Quantification of long-term hematopoietic stem cells (LT-HSC) in Pu.1 FL. **B. Q**uantification of short-term hematopoietic stem cells (ST-HSC) in Pu.1 FL. **C.** Quantification of MPP2 cells in Pu.1 FL **D.** Quantification of MPP3 cells in Pu.1 FL **E.** The quantification of MPP4 cells in Pu.1 FL. Data are presented as mean ± SEM. n= 5 KO, 6 Ctrl at E14.5, 5 KO, 11 Ctrl at E16.5, and 8 KO, 13 Ctrl at E18.5. ****P<0.0001, ***P<<0.001, **P<0.01, and *P<0.05, Wilcoxon test.

Investigating the multi-potent progenitors (MPP) numbers revealed that MPP2 and MPP3 did not change significantly during the hematopoiesis when comparing the Pu.1$^{KO}$ to Pu.1$^{Ctrl}$ embryos (Figure 16C-D). The only significant change was observed at E18.5 for the MPP4, where their number decreased in the Pu.1$^{KO}$ embryos compared to the Pu.1$^{Ctrl}$.

Studying the changes in hematopoiesis in the Id1/Id3 mouse model showed a pattern similar to Pu.1 cell number changes. There were no significant changes for the LT-HSC and ST-HSC. Analyzing the progenitors revealed no significant MPP changes (Figure 17A-E).
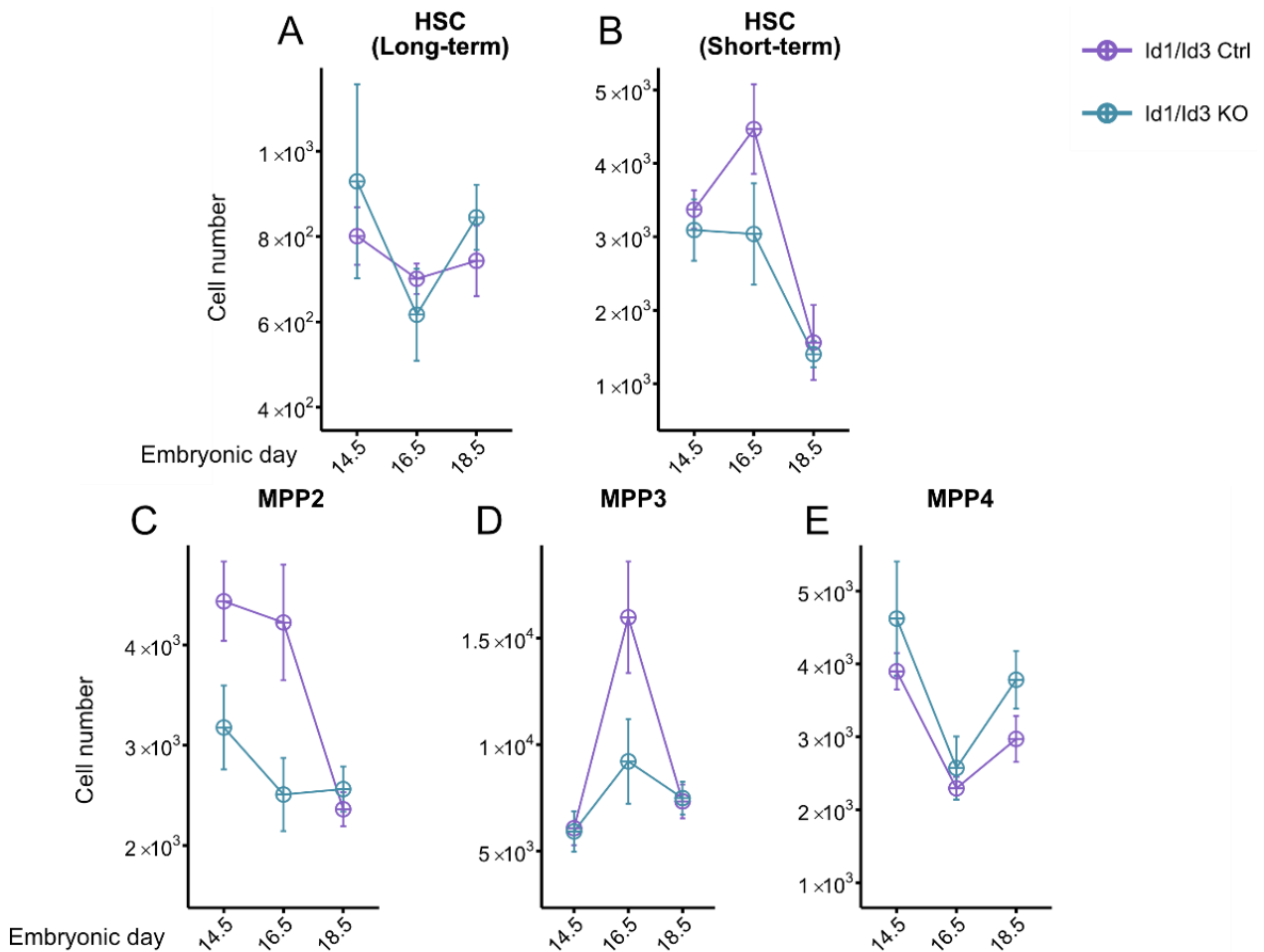


**Figure 17. Analysis of the HSC and progenitor cells in the Id1/Id3 model**

**A.** The quantification of LT-HSC in Id1/Id3 FL. **B.** The quantification of ST-HSC in Id1/Id3 FL. **C.** The quantification of MPP2 cells in Id1/Id3 FL **D.** The quantification of MPP3 cells in Pu.1 $^{f/f}$ FL **E.** The quantification of MPP4 cells in Id1/Id3 FL. Data are presented as mean ± SEM. n= 5 KO, 12 Ctrl at E14.5, n=6 KO, 7 Ctrl at E16.5, and n= 6 KO, 7 Ctrl at E18.5. ****P<0.0001, ***P<<0.001, **P<0.01, and *P<0.05, Wilcoxon test.

Similar to the Pu.1 model, the LT-HSC number was decreased at E16.5 in Id1/Id3 embryos when compared to E14.5, but increased again at E18.5. In contrast to the Pu.1 model, the ST-HSC were increased at E16.5 in Id1/Id3[Ctrl] embryos, but their cell number dropped at E18.5. When comparing the MPPs, MPP2 from Id1/Id3[KO] were lower in numbers compared to Id1/Id3[Ctrl] embryos at E16.5 and E18.5. Moreover, the MPP3 cell number at E16.5 showed the exact change observed in MPP2. Next, other progenitors downstream of MPPs, namely common myeloid progenitors (CMP), common lymphoid progenitors (CLP), granulocyte-macrophage progenitors (GMP), and megakaryocyte erythroid progenitors (MEP), were studied (Figure 18). In the Pu.1 model, the number of all of these cell type decreased during embryogenesis. The number of CMPs increases at E16.5 Pu.1[KO] embryos to the Pu.1[Ctrl]. This change becomes statistically significant by E18.5 (Figure 18A).
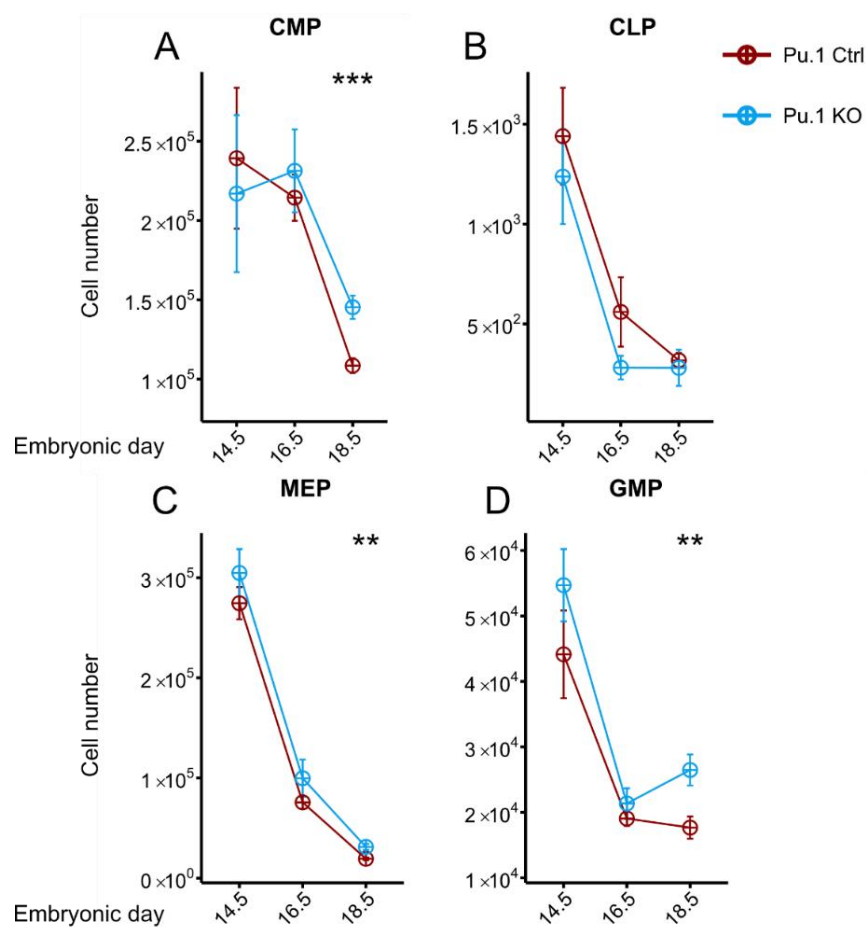


**Figure 18. Quantification of lymphoid and myeloid progenitors in the Pu.1 model**

**A.** Quantification of CMP cell number in Pu.1 FL. **B.** Quantification of CLP cell number in Pu.1 FL. **C.** Quantification of MEP cell number in Pu.1 FL **D.** Quantification of GMP cell number in Pu.1 FL. Data are presented as mean ± SEM. n= 5 KO, 12 Ctrl at E14.5, n=6 KO, 7 Ctrl at E16.5, and n= 6 at E18.5. ****$P<0.0001$, ***$P<<0.001$, **$P<0.01$, and *$P<0.05$, Wilcoxon test.

The same trend was observed in the MEPs and GMPs. A significant drop in the cell number of these two cell types at E18.5 happens in the cell numbers (Figure 18C-D). Furthermore, CLPs numbers were similar throughout development in Pu.1[KO] embryos when compared to

Pu.1$^{Ctrl}$ littermates, and the cell number differences between the conditions reached their lowest variance at E18.5 (Figure 18B).

In the next step, the changes in CMPs, CLPs, GMPs, and MEPs were studied in the Id1/Id3 model. Overall, the cell numbers among these cell types were not changed significantly when comparing the Id1/Id3$^{KO}$ to the Id1/Id3$^{Ctrl}$ embryos. Starting with the number of CMPs, no change was observed at any time point in KO vs. Ctrl (Figure 19A). Analysis of the CLPs also showed no significant changes. However, the number of the cells was higher at E16.5 in the Id1/Id3$^{KO}$ embryos (Figure 19B).
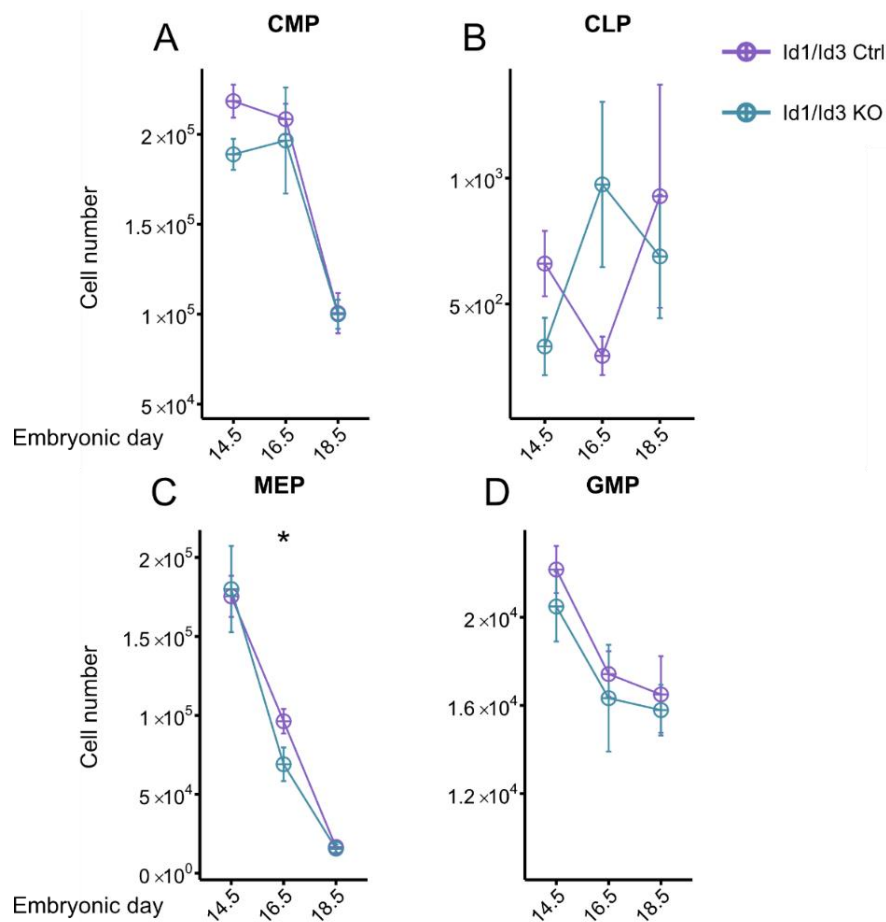


**Figure 19. Quantification of lymphoid and myeloid progenitors in the Id1/Id3 model**

**A.** Quantification of CMP cell number in Id1/Id3 FL. **B.** Quantification of CLP cell number in Id1/Id3 FL. **C.** Quantification of MEP cell number in Id1/Id3 FL **D.** Quantification of GMP cell number in Id1/Id3 FL. Data are presented as mean ± SEM. n= 5 KO, 12 Ctrl at E14.5, n=6 KO, 7 Ctrl at E16.5, and n= 6 KO, 7 Ctrl at E18.5. ****$P<0.0001$, ***$P<<0.001$, **$P<0.01$, and *$P<0.05$, Wilcoxon test.

The MEPs showed no changes at E14.5 and E18.5, while at E16.5, their number decreased in the Id1/Id3$^{KO}$ embryos (Figure 19C). The results of the GMPs were similar to the CMPs, as no change was observed among the two conditions at different time points. With time, the GMP cell numbers were constantly decreasing in both Id1/Id3$^{KO}$ and Id1/Id3$^{Ctrl}$ embryos (Figure 19D).

Figure 20 shows the analysis of the myeloid cells developing from the GMP. Considering the changes in the progenitor cells, the possible effect of such a change was tracked to investigate the alteration of granulocyte and monocyte numbers. It has been previously shown that monocytes at the E13.5 mouse embryonic stage do not express Cx3cr1 (Jappinen, Felix et al. 2019). However, it is also demonstrated that hepatic and all blood monocytes can express Cx3cr1 (Landsman, Bar-On et al. 2009, Lee, Kim et al. 2018). Hence, the Cx3cr1 expression of the monocytes in the FL at E14.5, E16.5, and E18.5 was studied.
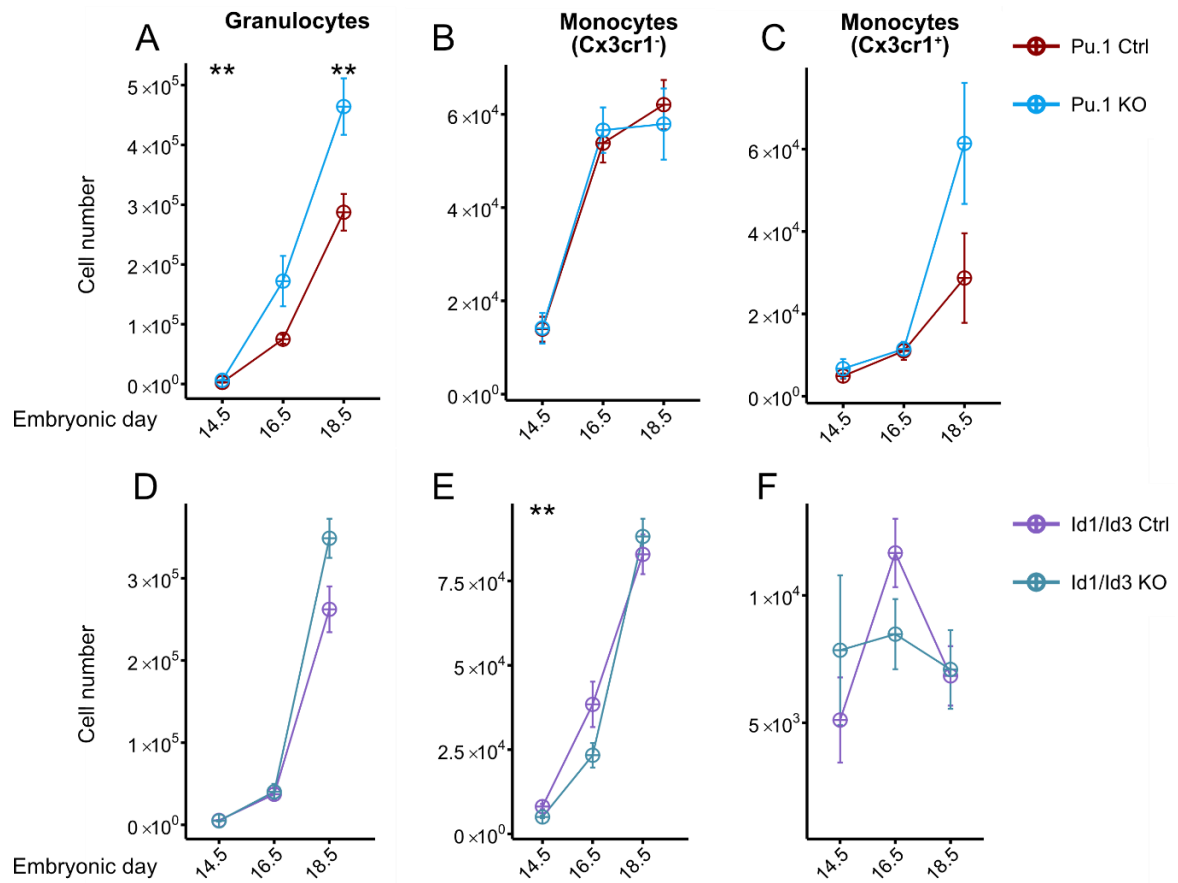


**Figure 20. Quantification of myeloid cells in the Pu.1 and Id1/Id3 models**

**A.** Quantification of Ly6G$^+$ granulocytes in Pu.1 FL. **B.** Quantification of Ly6C$^+$ Cx$_3$cr1$^-$ monocytes in Pu.1 FL. **C.** Quantification of Ly6C$^+$ Cx$_3$cr1$^+$ in Pu.1 FL **D.** Quantification of Ly6G$^+$ granulocytes in Id1/Id3 FL **E.** The quantification of Ly6C$^+$ Cx$_3$cr1$^-$ monocytes in Id1/Id3 FL. **F.** The quantification of Ly6C$^+$ Cx$_3$cr1$^+$ monocytes in Id1/Id3 FL. Data are presented as mean ± SEM. Pu.1 n= 5 KO, 11 Ctrl at E14.5, 5 KO, 11 Ctrl at E16.5, and 8 KO, 13 Ctrl at E18.5. Id1/Id3 n= 8 KO, 17 Ctrl at E14.5, 7 KO, 7 Ctrl at E16.5, and 6 KO, 7 Ctrl at E18.5. ****P<0.0001, ***P<<0.001, **P<0.01, and *P<0.05, Wilcoxon test.

The Pu.1 mouse model results show that granulocytes constantly increase in the Pu.1$^{KO}$ embryos. This increase is significant at E14.5 and E18.5. At the same time, at E16.5, the number of granulocytes varies between the biological replicates in the Pu.1$^{KO}$ samples leading to a non-significant change (Figure 20A). In contrast to the granulocytes, the number of Cx3cr1$^-$monocytes stays relatively the same while Cx3cr1$^+$ monocytes show none significant increase, the comparing the Pu.1$^{KO}$ to Pu.1$^{Ctrl}$ (Figure 20B and C).

Contrary to granulocyte number in the Pu.1 mouse model, the granulocytes in the Id1/Id3 samples did not show any change. However, the number of monocytes that lack Cx3cr1 expression significantly increased at E14.5 (Figure 20D and E). This increase was not observed in Cx3cr1$^+$ monocytes, and these cells showed high variance at E14.5 in both Id1/Id3$^{KO}$ and Id1/Id3$^{Ctrl}$ embryos.

In summary, results from the Pu.1 and Id1/Id3 mouse models showed that upon Mφ depletion cellular dynamics within hematopoiesis changes. The changes were particularly observable in the number of GMP and granulocytes in the Pu.1 model. However, the number of hematopoietic stem cells and their progeny in the Id1/Id3 model remained similar in both Ctrl and KO embryos.

## 4.2. Colony-forming assays confirm the increase in the granulocyte-macrophage progenitor in the Pu.1 model

Colony-forming assays (CFUs) were performed to investigate whether the depletion of Mφ in the Pu.1 and Id1/Id3 models could induce any changes in the differentiation of HSC in cell autonomous manner. In a previous study, FL HSC were harvested and cultured for 12 days to allow their differentiation into different hematopoietic lineages (Heider 2021).

After 12 days of cell culture, HSC-derived colonies were picked and analyzed using May-Grünwald-Giemsa staining to confirm their phenotype. The Pu.1$^{KO}$ showed no statistical significance of the total number of colonies compared to the Pu.1$^{Ctrl}$ (n=3 biological replicates per genotype). However, HCSs from the Pu.1$^{KO}$ model mainly differentiated into the granulocyte-macrophage colony-forming unit (CFU-GM), which were statistically significantly (p = 0.0241) increased compared to the Pu.1$^{Ctrl}$. Furthermore, Colony-forming unit-macrophage (CFU-M) showed a significant increase (p = 0.0232) in the Pu.1$^{KO}$. Colony-forming unit-granulocyte, erythrocyte, macrophage, megakaryocyte (CFU-GEMM) numbers were slightly higher in the Pu.1$^{Ctrl}$, but there were no statistically significant differences. Furthermore, Colony-forming unit-granulocyte (CFU-G) numbers were almost the same in Pu.1$^{Ctrl}$ and Pu.1$^{KO}$. Due to technical problems, it was not possible to compare Burst-forming unit-erythroid (BFU-E) in Pu.1$^{Ctrl}$ and Pu.1$^{KO}$ FLs.

In the Id1/Id3 model, the total colony number of the Id1/Id3$^{Ctrl}$ had no significant changes compared to the Id1/Id3$^{KO}$. Moreover, the colony distribution showed no significant differences and statistical significance.

In conclusion, the results from the CFU assays could show that depletion of Mφ in the Pu.1 model leads to the generation of more GMPs and granulocytes, confirming the observed results from the flow-cytometry.

## 4.3. Depletion of Mφ has a transient effect on erythroblast enucleation

Considering the role of Mφ in the erythroblast islands, where they support erythropoiesis (Manwani and Bieker 2008), the enucleation and maturation of erythroblasts were investigated in the KO and Ctrl embryos. The collected blood samples from the Pu.1 embryos showed that the percentage of immature red blood cells at E14.5 in the Pu.1$^{KO}$ samples was reduced to ~50%. In comparison, the Pu.1$^{Ctrl}$ embryos had around 75% erythrocytes (Figure 21 A, C, and D). This reduction of cells was not observable at later time points. At E16.5 and E18.5, both the Pu.1$^{KO}$ and Pu.1$^{Ctrl}$ showed the same percentage of erythrocytes, in this case around 100%. Examination of the Id1/Id3 blood samples showed a reduction in the percentage of enucleated cells in the Id1/Id3$^{KO}$ embryos at E14.5; however, this difference was not significant. Similar to the Pu.1 mouse model, at E16.5 and E18.5, the percentage of erythrocytes reached around 100%, and no difference could be seen in Id1/Id3$^{KO}$ and Id1/Id3$^{Ctrl}$ embryos (Figure 21 B).
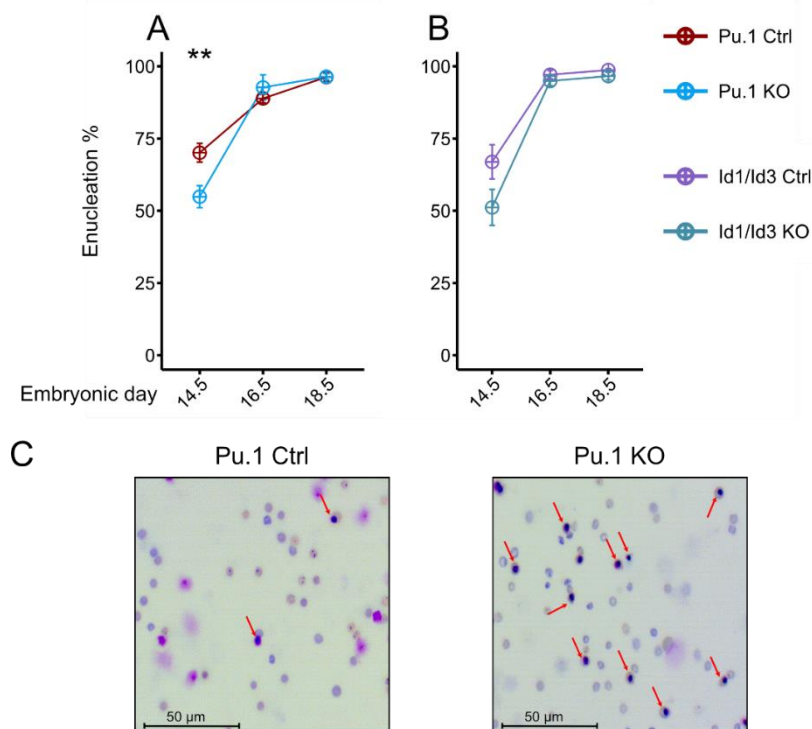


**Figure 21. Enucleation of erythroblasts in the Pu.1 and Id1/Id3 models**

**A.** Percentage of enucleated erythroblasts in Pu.1 FL at different time points. **B.** Percentage of enucleated erythroblasts in Id1/Id3 FL at different time points. Data are presented as mean ± SEM. Pu.1 n= 9 KO, 13 Ctrl at E14.5, n= 5 KO, 5 Ctrl at E16.5, and n= 6 KO, 5 Ctrl at E18.5. Id1/Id3 n=10 KO, 14 Ctrl at E14.5, n=6 KO, 5 Ctrl at E16.5, and n=5 KO, 5 Ctrl at E18.5. ****P<0.0001, ***P<0.001, **P<0.01, and *P<0.05, Wilcoxon test. **C.** Representative blood smear picture from Pu.1 E14.5 embryos. The red arrows show sill nucleated erythroblasts.

The different stages of erythrocyte maturation were investigated using flow cytometry to study the effects of Mφ depletion on the enucleation of erythroblasts in the FL. The results from the Pu.1 embryos showed that the maturation of erythrocytes was not affected in Pu.1$^{KO}$ except at the S1 and S2 stages. In these two stages at E18.5, the Pu.1$^{KO}$ samples had more cells compared to the Pu.1$^{Ctrl}$. The six different maturation stages of the erythrocytes showed constant and relatively similar percentages (Figure 22 A).



**Figure 22. Flow-cytometry of erythrocytes differentiation stages in Pu.1 embryos**

**A.** Comparison of differentiation stages of erythrocytes in Pu.1$^{KO}$ and Pu.1$^{Ctrl}$ embryos. Data are presented as mean ± SEM. Pu.1 1 n= 5 KO, 11 Ctrl at E14.5, 5 KO, 11 Ctrl at E16.5, and 8 KO, 13 Ctrl at E18.5. *P<0.05, Wilcoxon test. **B.** Representative gating strategy to capture differentiation stages of erythrocytes.

Figure 23 shows the maturation changes in the Id1/Id3$^{f/f}$ embryos. Altogether, the percentage of the cells in each maturation stage did not change between the Id1/Id3$^{KO}$ and Id1/Id3$^{Ctrl}$ embryos. Similar to the Pu.1 model, the percentages were relatively comparable between the conditions with no significant change. The percentage of the cells at the S0 stage at E14.5 showed variation, but this variation was resolved at E16.5 and E18.5. A similar variation could be observed at E14.5 in the S2 stage, which was no longer visible at the later time points.
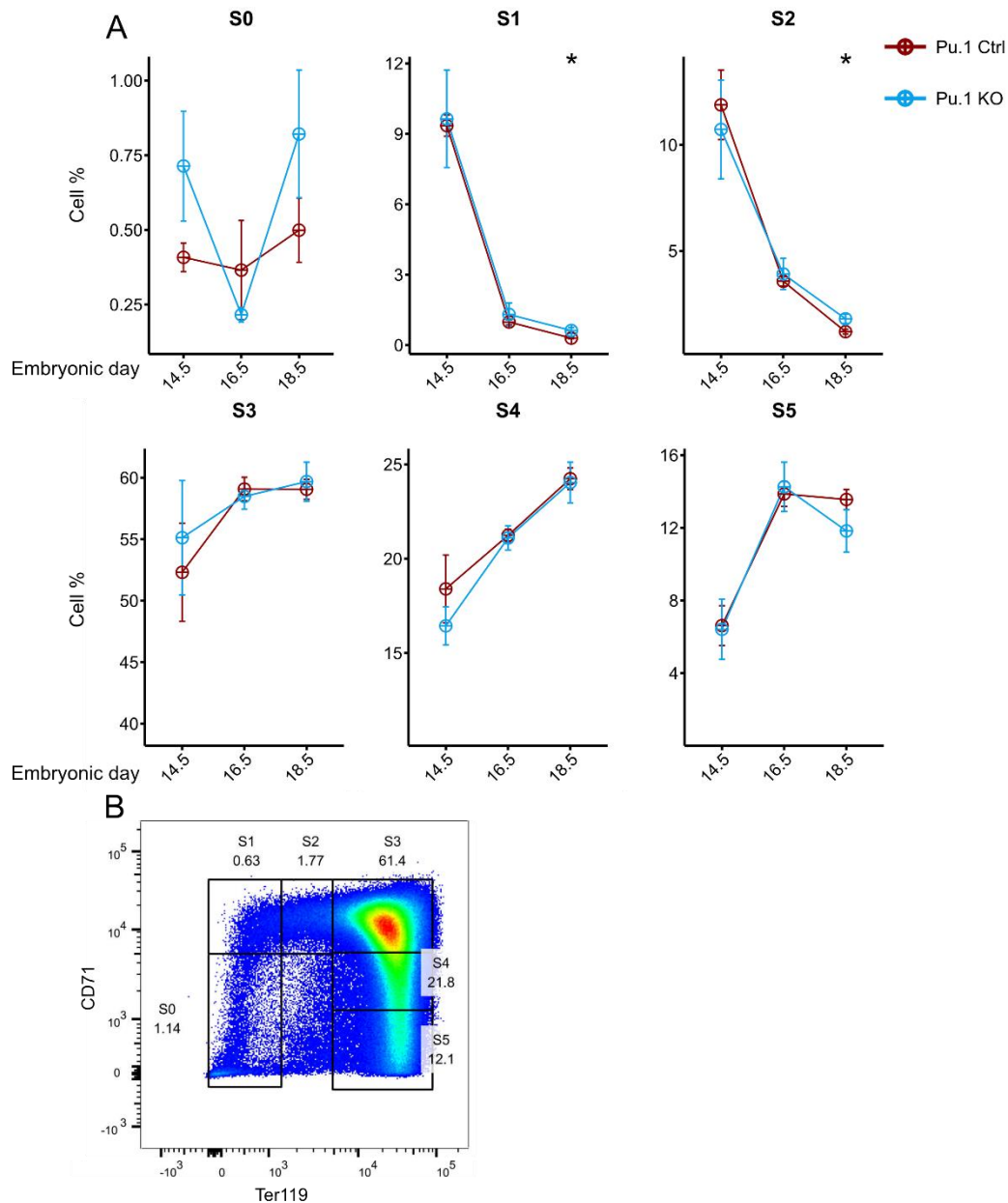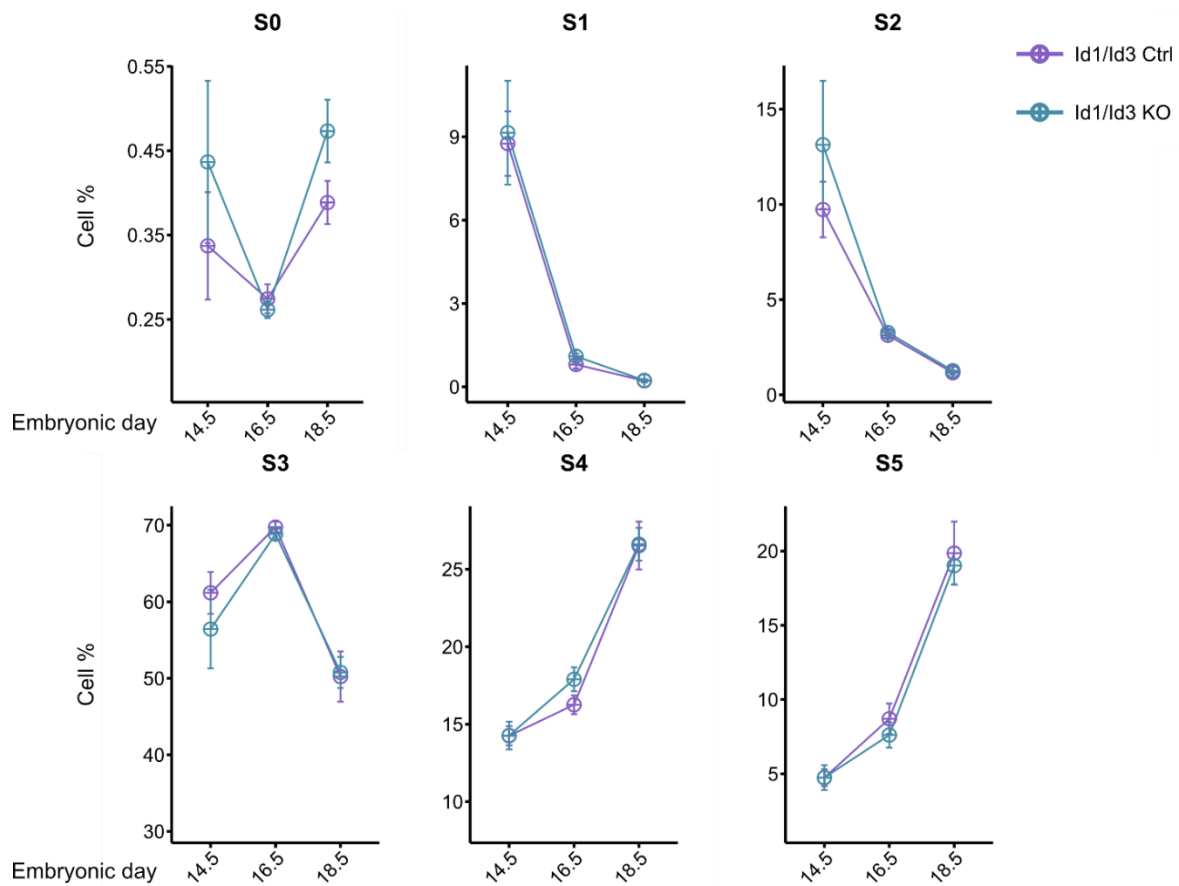


**Figure 23. Flow-cytometry of erythrocytes differentiation stages in Id1/Id3 embryos**

Comparison of differentiation stages of erythrocytes in Id1/Id3 $^{KO}$ and Id1/Id3$^{Ctrl}$ embryos. Data are presented as mean ± SEM. Id1/Id3 n= 8 KO, 17 Ctrl at E14.5, 7 KO, 7 Ctrl at E16.5, and n= 6 KO, 7 Ctrl at E18.5. Wilcoxon test.

## 4.4. Bulk-RNA sequencing reveals transcriptional changes in HSC upon Mφ depletion

The flow cytometry data analysis could show that depletion of Mφ can impact hematopoiesis. This impact was more significant in the Pu.1 mouse model. Here, changes in the hematopoiesis and its shift toward myeloid lineage were constant and observable at E16.5 and E18.5.

In the next step, these changes were investigated in more detail to understand the underlying causes and possible alterations in the gene expression of the HSC. To this end, bulk-RNA sequencing analysis was performed on sorted LT-HSC from E14.5 FLs from the Pu.1 mouse model. The expression data were analyzed and compared between the Pu.1$^{Ctrl}$ (n= 7) and Pu.1$^{KO}$ (n= 9), and the differentially expressed genes (DEG) were calculated.

In order to understand the function of the genes, which were affected by the loss of Mφ, DEG were determined (fold change (FC) greater than 0.5 or less than -0.5, p-value < 0.05). These settings resulted in 728 up-regulated DEG, and 515 downregulated DEG that were subtracted to a gene ontology (GO) analysis. The results of the overall DEG, regardless of their p-value, also could show a clear different expression pattern when comparing the KO embryos to the Ctrl (Figure 24). The top 10 up-regulated genes in the KO samples based on their FC were Pakap.1, Mybpc3, Prrt4, Pcdhga6, Slc25a41, Lilr4b, Rhov, Ctla4, Clnk, and Muc5b. Based on their FC, the top 10 down-regulated genes were Marco, Pdzd3, Clec4f, Hey2, Plppr5, Alk, Fmo4, Cyp7a1, Tdrd5 and Hao2.

The GO analysis revealed several processes and functions that were changed in the Pu.1$^{KO}$ LT-HSC compared to Pu.1$^{Ctrl}$ LT-HSC. The results could show that the genes associated with functions such as myeloid activation, lymphocytes differentiation and definitive hemopoiesis were up-regulated in KO samples (Figure 25A). Other up-regulated processes included Ras's protein signal transduction, calcium ion homeostasis, and developmental maturation. The down-regulated biological processes in the KO samples included nuclear division, cell cycle phase transition, erythrocyte homeostasis, and heme metabolic process.

Interestingly, the myeloid cell differentiation term occurred in both down and up-regulated genes among the GO terms. This means that part of the genes involved in this process were down-regulated in the KO embryos compared to the Ctrl, while the others were up-regulated in the KO samples compared to the Ctrl (Figure 25B). Investigating the genes that are involved in the myeloid cell differentiation process revealed that the down-regulated genes in the

Pu.1<sup>KO</sup> compared to Pu.1<sup>Ctrl</sup> samples are mostly known to be essential for Mφ development, e.g., Id2, Csf1r, and Klf1. However, the up-regulated genes in the Pu.1<sup>KO</sup> compared to Pu.1<sup>Ctrl</sup> such as Kit. Gata2 and Gata3 have a role in HSC proliferation and differentiation.
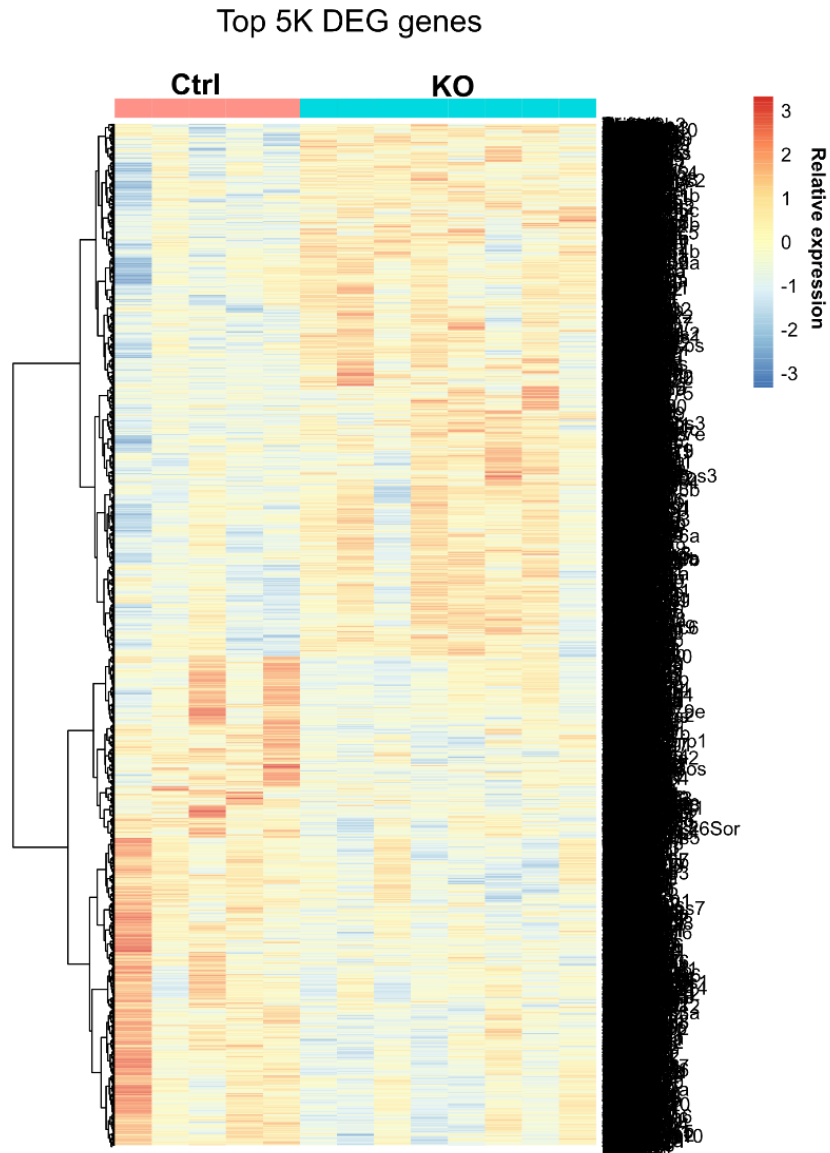


**Figure 24. The top 5k differentially expressed genes in the HSC of KO embryo compared to the Ctrl embryos.**
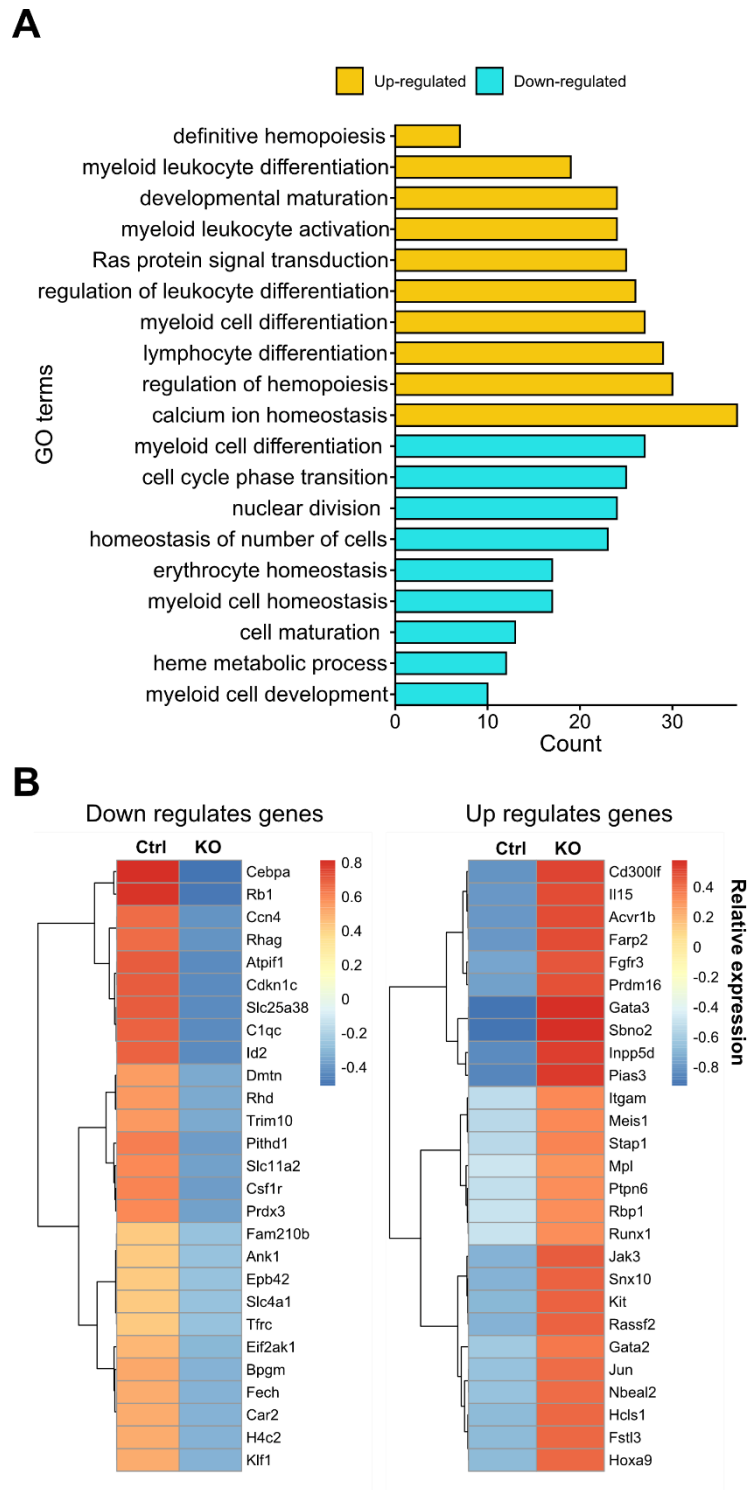
**Figure 25. The Bulk-RNA sequencing of HSC from Pu.1 embryos.**

**A.** Gene enrichment analysis of DEGs from KO and Ctrl embryos of Pu.1 model. n=16. **B.** Expression of genes involved in the myeloid cell differentiation term. P<0.0001

## 4.5. Characterization of macrophages at single-cell level reveal different sub-populations in the fetal liver

The results from the previous experiments provide evidence regarding the role of Mφ in the HSC niche and hematopoiesis. It is a known fact that Mφ are tissue-specific cells and that they are heterogeneous across different organs. Nevertheless, their heterogeneity in the same tissue, particularly during embryogenesis, remains elusive. Hence, a single-cell RNA-sequencing experiment was performed in the next step to investigate different subpopulations of Mφ within the FL that might have distinct functions, including direct interaction with HSC. In order to perform a single-cell RNA sequencing experiment to investigate the heterogeneity of Mφ, CD11b$^+$ F4/80$^+$ cells belonging to E14.5 wild-type FL were sorted and processed via Seq-well, a single-cell RNA sequencing technique. The results of the sequencing were analyzed through clustering of the cells followed by subsetting the clusters of interests which was done by overlaying different myeloid cell markers to exclude the cells belonging to cell types other than Mφ, such as dendritic cells, megakaryocytes, etc. and only to keep Mφ for further analysis.

The initial results of single-cell sequencing were processed through filtering cells and genes. This cleaning process filtered 523325 cells and 3538 genes out, resulting in the final dataset of 32431 cells and 18631 genes. This dataset was further processed for further analysis and clustering. The initial clustering resulted in 11 (Figure 27) groups which are visualized using Uniform Manifold Approximation and Projection (UMAP) method (McInnes, Healy et al. 2018). To find the cluster(s) of interest, namely the clusters representing the Mφ, five signature lists (Mass, Ballesteros et al. 2016) were overlaid on all the clusters (Figure 27). Four clusters out of eleven were selected based on their expression of these signatures.
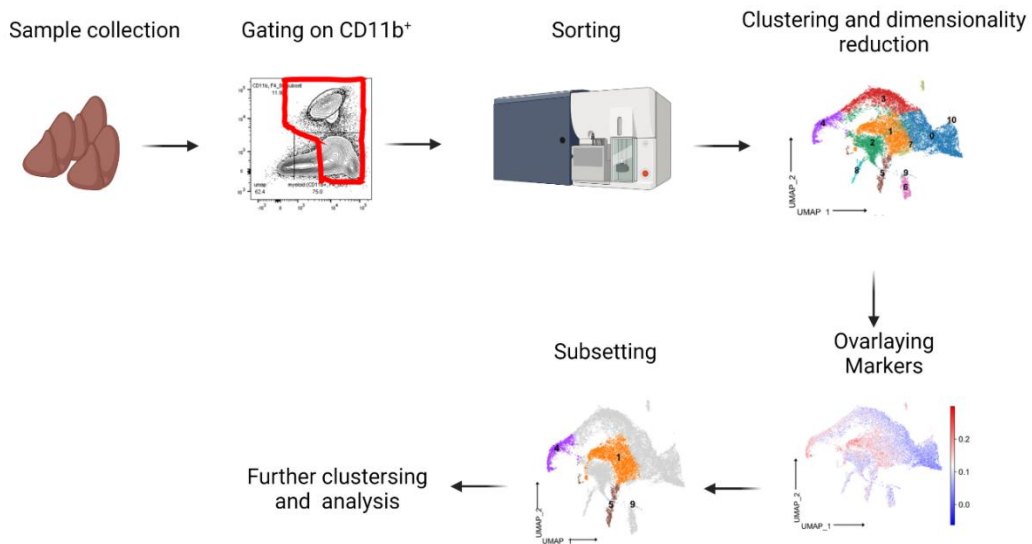
**Figure 26. The overall schematic process of analyzing the single-cell sequencing data.**

The FL livers were collected and analyzed through flow-cytometry; the data was down-sampled and analyzed using cluster and dimensionality reduction. The clusters of interests were subset and further analyzed.



**Figure 27. Visualization of sc-RNA sequencing result using UMAP**

UMAP plots of sc-RNA sequencing clustering and the cells' expression of different signature lists overlaid on the cells. These lists include the genes differentially expressed in EMP, pMφ, Mφ, and also the genes up-regulated in Mφ compared to pMφ and EMPS.

Figure 28A shows the selected four clusters. These clusters were subset and re-analyzed to identify the possible different Mφ and possibly Mφ precursor populations. The clustering of the subset data returned seven different groups. Two different signature markers were 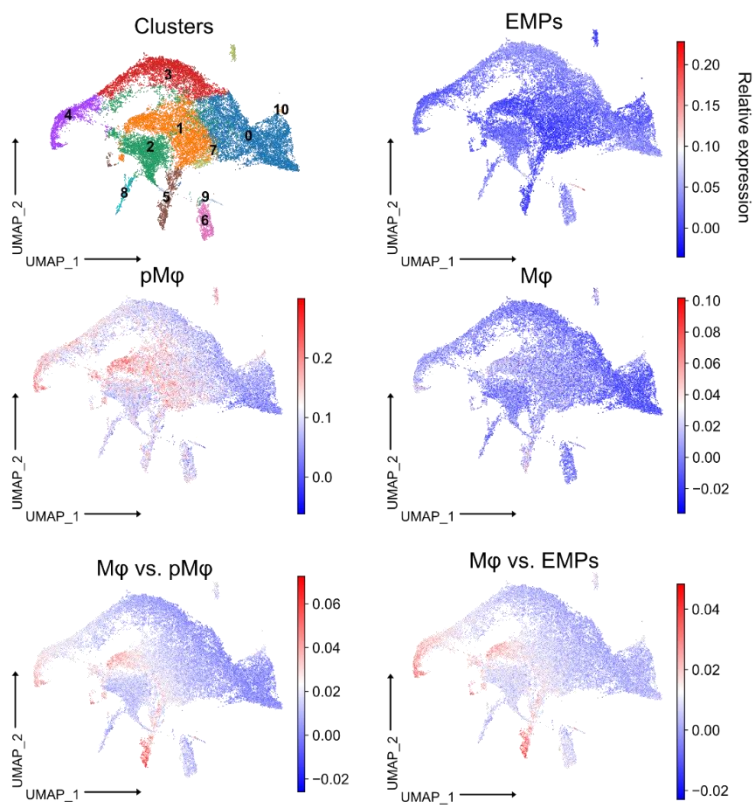overlaid on top of the clusters, similar to the previous step. These two signature lists included the genes that are expressed in Mφ (Figure 28C). The resulted clusters were subjected to subsetting again based on their expression of the two signature lists. In this step, five groups within which most cell showed high expression of genes specific to mature Mφ were selected for further analysis.
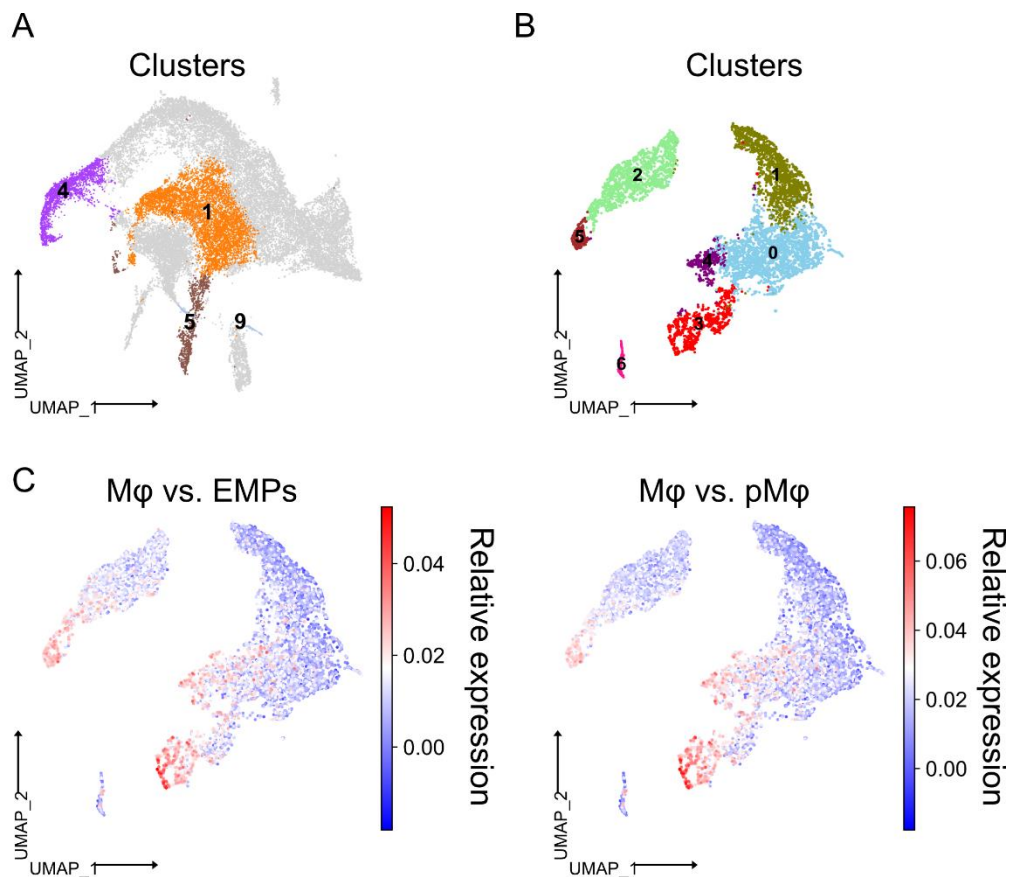


**Figure 28. First sub-set clusters and the newly generated clusters**

**A.** UMAP plot of selected clusters for the first subsetting. **B.** The newly formed cluster on the subset data and the cells' expression of different signature lists overlaid on the cells. **C.** Overlaying of two signature lists on the cells

The selected five clusters (Figure 29A) were subjected to the last clustering round. The clustering was done in a non-stringent way allowing the cells to form many clusters to separate the cells that represent Mφ from the other cell types. The re-analysis of the data produced 18 clusters. The non-stringent clustering showed to be effective as the initial screening of the groups immediately detected three clusters, clusters 15, 16, and 17, that were different from the other cells (Figure 29B). The two signature lists that included the genes up-regulated in adult Mφ compared to the immature Mφ were overlaid on all clusters.

Furthermore, the DEGs of the clusters were investigated, and several markers associated with the Mφ were selected for their expression pattern within the clusters (Figure 29D). The aim was focused on analyzing clusters that expressed more than one marker associated with Mφ (Figure 29C). These clusters were 1, 2, 7, 8, and 11. Furthermore, cluster 9 could be identified as the erythroblastic island. This cluster has a low expression of Mφ associated markers but is highly expressing gene related to erythroblasts and erythrocytes, e.g., *Hbb-bt*, which correspond to the characterization of erythroblastic islands.
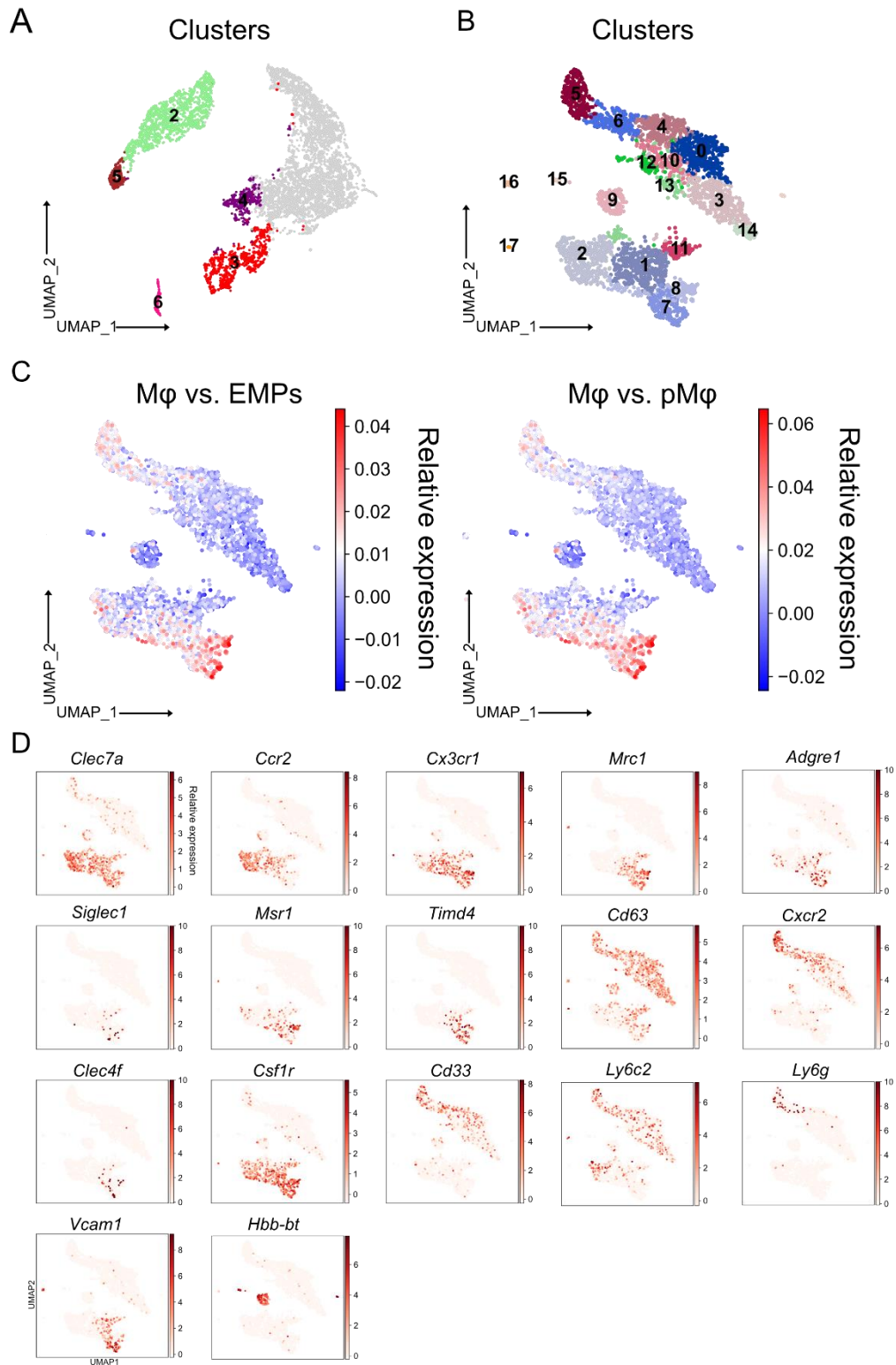
**Figure 29. Second sub-set clusters and the subsequently generated clusters**

**A.** UMAP plot of selected clusters for the second analysis. **B.** Results of second clustering on the second subset data and the cells' expression of different signature lists overlaid on the cells. **C.** Overlaying of two signature lists on the cells **D.** Expression of selected genes on the single cells

Focusing on the six selected clusters (Figure 30A), further downstream analysis was done to confirm the identity of each of the clusters. Figure 30B shows the dot-plot of eleven selected genes. *Csf1r*, *Clec7a*, and *Cx3cr1* are Mφ core genes that are up-regulated during development from EMP to fetal Mφ (Dai, Ryan et al. 2002, Taylor, Brown et al. 2002, Burgess, Wicks et al. 2019). All selected clusters express these genes to some extent, confirming the Mφ identity of the cells within these groups. The expression of other Mφ genes such as *Adgre1*, *Timd4*, *Vcam1*, and *Mrc1* indicate a heterogeneity among these Mφ populations in the fetal liver. The dot-plot and the heatmap of top expressed genes within each cluster indicated that clusters 7, 8, and 2 represent the Mφ. In these clusters genes that are attributed with Mφ such as Clec4e, Clec1b, and MS4a7 are highly expressed. However, clusters 1 and 11 are still differentiating or immature cells. In cluster 1, there is no specific pattern in the gene expression and this cluster express different genes at low level (Figure 30B and C). As expected, cluster 9 represented the erythroblastic islands and central Mφ based on the gene expression.
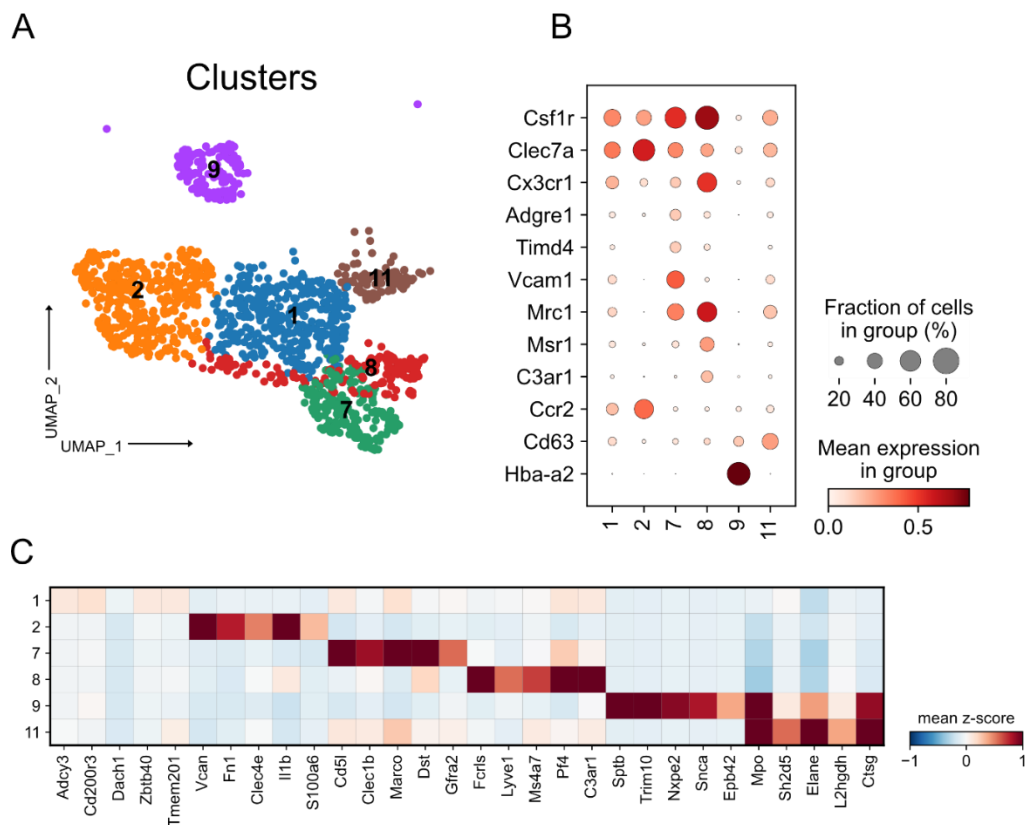


**Figure 30. Second sub-set clusters and the final generated clusters**

**A.** UMAP plot of the final clusters that represents Mφ cells. **B.** Dot plot expression of selected genes in the final clusters **C.** Heatmap of top 5 expressed genes in the final clusters.

To analyze whether the identified populations have unique cell functions and each cluster is distinct from the other discovered clusters, all clusters were compared against each other and the top 100 differentially expressed genes (DEG) were used as an input for GO analysis. Figure 31 shows the GO terms linked with each of the clusters. For example, the terms "macrophage activation" and "regulation of inflammatory response" are associated with clusters 2, 7, and 8. In contrast, cluster 1 expresses genes that reflect the proliferation/differentiation phase of the cells. These terms are in accordance with the previous assumptions that clusters 2, 7, and 8 consist of mature Mφ, and cluster 1 represents immature or differentiating cells. Terms such as "erythrocyte differentiation" and "erythrocyte homeostasis" confirmed the erythroblastic island identity of cluster 9. Cluster 11 had similar GO terms as cluster 9 but with fewer genes for each term, indicating that this cluster is probably not fully maturated.
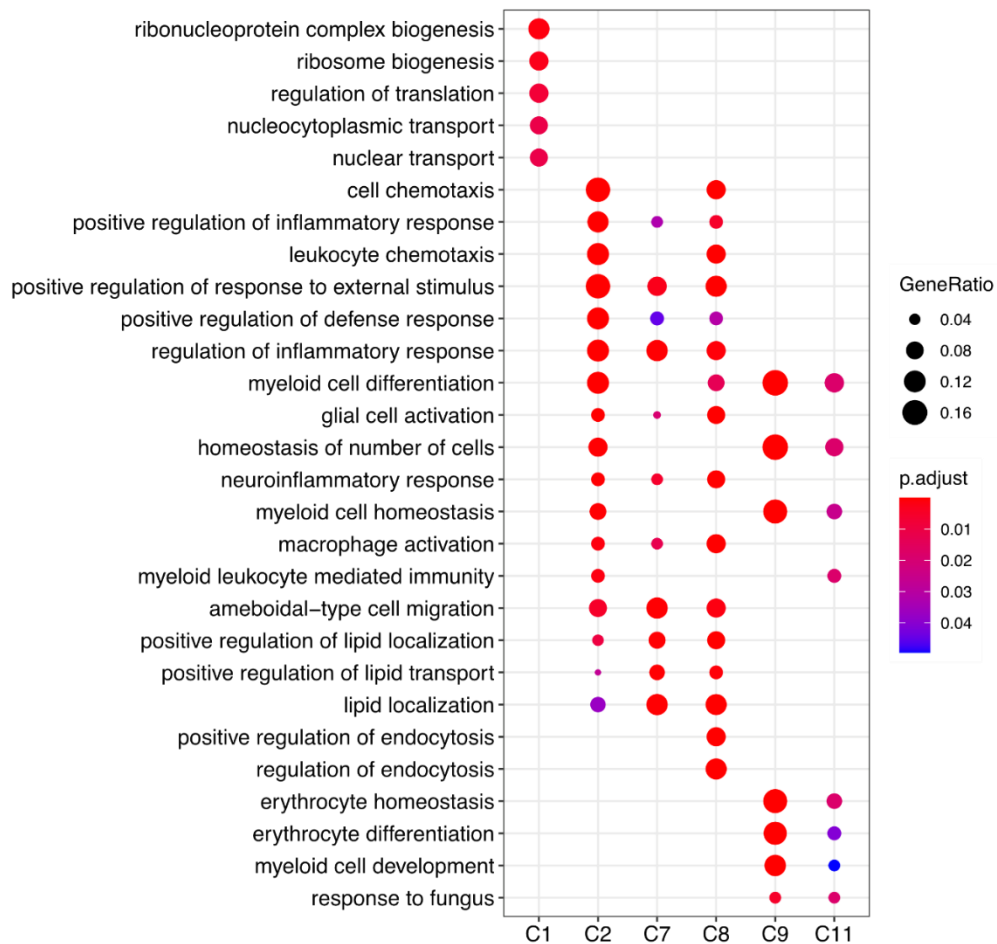


**Figure 31. Gene ontology (GO) analysis on the differentially expressed genes (DEG)**

The dot plot of the terms that are associated with the DEG of the final clusters.

To study whether the identified macrophage subpopulations were indeed undergoing a developmental trajectory, the Partition-based graph abstraction (PAGA) method was used. In this analysis, five out of six final clusters (clusters 1, 2, 7, 8, and 11) were examined (Figure 32A). Cluster 9 was excluded from this analysis as its identity was apparent due to the gene expression and the GO terms. Cluster 1 is the center of the network. This cluster differentiates into the other groups and strongly relates to cluster 11. Since PAGA uses to expression profile of the cells to predict their relation, it can be assumed that cluster 1 expresses core genes involved in all other clusters. Furthermore, clusters 7 and 8 show substantial similarity to each other. Finally, the pseudotime analysis of the clusters also confirmed the differentiating stage of cluster 1 (Figure 32B).



**Figure 32. The trajectory analysis of the clusters**

**A.** Trajectory analysis of five Mφ clusters using PAGA algorithm **B.** The pseudotime analysis of the clusters visualized using the distributed recursive layout (DRL).

## 4.6. Flow-cytometry data confirms the observed heterogeneity in the single-cell data

The results from the single-cell sequencing and the following downstream analysis could show that tissue-resident Mφ in the FL are heterogeneous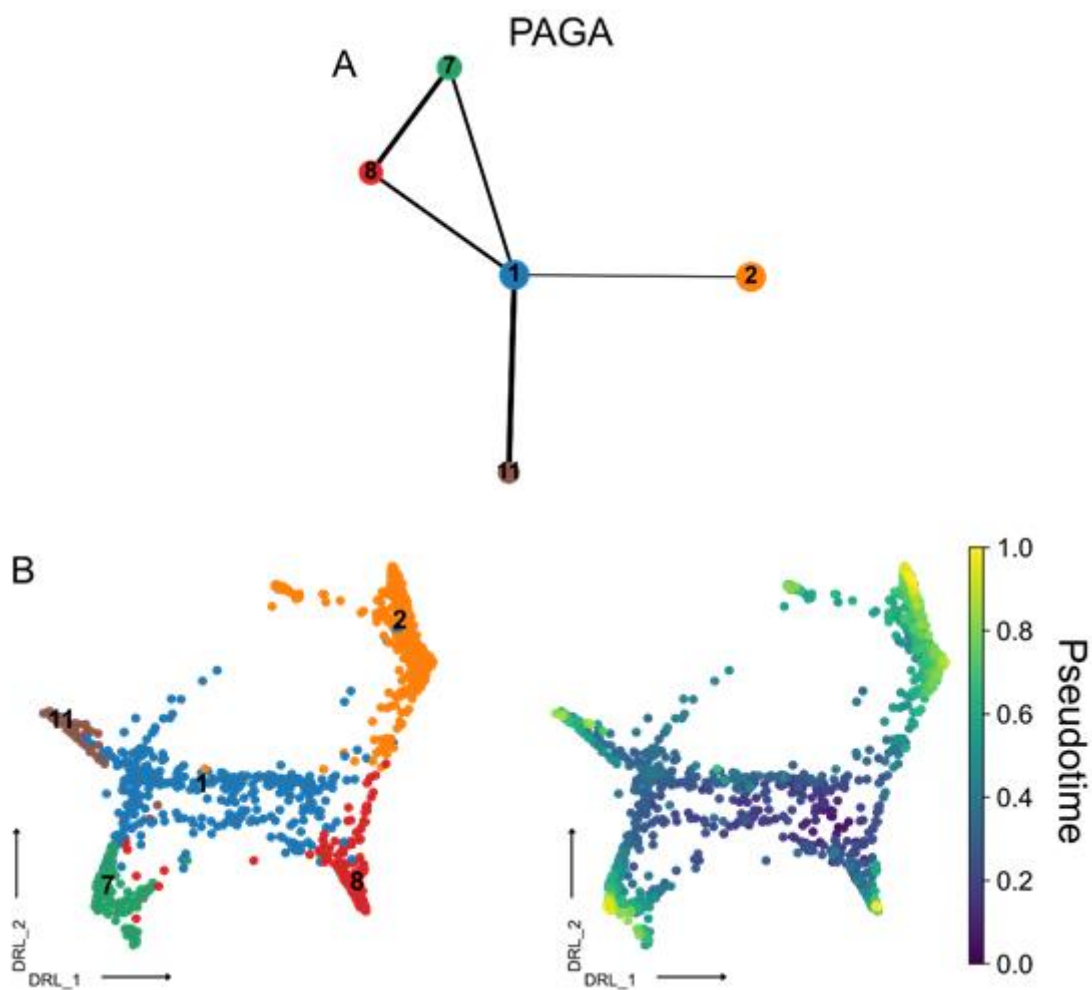 and different subpopulations of Mφ exist in the FL. In summary, six different groups were identified. Three out of the six clusters were regarded as main clusters representing mature Mφ. In addition, one cluster was labeled as erythroblastic island and represented central Mφ. The two remaining clusters were considered immature or differentiating groups.

To validate the heterogeneity observed using scRNA-seq, a flow-cytometry panel consisting of 20 markers was developed. Most of the markers were selected based on the DEGs of the six clusters from the single-cell analysis. Additionally, to address the ontogeny of the distinct macrophage populations, E14.5 FL from three different fate-mapping models was analyzed. The first reporter mouse is the $Rank^{Cre}Rosa26^{eYFP}$ model (Percin, Eitler et al. 2018). Rank is an essential gene for Mφ development; hence, the expression of this gene is expected in the identified Mφ clusters. The other two reporter mice are $Ms4a3^{Cre}Rosa26^{eYFP}$ reporter and $Cxcr4^{Cre}Rosa26^{eYFP}$ reporter models (Liu, Gu et al. 2019, Werner, Mass et al. 2020). The expression of these two genes in any cluster would hint that those cells have originated from HSC and not EMPs.

### 4.6.1. Flow-cytometry confirms the heterogeneity of Mφ

The flow cytometry data from *Ms4a3^CreRosa26^eYFP* FLs were imported into R after compensation and down-sampling on CD11b$^+$ F4/80$^+$ cells for further analysis. The data were clustered in an unsupervised way into 35 clusters. The clusters of interest were identified via the expression of the Mφ markers. These clusters were subset and clustered again. Some were merged based on the heatmaps and their similarity (Figure 33). The final clusters represented all Mφ, and the heterogeneity of the clusters was further investigated according to the results of single-cell analysis. Figure 34A shows the initial clustering and dimensionality reduction results using the UMAP method. In total, 35 clusters were generated. This cluster number could allow more homogeneity within each group of the cells regarding their expression pattern, making subsetting easier. Subsetting was done through overlaying six Mφ markers; F4/80, Tim4, Cx3cr1, CD169, CD206, and Vcam1. Moreover, Ly6G and Ly6C were used to identify granulocyte and monocytes (Figure 34B).
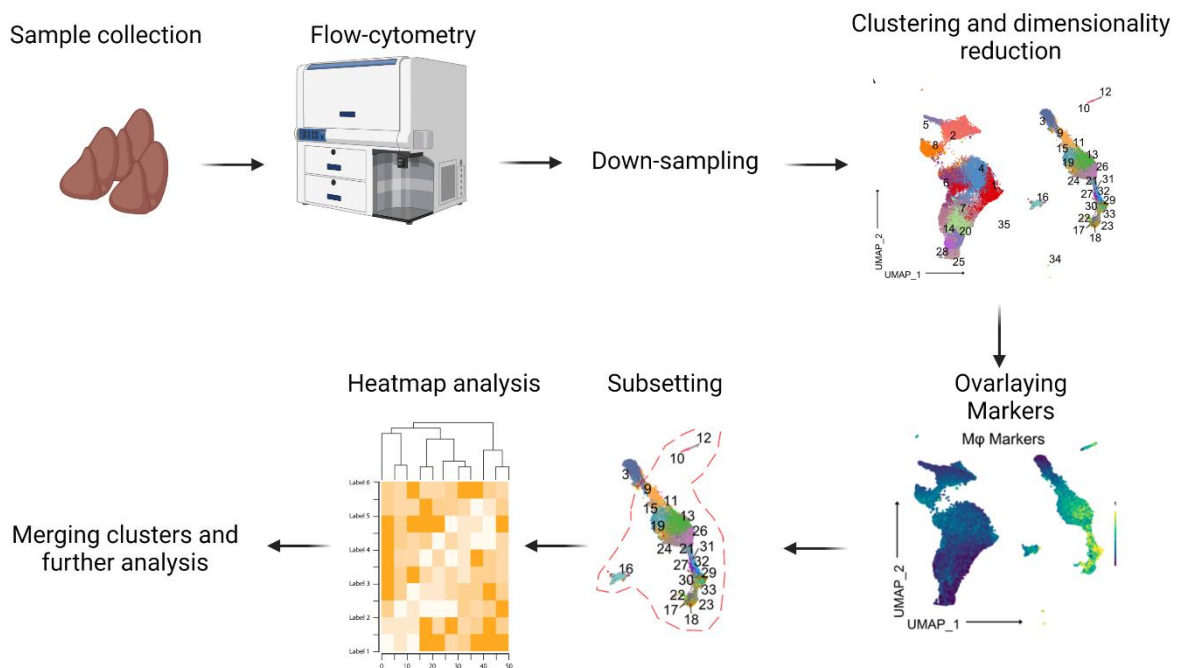


**Figure 33. The overall schematic process of analyzing the flow-cytometry data.**

The FL livers were collected and analyzed through flow-cytometry; the data was down-sampled and analyzed using cluster and dimensionality reduction. The clusters of interests were subset and further analyzed.
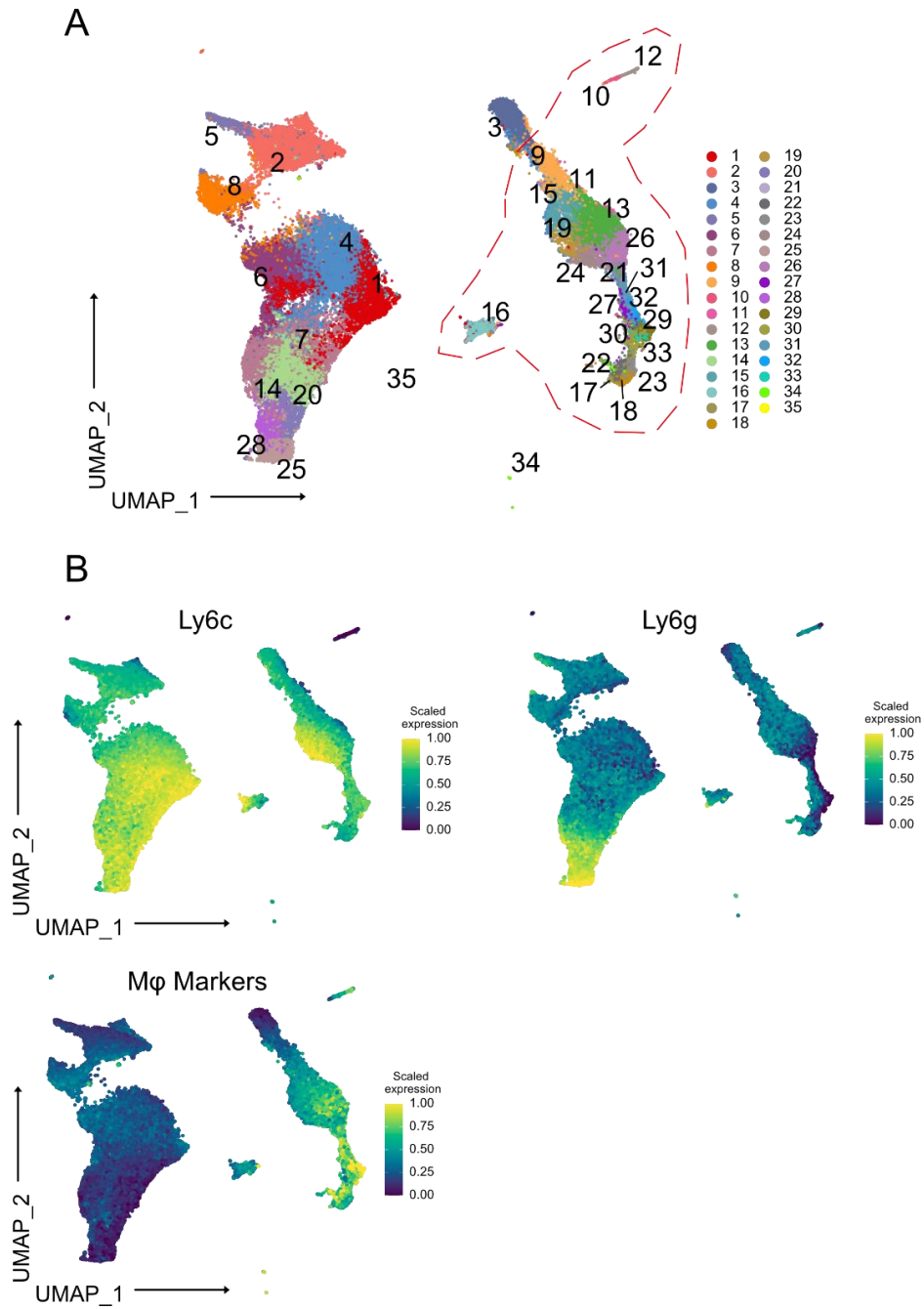
**Figure 34. The down-stream analysis of the flow-cytometry data**

**A.** UMAP plot of initial clustering of the flow-cytometry data. The red dashes indicated the selected cluster for further analysis **B.** Overlaying of Ly6c, Ly6g, and Mφ signature expression on the cells.

Based on the average expression, the clusters 1, 2, 3, 4, 5, 6, 7, 8, 14, 20, 25, 28, 34, and 35 were removed from further analysis as they were not expressing markers that could hint toward a Mφ identity of these groups. The remaining cells were re-clustered, and the UMAP was re-calculated. The re-clustering of the cells yielded 15 clusters in total (Figure 35A).
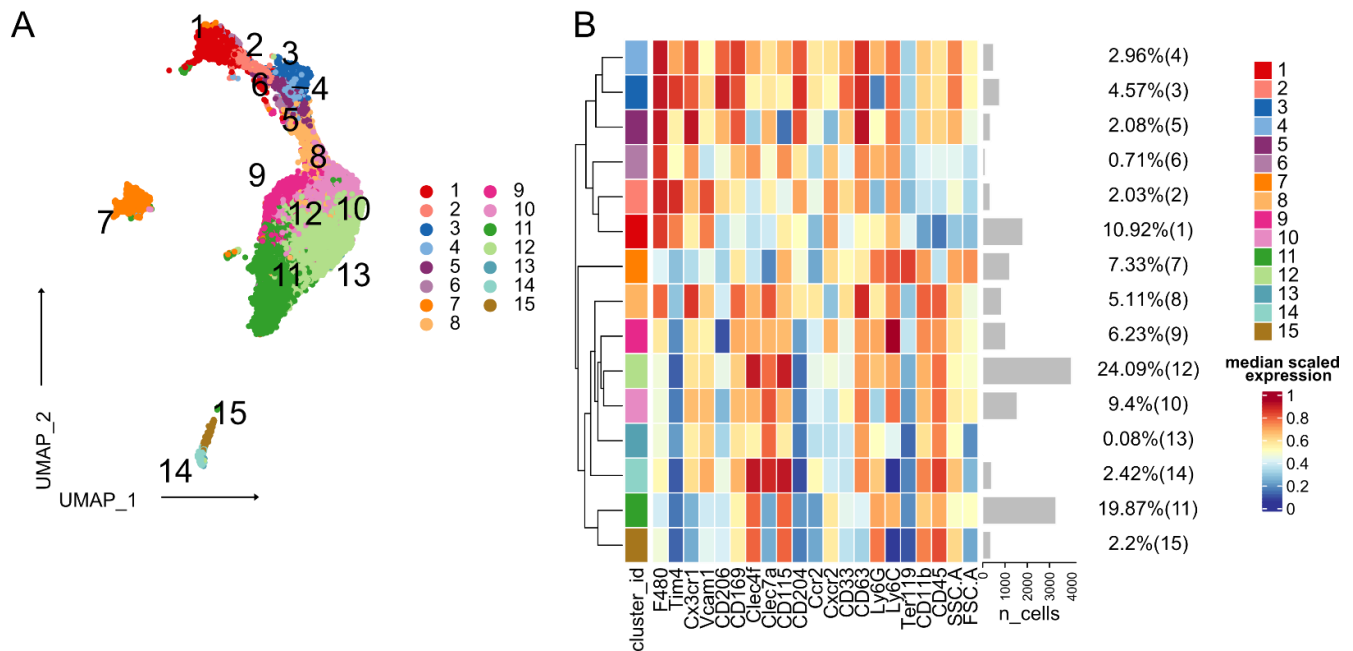


**Figure 35. The re-analysis and clustering of subset flow-cytometry data**

**A.** UMAP plot of second clustering of the subset data. **B.** The heatmap of newly generated clusters.

Considering the new cluster heatmap (Figure 35B) and the positions of clusters on the UMAP, some of the groups were merged as they were very similar, and the newly merged clusters were also re-named (Table 12).

| Old Clusters | 1 | 2 | 3 | 4 | 5 | 6 | 7 | 8 | 9 | 10 | 11 | 12 | 13 | 14 | 15 |
|---|---|---|---|---|---|---|---|---|---|---|---|---|---|---|---|
| New Clusters | A | A | B | B | B | A | C | D | G | H | F | G | H | E | E |

**Table 12. Merged clusters based on their similarity.**

Figure 36 A shows the re-calculated UMAP of the final merged clusters. The overlay of the 11 Mφ markers shows that some of the clusters express these markers higher than the others (Figure 36B). Based on the heatmap (Figure 36C), clusters A, B, and D looked the most like mature Mφ cells. The expression of clusters F, G, and H hinted toward immature/proliferating cells. Finally, cluster C was identified as the erythroblastic island and central Mφ. These clusters follow the previous results from the single-cell analysis and confirm it. The identity of

cluster E based on its expression looked very much like clusters F and G, implying that this cluster might still be differentiating toward mature Mφ cells.

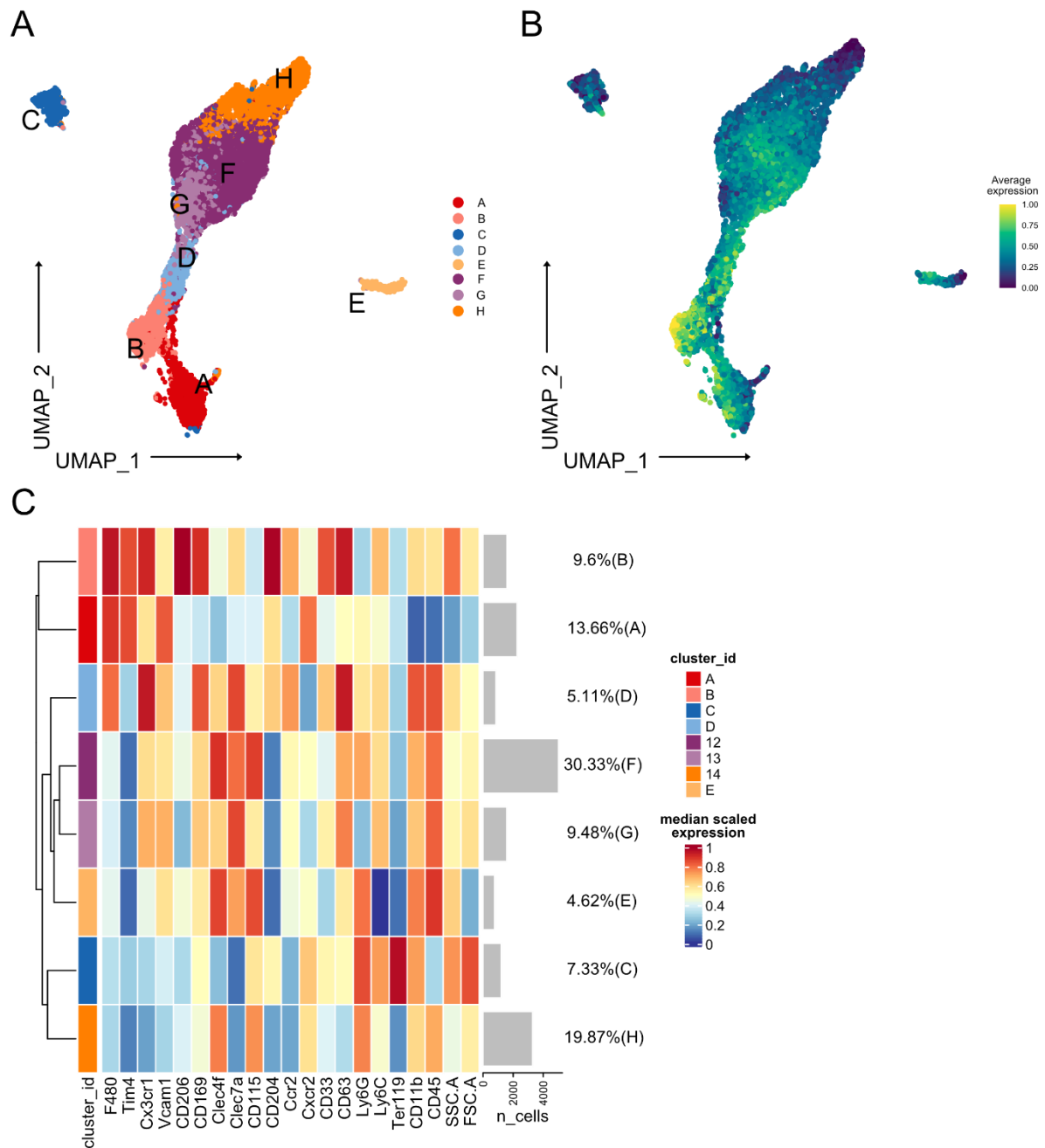

**Figure 36. The final clustering resulted from the flow-cytometry data**

**A.** UMAP plot of the final clusters after subset and merging **B.** UMAP plot of overlaid Mφ signature expression on the cells. **C.** The heatmap of final clusters.

As mentioned before, the identified clusters in the previous part belonged to *Ms4a3^{Cre}Rosa26^{eYFP}* reporter fetal livers. The same experiment was also performed on *Rank^{Cre}Rosa26^{eYFP}* and *Cxcr4^{CreERT}Rosa26^{eYFP}* fetal livers. The *Rank^{Cre}Rosa26^{eYFP}* model efficiently can label YS-derived tissue-resident Mφ (Percin, Eitler et al. 2018) while, *Ms4a3^{Cre}Rosa26^{eYFP}* and *Cxcr4^{CreERT}Rosa26^{eYFP}* models can be used for tracing monocytic-derived Mφ (Liu, Gu et al. 2019, Werner, Mass et al. 2020).

The clustering results from the flow-cytometry data identified the same clusters found in the *Ms4a3^{Cre}Rosa26^{eYFP}* FLs, the *Rank^{Cre}Rosa26^{eYFP}* and the *Cxcr4^{CreERT}Rosa26^{eYFP}* embryos (Figure 37A). All the four main Mφ clusters (A, B, C, and D) could be identified in all samples. Their marker expression correlates to each other in general despite showing some differences in intensity. Cluster E showed a heterogeneous expression of markers across different embryos. Cluster E from the *Cxcr4^{CreERT}Rosa26^{eYFP}* model was more similar to the cluster A of *Ms4a3^{Cre}Rosa26^{eYFP}* model, and the identified cluster E in *Rank^{Cre}Rosa26^{eYFP}* and *Ms4a3^{Cre}Rosa26^{eYFP}* embryos were not similar to any other clusters. It could be concluded that cluster E is most likely a differentiating cluster that contains heterogeneous cells at different stages which express the selected markers at a different level. Hence, this cluster was excluded from further analysis and comparison of the four main Mφ clusters after removal of cluster E could show an overlap of these clusters between different models (Figure 37B).
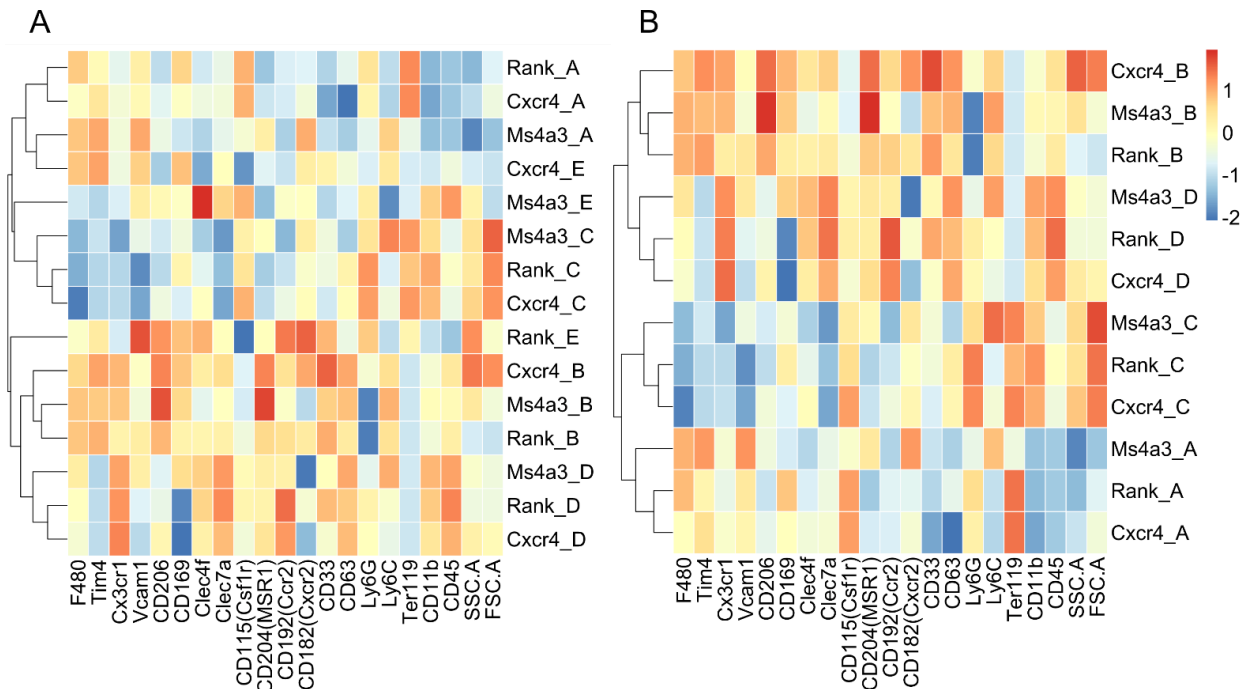


**Figure 37. The comparison of clusters among the three different fate-mapper models**

**A.** The heatmap of all possible Mφ clusters. **B.** The heatmap of four main Mφ clusters after excluding cluster E.

### 4.6.2. Flow-cytometry reveals the ontogeny of the Mφ clusters

The percentage of the cells that are expressing YFP in the $Rank^{Cre}Rosa26^{eYFP}$ samples differs between the clusters. Cluster C, which has been identified as the erythroblastic island, has the least expression, around 10%. This Rank-associated YFP expression percentage is in accordance with the fact that in an erythroblastic island, a central Mφ is surrounded by multiple erythroblasts, and Rank is not expressed in those cells. 50% of the cells in clusters A and D express YFP signal resulting from the Rank activity, which can confirm the Mφ identity of these two clusters. Cluster B has the highest cell percentage for Rank-associated YFP expression among all clusters. The YFP expression result from the $Cxcr4^{CreERT}Rosa26^{eYFP}$ model could show that only the cells in cluster C have been associated with Cxcr4 expression, which can be related to the erythroblasts generated during the second wave of hematopoiesis from HSC. The expression of YFP from the $Ms4a3^{Cre}Rosa26^{eYFP}$ model was not detected in any cluster except cluster C. Analyzing the YFP signal from the reporter mice could reveal that all of the four Mφ clusters were labeled, and they are yolk sack-derived macrophages.
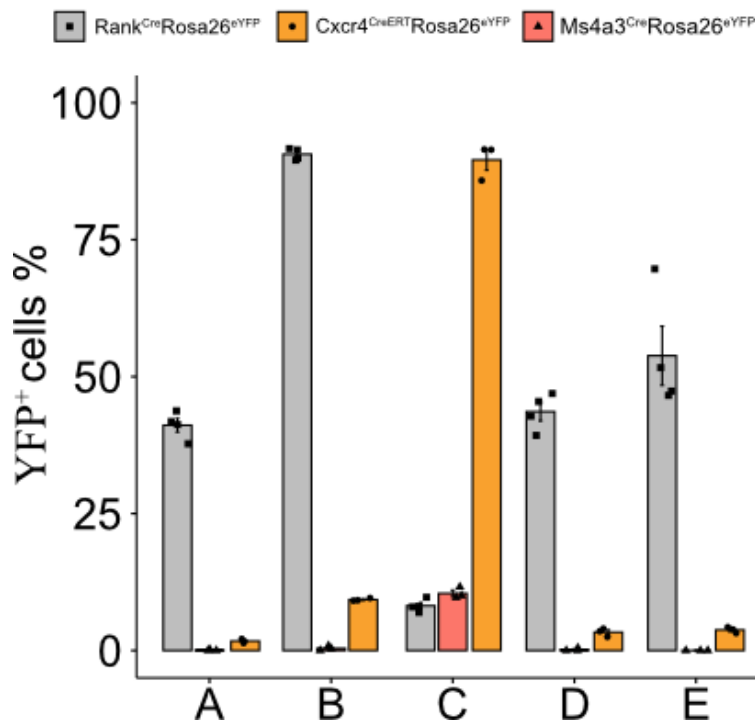


**Figure 38. The percentage of the cells within each cluster that express YFP**

### 4.6.3. Correlation of single-cell RNA-seq analysis with flow-cytometry data

A correlation matrix between the two data was calculated to confirm the similarity between the six aforementioned clusters with the results of SC analysis. In this analysis, cluster C from the flow-cytometry data was omitted as it perfectly matched with cluster 9 of the SC data, both identified as erythroblastic islands. Cluster E was also omitted due to its ambiguous and uncertain identity. Clusters F, G, and H from the flow-cytometry correlate with clusters 1 and 11 from the SC data, which resembled proliferating/immature cells (Figure 39B). Clusters A, B, and D from the flow-cytometry correspond to clusters 2, 7, and 8, resembling mature Mφ clusters.
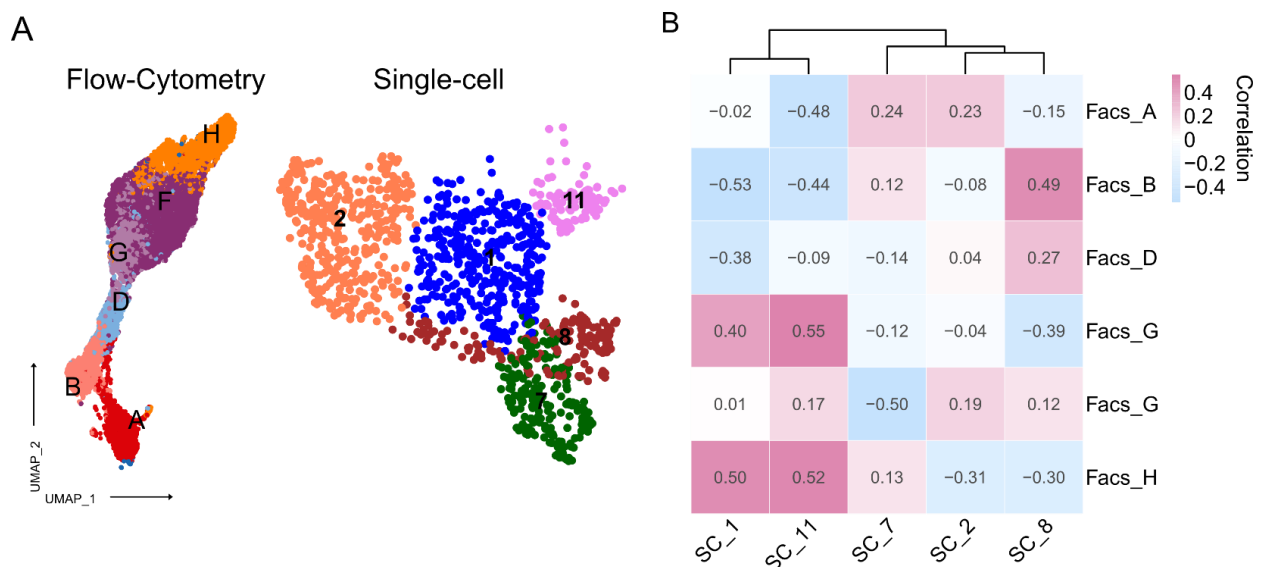


**Figure 39. The comparison between single-cell and flow-cytometry cluster**

**A.** The final clusters achieved from the flow-cytometry data and single-cell analysis (the colors have been changed to avoid confusion). **B.** The correlation matrix between the clusters of single-cell and flow-cytometry analysis

## 4.7.  Mφ heterogeneity in the human fetal liver

In order to investigate the existence of the discovered Mφ clusters from the mouse in humans, the single-cell data of human fetal liver atlas was re-analyzed (Popescu, Botting et al. 2019) with a focus on the identified Kupffer cell, the monocytes-Mφ (mono-mac) and Vcam1$^+$ erythroblastic island Mφ (Vcam1$^+$ EI Mφ) clusters. The human data sets consisted of fetal tissues between 7-17 post-conception weeks (PCW), corresponding to the mouse embryos from E12.5 and older (Xue, Cai et al. 2013).

Figure 40.A and B show the identified Mφ clusters in the mouse and the selected clusters from the human dataset. After the integration of the two datasets, the clusters from the mouse dataset were selected as a reference. In contrast, the cells in the human dataset were selected as the query. This allowed for searching the human cells that resemble the most with the identified Mφ clusters in the mouse.

Figure 28C shows the concatenated datasets from mouse and human. Projecting the mouse Mφ clusters on the human dataset showed that clusters 2, 7, and 8 from the mouse data were found in human cells. Clusters 7 and 8 were be identified among the human cells that have been assigned to the Kupffer cell cluster. In contrast, cluster 2 is primarily identified among the mono-mac cluster. Interestingly cluster 9, which represents the erythroblastic island, has been projected on the human cells assigned to the Vcam1$^+$ EI Mφ. However, some other cells from the mono-mac cluster fell into the same category (Figure 28C and D).

However, the overlay of Mφ markers from the mouse dataset on the human dataset could not show a similar expression on the human cells. Except for a few markers such as CD63 and TIMD4 that mainly were expressed on the cells projected as cluster 7, the rest of the markers were randomly expressed (Figure 28E).
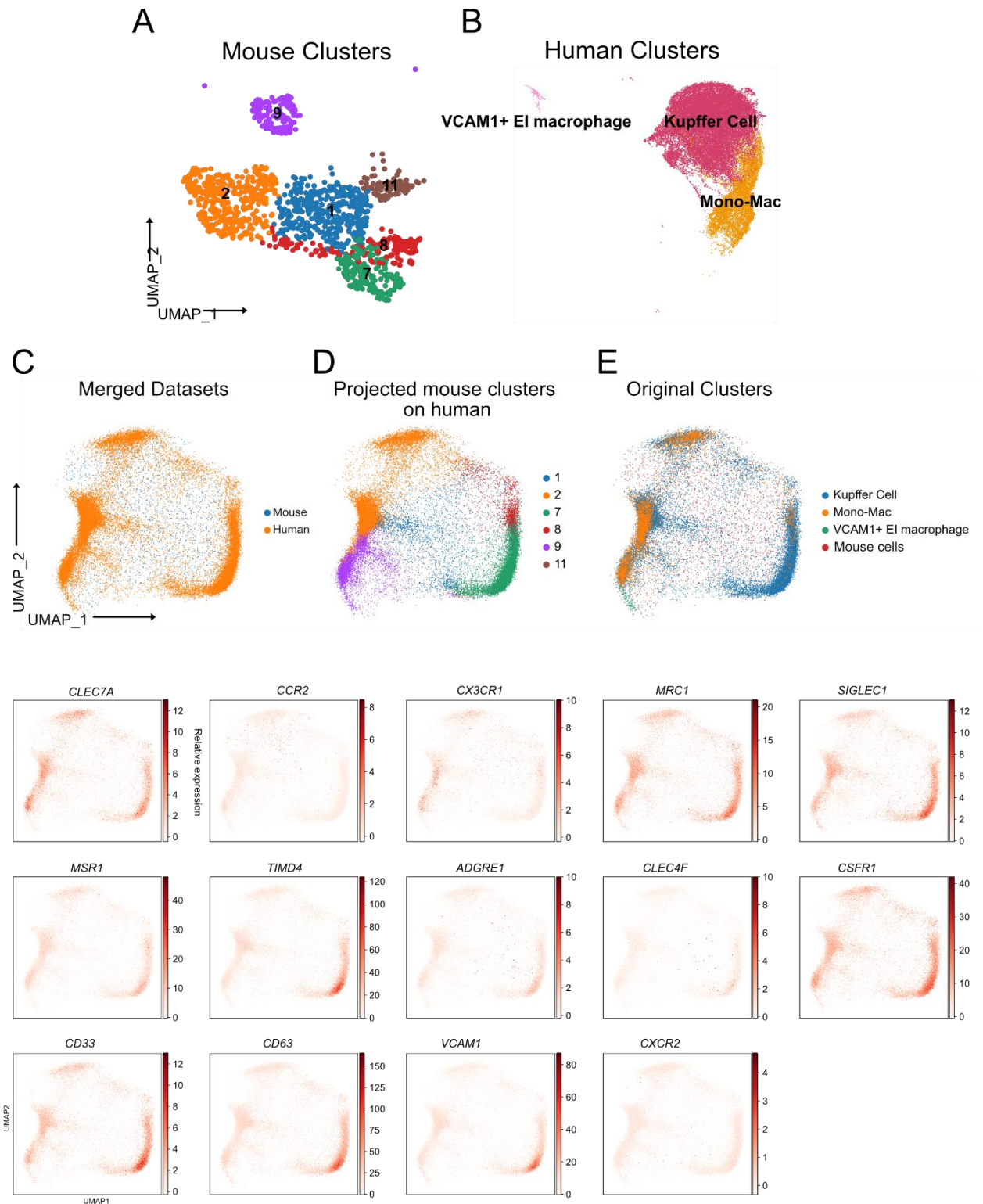
**Figure 40. Integration of the mouse and human Mφ datasets**

**A.** The mac clusters from the mouse data **B.** The mac clusters from the human data **C.** UMAP of merged human and mouse mac data **D.** The prediction and projection of five mac clusters from the mouse on the human data **E.** The original clusters from the human dataset **F.** The overlaid different markers on the integrated dataset.

## 4.8. Fetal liver macrophages interact with HSC

Macrophage heterogeneity in the mouse FL may hint towards a distinct function of subpopulations. While the interaction of macrophages with erythroblasts is well established, it remains unknown whether specific macrophage populations crosstalk with other neighboring cells, thereby contributing to distinct subtissular niches. Due to the cellular and molecular changes observed in HSC in the Pu. 1 model, we hypothesized a direct interaction between Mφ and HSC in the FL. To this end, cryosections of the wild-type fetal livers at E14.5 were stained using six markers (Figure 41). F4/80, Tim4, and Iba1 were used to identify Mφ. c-kit and CD150 were used to identify progenitors and LT-HSC. Ter119 was used to stain erythrocytes/erythroblasts.

Mφ expressing F4/80 and Tim4 interact with Ter119+ cells (top row, Figure 41.). Additionally, a direct interaction between Mφ and c-Kit+ progenitors (middle row) and CD150-expressing cells (bottom) was observed Mφ.
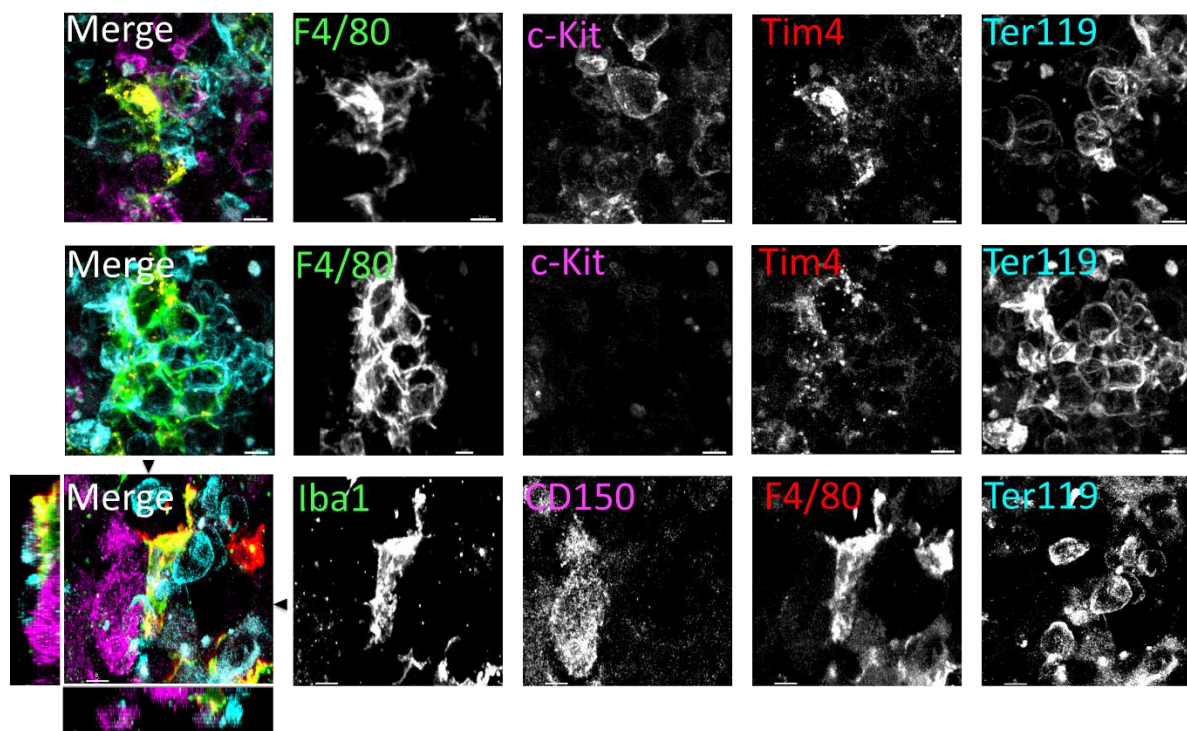


**Figure 41. The immunofluorescence staining of Mφ and HSC in the E14.5 FL.**

Immunostaining with antibodies against, F4/80, c-Kit, Tim4, Ter119, and CD150 on cryosections from E14.5 FL. The black arrows on the third row indicate the yz and xz dimensions which have been shown on the left and bottom side.

# 5. Discussion

The aim of thesis was to study the contribution and possible roles of Mφ in hematopoiesis during mouse embryogenesis at different time points. Two genetic mouse models were utilized to investigate such contributions, the Pu.1 and Id1/Id3. Using these models revealed that the depletion of Mφ affects the hematopoiesis and the enucleation of erythroblasts. Pu.1KO embryos produced more granulocytes during hematopoiesis than Pu.1$^{Ctrl}$, and the HSC differentiated into more GMPs. The depletion and changes in hematopoiesis were confirmed using immunofluorescence and CFU assay. Additionally, bulk RNA-sequencing of HSC showed transcriptome changes upon depletion of Mφ. Furthermore, a transient change in the number of enucleated erythroblasts was evident at E14.5 resulting in more nucleated erythroblasts in the Pu.1$^{KO}$ embryos than the Pu.1$^{Ctrl}$.

Confirming the effect of Mφ on HSC and hematopoiesis, the next goal of this thesis was investigating the heterogeneity of tissue-resident Mφ in the FL, their ontogeny and discovering the possible sub-population responsible for the observed changes. Using single-cell sequencing on E14.5 wild-type FL, five different sub-populations of Mφ and their precursors were discovered in addition to the central Mφ in the erythroblastic islands. Three of the five groups were identified as mature Mφ, while the other two exhibited proliferating and differentiating signatures. Furthermore, analyzing a human FL dataset could hint toward the existence of different Mφ populations.

The result of the single-cell analysis was confirmed using flow-cytometry. Investigating the ontogeny of the identified clusters using three fate-mapping models revealed that all FL Mφ clusters originated from pMacs and not HSC.

The immunofluorescence of the FL implied a direct interaction between Mφ and HSC, and a ligand-receptor analysis on the data could reveal possible ligands and receptors that are responsible for this interaction.

## 5.1. Mφ effect on the hematopoiesis

### 5.1.1. Mφ depletion across the tissues using the genetic models

Studying the effect of Mφ on hematopoiesis showed that depletion of Mφ has a significant impact on the HSC differentiation. The Pu.1$^{KO}$ embryos showed a significant loss of tissue-resident Mφ in the FL, brain and lung at E14.5, which was expected due to the critical role of Pu.1 in the development and proliferation of Mφ (Zhang, Hetherington et al. 1994, Celada, Borràs et al. 1996, DeKoter and Singh 2000). Furthermore, since a full knockout of Pu.1 affects myeloid cells and B lymphocytes development (McKercher, Torbett et al. 1996, Anderson, Smith et al. 1998), the results could also prove the efficiency of using Tnfrsf11a (also known as RANK) in selectively depleting Mφ. Mass et al. already showed that Tnfrsf11a is expressed in the fetal and adult tissue-resident macrophages but not HSC and their progeny (Mass, Ballesteros et al. 2016). Hence, using the combination of this gene and Pu.1, in the *Tnfrsf11a$^{Cre}$; Pu.1$^{flox/flox}$* model, Mφ were depleted without depletion of other cell types. However, in contrast to the initial expectation, Mφ re-populated the FL at E16.5 and E18.5. This re-population was not observed in the brain, and the lung and a significant reduction in Mφ was still evident in these tissues when comparing Pu.1$^{KO}$ embryos to the Pu.1$^{ctrl}$ at all studied time-points. The mechanism of Mφ re-population in the FL through a knocking-out of Pu.1 is not clear, and there might be different underlying reasons for this observation.

One theory could be that the re-populated Mφ differentiated from monocytes. Previous studies have already shown that the depletion of tissue-resident Mφ in the liver, whether through genetic tools or infection models, can cause the recruitment and differentiation of blood monocytes into tissue-resident Mφ (Bleriot, Dupuis et al. 2015, Scott, Zheng et al. 2016, Lai, Sheng et al. 2018, Scott, T'Jonck et al. 2018, Bonnardel, T'Jonck et al. 2019). This could also explain the higher number of F4/80$^+$ cells in the Pu.1$^{KO}$ embryos compared to Pu.1$^{Ctrl}$ as it was shown that the number of recruited monocytes could surpass the number of depleted tissue-resident Mφ. However, only a tiny percentage of the recruited monocytes can differentiate into tissue-resident cells (Guilliams, Thierry et al. 2020). Therefore, monocyte-derived Mφ are most likely able to express F4/80$^+$ but will not be able to exhibit the properties of tissue-resident Mφ.

Unlike the FL, the brain and the lung of Pu.1$^{KO}$ embryos do not show the same re-population of Mφ. However, the number of F4/80$^+$ cells increased at E16.5, but this increase cannot compensate for the loss of Mφ in the brain and the lung. At E18.5, the population drops again in Pu.1$^{KO}$ brain and lung. It can be likely that the same process of monocytes recruiting happens inside the brain, but F4/80 is not sufficient to capture the monocytes-derived Mφ;

however, due to the blood-brain barrier (BBB), this process should happen before E18.5 as by 16.5 to E18.5. The BBB is fully developed and functional (reviewed here: Haddad-Tovolli, Dragano et al. (2017)). Whether the repopulation of the Mφ could result from monocyte differentiation needs further investigations using fate-mapper models. A previous study could show upon depletion of tissue-resident Mφ in the brain using a genetic model, and the tissue-resident Mφ niche was re-populated by a combination of two subsets of Mφ; a Cx3xr1$^+$F4/80$^{low}$ Clec12a$^-$ and Cx3cr1$^+$ F4/80$^{hi}$ Clec12a$^+$ Mφ that originated directly from Ly6C$^{hi}$ monocytes (Lund, Pieber et al. 2018). Hence, it could be that using F4/80 solely, only the second population was captured. Moreover, it has been demonstrated that upon depletion of Mφ in the brain, a small subset of Mφ progenitors can regenerate the depleted cells and repopulate the brain (reviewed here: Han, Harris et al. (2017)). Therefore, further investigation in future studies would be necessary to clarify the re-population of Mφ in the brain.

A similar progression could be assumed in the lung as it has been shown that the depletion of tissue-resident Mφ in the lung can induce monocytes-derived Mφ that are identified by high expression of CD64 and CD11c (McQuattie-Pimentel, Budinger et al. 2018). It would be interesting for future studies to include other markers to analyze the re-populated Mφ in the tissues. Furthermore, genetic models such as the Ms4a3$^{TdT}$ reporter mouse could be beneficial in fate-mapping the observed Mφ population in the Pu.1$^{KO}$ embryos (Liu, Gu et al. 2019).

Coming to the Id1/Id3 mouse model, the results of Id1/Id3$^{KO}$ embryos showed a less efficient Mφ depletion in comparison to the Pu.1 model. Id1 and Id3 are co-expressed transcription regulators in pre-Mφ and Mφ (Mass, Ballesteros et al. 2016). They belong to the murine dominant negative helix-loop-helix (dnHLH) family. They can inhibit the activities of bHLH transcription factors in different cell types (Benezra, Davis et al. 1990, Christy, Sanders et al. 1991, Sun, Copeland et al. 1991, Riechmann, van Cruchten et al. 1994). So far, four members of this family have been identified; Id1, Id2, Id3, and Id4.

Id3 has a significant role in developing and maintaining tissue-resident Mφ in the liver. However, the proliferation of the tissue-resident Mφ in the liver during steady-state is not affected by Id3 deficiency (Mass, Ballesteros et al. 2016). Since Id1 and Id3 are co-expressed, it was ambiguous if the expression of Id1 could compensate for the Id3 deficiency (Jen, Manova et al. 1996, Lyden, Young et al. 1999). A recent study has shown that upon depletion of Id3, the Id1 is up-regulated (Mass, Ballesteros et al. 2016), supporting the assumption that Id1 can compensate for the Id3 deficiency; hence, a double knock-out was necessary to ensure the depletion of Mφ in combination with Tnfrsf11a$^{Cre}$. Despite having the double knock-out model, FL Mφ in Id1/Id3$^{KO}$ embryos was reduced only by around 30-40 % compared to

Id1/Id3 $^{Ctrl}$ embryos. A similar result was also evident in the immunofluorescence picture of Mφ in the Id1/Id3$^{KO}$ compared to Id1/Id3$^{Ctrl}$ FLs. Since the efficiency of the Rank-Cre model was already demonstrated in the Pu.1 model, the flow-cytometry results suggested that the double knock-out of Id1 and Id3 is either not sufficient to disturb the tissue-resident Mφ development in the FL or only a certain subset of tissue-resident Mφ in the FL depends on the Id1 and Id3 for their differentiation and not all of them. The previous study of the dnHLH family could show that Id1, Id2, and Id3 belong to the same subclass. Their expression patterns overlap in many organs, except in the tissue derived from the primitive gut. These three members are distinct from Id4, which is expressed only in neuronal tissues and in the ventral portion of the epithelium of the developing stomach (Jen, Manova et al. 1996). Considering the highly related expression pattern of Id1, Id2, and Id3, it might be that Id2 can compensate the other two proteins' role, therefore allowing proliferation and differentiation of tissue-resident Mφ.

The results from the brain were according to the expectation as Id1 and Id3 are not playing a role in the development of tissue-resident Mφ in the brain. However, the results of the lung at E16.5 showed a decrease in the number of Mφ in the Id1/Id3$^{KO}$ compared to the Id1/Id3$^{Ctrl}$. The previous studies have shown the importance of Peroxisome proliferator-activated receptors (PPARs) in developing lung tissue-resident Mφ, especially the PPAR-γ (Smith, Standiford et al. 2007, Mass, Ballesteros et al. 2016). Interestingly, it has been shown that Id1 has the highest binding affinity with PPAR-γ, and Id1 alone is sufficient to mediate the full interaction with PPAR-γ (Shi, Hon et al. 2002, Li, Kovach et al. 2008). Thus, the depletion of Id1 could impact the activity of PPAR-γ, resulting in impaired development of lung resident Mφ since it is also shown that Id2 is not able to interact with PPAR-γ. However, assuming this, it's unclear why this decrease of cells occurs specifically at E16.5 and is not evident anymore and E18.5. The technical issue in preparing the lung and doing the flow-cytometry should also not be neglected. The results could be a consequence of such issues.

Additionally, the Mφ in the lung have been shown to have two main origins; embryonic-derived and monocyte-derived (reviewed here: Evren, Ringqvist et al. (2020)). As neither of the two used models in this thesis targets the monocytes, the assumption of Mφ repopulation in the lung by monocytes should not be ignored. Altogether, further samples and mouse models would be required to validate the results.

## 5.1.2. Mφ are part of the HSC niche

The data presented in this thesis could show that upon depletion of Mφ in the FL, the hematopoiesis shifts toward myeloid linage so that more GMPs and granulocytes are produced. As presented in the result part, in the Pu.1$^{KO}$ embryos, the number of granulocytes increased at all-time points. However, only E14.5 and E18.5 were statically significant. At E16.5, despite the increase in the number of granulocytes in the Pu.1$^{KO}$, the difference is insignificant due to the data variance. Furthermore, the GMPs in the Pu.1$^{KO}$ showed a constant increase compared to the Pu.1$^{Ctrl}$ embryos, which became statistically significant at E18.5. Taking these main results together, it can be assumed that FL Mφ are part of the HSC niche along with the other cell types. It has already been shown that the FL is a unique microenvironment to HSC and can regulate them through cell-cell interactions that can be direct or by the help of cytokines (Lewis, Yoshimoto et al. 2021). However, the exact compartment and participating cell within this niche is not yet fully understood, particularly the possible role of Mφ within this niche.

The immunofluorescence results performed on wild-type E14.5 FL provided an insight into possible Mφ-HSC interaction. The results showed that many of the Mφ were interacting with Ter119$^+$ cells, indicating the erythroblastic islands. Additionally, an interaction between F4/80$^+$, Tim4$^+$ Mφ, and Kit$^+$ cells was evident in the result. F4/80 is a glycoprotein that is highly expressed on most resident tissue Mφ and is one of the most specific surface markers for mouse Mφ (Austyn and Gordon 1981, Morris, Graham et al. 1991). T-cell immunoglobulin and mucin domain-containing 4 known as Tim-4, is a phosphatidylserine receptor and it has been shown that it can be selectively expressed in Mφ and other antigen-presenting cells (Wong, Valdez et al. 2010). The FL-stained sections could interestingly show that not all Mφ have interaction with Kit, but some exhibited this interaction. The Kit role in the maintenance and survival of HSC is well recognized. However, the expression of Kit is not limited to the HSC, and the progenitor cells express this marker (Pietras, Reynaud et al. 2015). This could also imply the interaction between the Mφ and progenitors. Although the cooperation of Mφ and progenitor cells during tissue repair has been reported before (Anghelina, Krishnan et al. 2006) but the direct interaction between the Mφ and progenitors in the FL has not been reported.

In order to exclude the possible progenitors other than the HSC from the result, further staining using CD150 antibody together with Iba1 antibody was performed. CD150, also known as SLAM (signaling lymphocyte activation molecule) is a surface marker that has been reported to express on LT-HSC (Kiel, Yilmaz et al. 2005). Ionized calcium-binding adaptor molecule 1

Iba1) is a protein whose expression is restricted to Mφ (Imai, Ibata et al. 1996). The staining results using these two markers could demonstrate an interaction between a CD150⁺ HSC and an Iba1⁺ Mφ, which has not been reported before.

In conclusion, the staining results could indicate a direct interaction between Mφ and HSC. This interaction could be vital for the maintenance and function of HSC during hematopoiesis. However, the nature of this interaction and the possible ligands and receptors that might be involved need further investigation.

Previous studies have already demonstrated the importance of HSC interaction with other cell types. One of the best-known communications of HSC within the niche is their interaction with Nestin⁺ stromal cells that are adjacent to portal vessels. This interaction is crucial for HSC expansion through producing angiopoietin-like 2 and 3 (Angptl2, 3). (Zhang, Kaba et al. 2006, Chou and Lodish 2010, Khan, Mendelson et al. 2016). Endothelial cells, another type of stromal cell, have been reported to express membrane-bound SCF, support erythropoiesis, and role in HSC expansion (Neo, Booth et al. 2018). To this date, the role of Mφ in the HSC niche in the FL has been described as a third-party that is acting as a mediator between HSC and the hepatocytes. The development of the HSC and progenitors happens around the same time as the hepatic linage, and this has led to a complex interaction network that is still not fully defined (Figure 42) (Soares-da-Silva, Peixoto et al. 2020) but has also been observed in the human (Yong, Keng et al. 2016).

As mentioned before, Mφ has a mediator role within this network. A previous study has shown that Mφ in the FL release Oncostatin M (OSM), which is crucial for hepatocyte differentiation (Kamiya, Kinoshita et al. 1999). Furthermore, Dlk1⁺ fetal hepatic progenitors secrete SCF and Epo, which are crucial for HSC expansion. SCF-signaling is known to be necessary for definitive hematopoiesis (Ogawa, Nishikawa et al. 1993, Sugiyama, Kulkeaw et al. 2011). Hepatoblasts express angptl3, in addition to alpha-fetoprotein (AFP), CXCL12, and essential hematopoietic cytokines, including SCF, thrombopoietin (TPO), and insulin-like growth factor 2 (IGF2). Therefore, it can be assumed that Dlk1+ fetal hepatoblasts can secrete essential hematopoietic cytokines to support HSC expansion (Sugiyama, Kulkeaw et al. 2011).
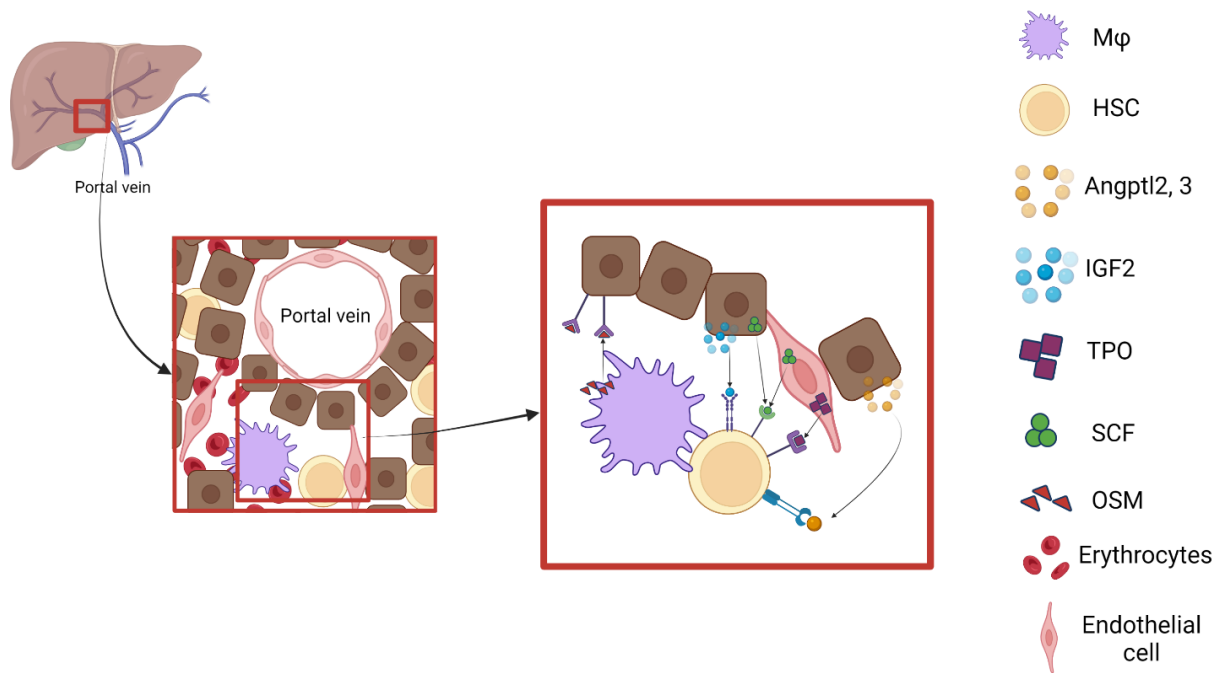
**Figure 42. The HSC niche in the fetal liver and cellular cross talk.**

Mφ produce OSM to promote the maturation of hepatocytes, and the mature hepatocytes produce IGF2, TPO, and angptl2 and 3, which is received by HSC as they also get SCF from endothelial cells. (Figure was adapted from Lewis, Yoshimoto et al. (2021) and recreated using biorender.com)

Taken together, previous studies and the results presented in this thesis indicate that the role of Mφ in the HSC niche is more than just supporting the HSC indirectly through hepatoblasts. In support of this assumption, a recent study in zebrafish showed that VCAM$^+$ Mφ are required to guide and retain HSC in their embryonic niche through a binding to α4-integrin expressed on the HSC (Li, Xue et al. 2018). Further, Mφ play a role in the migration of the HSC from the FL to the BM. The migration of the HSC from the FL to the BM happens as soon as the fetal BM is generated, and this process is facilitated by the help of different cytokines, ECM signals and adhesion molecules such as Cxcl12 and SCF (Ciriza, Thompson et al. 2013). It has been shown that Mφ provide and modulate the accessibility of HSC to Cxcl12 by expression of Mmp9 (Theodore, Hagedorn et al. 2017). Hence, it can be expected that the HSC number in the FL might exceed slightly by the time due to the slower migration to the BM upon depletion of Mφ. This slight increase could be observed in both Pu.1$^{KO}$ and Id1/Id3$^{KO}$ embryos. However, this was not statistically significant due to the variability of the data. Hence, it would be interesting for future studies to analyze the number of HSC also in the BM.

One of the important changes observed in the hematopoiesis was the increase of the GMPs and granulocytes in the Pu.1$^{KO}$ embryos, which were also confirmed by the CFU analysis. The bulk-RNA analysis of the Pu.1$^{KO}$ and Pu.1$^{Ctrl}$ embryos could show the underlying changes in

the gene expression of the HSC that were caused most likely due to the lack of interactions with the Mφ. The Gene Ontology (GO) highlighted the main function of the differentially expressed genes (DEG). The function of DEGs were in line with the changes in the number of GMPs and granulocytes and also the observed changes in the erythropoiesis.

Many of the up-regulated genes in the Pu.1[KO] embryos had a role in myeloid cells differentiation and maturation in addition to the genes that were responsible for definitive hematopoiesis. Furthermore, among the down-regulated DEGs in the Pu.1[KO] embryos, several genes had a role in erythrocyte hemostasis and the heme metabolic process. These findings support the essential role of Mφ in hematopoiesis. The results from the both Pu.1[KO] and Id1/Id3[KO] embryos showed that Mφ deficiency can delay the enucleation of erythroblasts. This effect could be seen at E14.5 embryos. The relation between the Mφ and erythroblasts within the erythroblastic islands has been described in different studies (de Back, Kostova et al. 2014). Previous data has shown that erythroblastic islands contain a Mφ surrounded by developing erythroblasts. Within this structure, Mφ actively participate in erythroblast development by providing iron for heme synthesis and phagocytosing expelled nuclei during final erythroid differentiation (Chasis 2006). It has been suggested that Mφ promote erythropoiesis by directly transferring iron to erythroid progenitors (Zhang, Hetherington et al. 1994, Celada, Borràs et al. 1996). Hence, the deficiency of Mφ can interrupt this process which could be one of the reasons that the percentage of erythrocytes has dropped in KO embryos.

The deficiency of erythrocytes due to the malfunctioning of Mφ has also been reported previously. It has been demonstrated that abnormal Mφ can directly affect erythroblastic island function. In severe cases, this can lead to lethal anemia (Clarke, Maandag et al. 1992, Jacks, Fazeli et al. 1992, Lee, Chang et al. 1992). The interaction between the central Mφ and the erythroblasts occurs via several interactions, which have been summarized in Figure 43; therefore, the impairment of any of them could impact the erythrocytes formation.

One of the essential interactions has been identified via Erythroblast macrophage protein (Emp) that is expressed on the surface of both central macrophages and erythroblasts and promotes binding between the two cell types. Lack of this interaction can promote apoptosis among erythroblasts and leads to aberrant erythropoiesis (Hanspal and Hanspal 1994, Hanspal, Smockova et al. 1998). Additionally, several adhesion molecules found on the Mφ within the erythroblastic islands, such as CD163 and CD169, have a confirmed role in promoting proliferation and maintenance of erythropoiesis (Fabriek, Polfliet et al. 2007, Chow, Huggins et al. 2013). Another crucial molecular interaction between the Mφ and erythroblast happens between the α4β 1 integrin (Very Late Antigen 4; VLA-4) on erythroblasts and

vascular cell adhesion molecule 1 (Vcam-1) on Mφ (Sadahira, Yoshino et al. 1995, Ulyanova, Jiang et al. 2011). Another known interaction contributing to the decreased number of erythrocytes in KO embryos is between intercellular adhesion molecule 4 (ICAM-4) expressed on erythroblasts and αV integrin on Mφ (Lee, Spring et al. 2003, Lee, Lo et al. 2006). This interaction has a vital role in maintaining the erythroblastic island integrity; hence, its disruption can lead to a diminished number of erythroblastic islands.
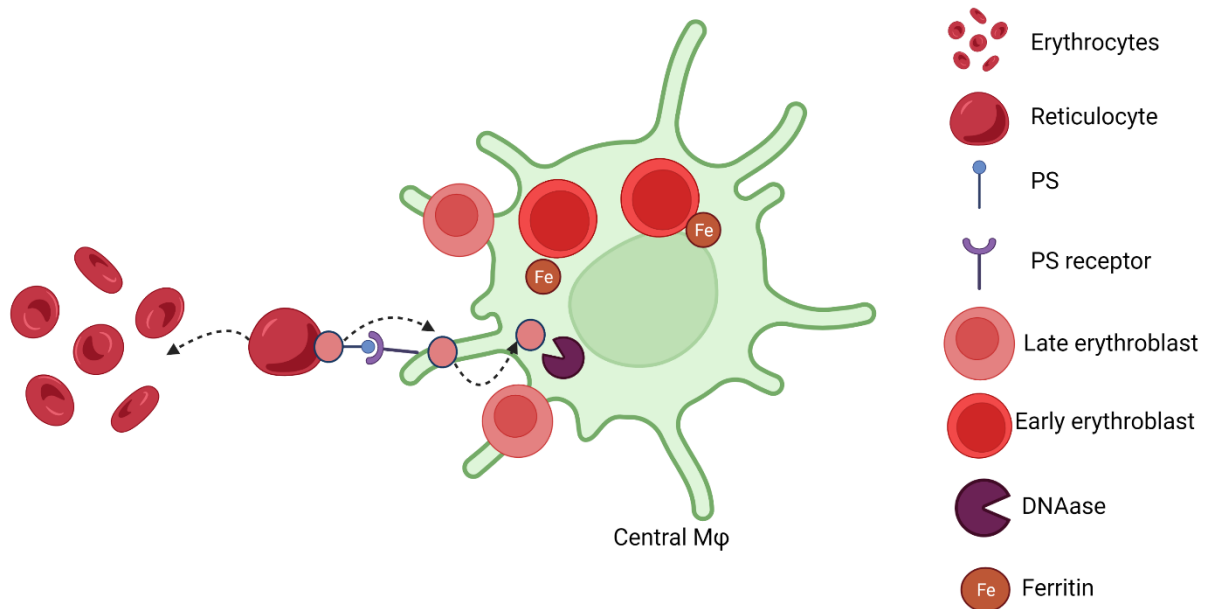


**Figure 43. Role of Mφ in erythropoiesis.**

Mφ not only provide iron for developing erythroblasts but also phagocytose expelled nuclei. The expelled nuclei expose phosphatidylserine (PS) on their surface and bind with the PS receptors, and will be phagocytosed. The expelled nuclei will be broken by DNaseII (Figure was adapted from de Back, Kostova et al. (2014) and recreated using biorender.com)

In summary, considering the results from the flow-cytometry analysis, it could be concluded that the deficiency of Mφ in the KO embryos impaired the essential interactions between the Mφ and erythroblasts, which most likely led to more apoptosis and less differentiation of erythroblasts. In KO embryos at E14.5, the erythroblasts most likely were stressed due to their limited access to iron. However, the results did not significantly change between different stages of erythrocyte maturation in KO and Ctrl embryos at the same time-point. Considering the re-population of the FL at E16.5 and E18.5, it could be assumed that the generated F4/80+ cell could interact with erythroblasts, leading to sufficient enucleation of erythroblasts in KO embryos later during embryogenesis. Nevertheless, concerning the role of Mφ in the maturation of erythrocytes, it would be interesting to investigate the maturation states of erythroblasts using more samples and also by the total cell numbers in each phase instead of looking into the percentages.

Exploring the DEG result further, one of the interesting functions of them was their role in myeloid cell development. Interestingly these genes were found in both down and up-regulated lists. Investigating these genes showed that the up-regulated ones have a role in GMPs and granulocytes modulation and differentiation, while the down-regulated genes were important for the development and maintenance of the Mφ.

In LT-HSC from the Pu.1$^{KO}$ samples, particular genes such as *Gata2*, *Gata3*, *Kit*, and *Jak3* were significantly upregulated compared to the Pu.1$^{Ctrl}$ embryos. Previous studies have shown the importance of the *Gata2* and *Gata3* for maintaining HSC (Orkin 1995, Orkin 2000). *Gata2* acts as a crucial regulator of HSC and their committed progenitor cells (Rodrigues, Tipping et al. 2012). Furthermore, *Gata2* is well known for expanding immature HSC (Tsai, Keller et al. 1994, Tsai and Orkin 1997, Yoshida and Georgopoulos 2013). Thus, *Gata2* could be one of the leading role players in increasing GMPs and granulocytes. The *Gata2* deficient mice have shown fewer GMPs than the control mice (Rodrigues, Boyd et al. 2008). Also, a previous study from *Gata2* heterozygote (Gata2$^{+/-}$) mice displayed reduced GMPs in colony-forming cell (CFC) and serial re-plating CFC assays (Rodrigues, Boyd et al. 2008). Another study done in humans could show that the deficiency of *Gata2* leads to a lack of production of granulocytes (Huang, Du et al. 2015). These data highlight the importance of *Gata2* regulation for GMPs and granulocytes. They indicate that the up-regulation of *Gata2* could be one of the main reasons of the observed increase of granulocytes in Pu.1$^{KO}$ embryos.

Similar to *Gata2*, *Gata3* can also regulate HSC maintenance and differentiation. It has been previously in different studies demonstrated that *Gata3* is abundantly expressed in LT-HSC and is required for maintaining the number of LT-HSC (Fitch, Kimber et al. 2012, Ku, Hosoya et al. 2012, Frelin, Herrington et al. 2013). This could also suggest that the dysregulation of the *Gata3* in the absence of Mφ led to a slight increase of the LT-HSC in both Pu.1$^{KO}$ and Id1/Id3$^{KO}$ embryos. Despite the evident effect of Mφ deficiency on the expression of *Gata2* and *Gata3*, the mechanism of this dysregulation is not clear. However, it is already known that several transcription factors that play a role in the Wnt and Notch signaling pathways participate in regulation (Trompouki, Bowman et al. 2011, Guiu, Shimizu et al. 2013). A recent study in humans has identified several genes that could potentially activate *Gata2,* such as *CXXC1, BRCA1, ERG1,* and *PPARD (Saito, Fujiwara et al. 2015).* The ERG*1,* and *PPARD* have already been identified as important for Mφ. *Egr1* has an essential role in regulating Mφ differentiation and is expressed within Mφ differentiating cells (Nguyen, Hoffman-Liebermann et al. 1993, Krishnaraju, Hoffman et al. 2001). PPARD belongs to the PPAR family which their role in Mφ function has been recognized however, the knowledge over their role in molecular and cellular signaling in immune cells is limited (Toobian, Ghosh et al. 2021). All in all, it is

possible that the lack of Mφ might disturb the signaling pathways important HSC, leading to dysregulation of several genes such as *Gata2*.

*Kit* expression and its signaling have a significant role in regulating HSC function. Previous studies have shown that deficiencies of Kit can lead to a reduced number of HSC (Yee, Paek et al. 1994, Miller, Rebel et al. 1996). It has been observed that gain of function mutations in *K*it result in a noticeable expansion of myeloid cells (Bosbach, Deshpande et al. 2012). The up-regulation of *Kit* could be a direct response of HSC to the lack of necessary cell-cell interactions with Mφ and an attempt to promote Mφ differentiation as studies have shown that binding of the Kit receptor with the stem cell factor (SCF) induce a chain of signaling events that can result into cell differentiation (Bernstein, Forrester et al. 1991, Antonchuk, Hyland et al. 2004). *Jak3* belongs to one of four members of Janus kinases, a family of non-receptor tyrosine kinases involved in different cytokine-mediated aspects of immunity (Shuai and Liu 2003). It is expressed at low levels in immature HSC, and its expression is up-regulated during the differentiation of HSC. The role of *Jak3* in the development of the lymphoid lineage such as B cells and T cells is well characterized (Nosaka, van Deursen et al. 1995, Park, Saijo et al. 1995, Thomis, Gurniak et al. 1995). It has also been shown that overexpression of *Jak3* can accelerate granulocytic differentiation, which is associated with growth arrest in the G1 phase in the cell cycle (Rane, Mangan et al. 2002).

As aforementioned, while the up-regulated genes that played a role in myeloid cell development mainly took part in GMPs and granulocytes differentiation, the down-regulated genes are vital for Mφ development, particularly *Id2*, *Klf1, Csfr1*, and *C1qc* were down-regulated in the Pu.1$^{KO}$ LT-HSC compared to Pu.1$^{Ctrl}$. The role of these genes for Mφ development has been investigated in several studies (Sontheimer, Racila et al. 2005, Stanley and Chitu 2014, Mass, Ballesteros et al. 2016, Mukherjee, Xue et al. 2021). It can be assumed that down regulation of these genes is a direct result of the inability of HSC for differentiation into Mφ. Based on this data, it can be assumed that the lack of Mφ interaction with HSC has forced these cells into differentiation into GMP, which has been reflected in the up-regulated genes but, at the same time, the inability of HSC for differentiation into Mφ has led into down-regulation of Mφ associated genes.

In conclusion, the result of bulk-RNA sequencing from the Pu.1 mouse model could shed light on transcriptional changes that HSC undergo upon depletion of Mφ. These results indicate an essential role for Mφ in hematopoiesis during embryonic development. Lack of Mφ within the FL has resulted in up-regulation of important genes for definitive hematopoiesis and myeloid differentiation, while genes associated with Mφ development and homeostasis of cell number have been down-regulated.

## 5.2. Characterization of Mφ heterogeneity in the fetal liver using single-cell OMICs

The results from the flow-cytometry could show an impact of Mφ on the hematopoiesis. Furthermore, the bulk-RNA sequencing analysis also revealed that HSC gene expression profile changes upon depletion of M, confirming the contribution of Mφ in HSC maintenance. These results opened a new vista about Mφ's role in the HSC niche. Nevertheless, at the same time led to some questions regarding the heterogeneity of Mφ in the fetal liver. Heterogeneity of Mφ across different tissues is already well-known and investigated (Gordon and Pluddemann 2017). However, the heterogeneity of Mφ within the FL is still not well studied. Considering the different functions of Mφ, this thesis also aimed to study the existence of possible different populations of Mφ in the FL and whether all Mφ populations can interact with HSC or not.

A single-cell analysis on E14.5 wild-type FL was performed to answer those questions, and CD11b$^+$ F4/80$^+$ cells were sorted and prepared for library preparation and sequencing. After quality control, the sequencing results were analyzed, cleaning up the data followed by subsetting the data to exclude cell types other than Mφ (Figure 26). The final analysis revealed six clusters that resembled the Mφ based on their gene expression. Among these clusters, the erythroblastic islands were also recognized as one cluster (cluster 9 from the single-cell analysis) based on its high expression of genes related to erythroblasts/erythrocytes in addition to the expression of Mφ markers such as Csf1r and Clec7a. This cluster also has been recognized in human FL in a previous study (Popescu, Botting et al. 2019). The expression of the aforementioned genes was relatively low, but this can be because, in an erythroblastic island, a central macrophage can be surrounded by multiple erythroblasts. The exact number of surrounding cells in the mouse is yet to be determined. However, previous studies in rats and humans have shown as many as 10 and 30 erythroblasts per Mφ, respectively (Lee, Crocker et al. 1988, Yokoyama, Kitagawa et al. 2002).

The analysis of the other five clusters could show that all of these groups express genes essential for Mφ fate and development. All of the five clusters were expressing Csf1r. Csf1r is expressed in the fetal macrophages and their progenitors that are found in the yolk sac. It is a highly conserved gene among different species and has been shown to be crucial for proliferation, differentiation, and survival of Mφ (Sherr, Rettenmier et al. 1985, Garceau, Smith et al. 2010, Wang, Kono et al. 2013). Clec7a (Dectin-1) was also among the expressed genes in the five clusters. This gene encodes a lectin-like innate immune receptor that can bind to beta-glucans; hence, it has a vital role in the recognition and phagocytosis of pathogenic fungi

by Mφ (Lefevre, Gales et al. 2010, Dambuza and Brown 2015). Another vital gene expressed by these clusters was $Cx_3cr1$, a member of the seven-transmembrane G-protein coupled receptor (GPCR). It can bind to its sole ligand, $Cx_3cl1$ (fractalkine or neurotactin). $Cx_3cr1$ is involved in the colonization of pre-Mφ at the embryonic stage and their differentiation into tissue-resident macrophages (Mass, Ballesteros et al. 2016). Although $Cx_3cr1$ can be expressed by monocytes, T cells, natural killer cells, and smooth muscle cells (Julia 2012, White and Greaves 2012), it is not expressed in fetal liver-derived monocytes or their precursors (Yona, Kim et al. 2013). Hence, making it a unique marker for detection of Mφ at early time points of development. Despite having the expression of these genes in common, the five clusters express further Mφ markers in which they show a different level of expression, making them distinct populations from each other, e.g., cluster 7 expresses Vcam1 abundantly.

In contrast, other clusters either do not express it or express it at a very low level. Vcam1 has been previously shown to be expressed on the surface of Mφ (Yona, Kim et al. 2013, Sharma, Sharma et al. 2017). It can regulate trans-endothelial migration of leukocytes, including Mφ (Deem, Abdala-Valencia et al. 2007). More interestingly, $Vcam1^+$ Mφ have been shown recently to be essential for guiding HSC and the progenitor cells during their migration to caudal hematopoietic tissue of zebrafish, which is equivalent to the FL in mammals (Li, Xue et al. 2018). Investigating other clusters indicated that Msr1 expression is unique to cluster 8, and Ccr2 expression is exclusive to cluster 2. The macrophage scavenger receptor 1 (Msr1) is expressed on myeloid cells, such as macrophages and dendritic cells and participates in different pathophysiological events, such as host defense, endotoxemia, and endocytosis (Areschoug and Gordon 2009, Kelley, Ozment et al. 2014). Ccr2, similar to $Cx_3cr1$, is also a GPCR and is the main receptor for Ccl2. Ccl2 role has been described as a chemoattractant through binding to Ccr2 on monocytes, Mφ, and lymphocytes (Balkwill 2003). Considering the cluster 2 expression profile, the Ccr2 gene might suggest that either majority or part of these cells are monocytic-derived rather than embryonic-derived.

Despite expressing important Mφ markers on cluster 1, this cluster did not express any specific marker distinguishing it from the rest of the groups. Instead, the absence of any other Mφ markers made this cluster distinct. The top expressed genes in this cluster revealed that it expresses genes found on proliferating/differentiating cells such as Dach1 and Adcy3. The top expressed genes in cluster 11 showed a similar expression pattern to cluster 9. This cluster expressed genes such as Ctsg, Mpo, and Elane, which are also only expressed on cluster 9. Both clusters 9 and 11 expressed Cd63; however, the expression of this gene was more abundant on cluster 11 compared to cluster 9. Taking all of these observed results, it

was concluded that these five clusters have an Mφ fate. However, among these five groups, the expression profile of clusters 2, 7, and 8 hinted toward already mature/adult Mφ cells.

In contrast, cluster 1 expression implied proliferating and still differentiating cells. Cluster 11, due to its high resemblances to cluster 9, could be interpreted as differentiating cells that most likely would participate in the erythroblastic islands. Furthermore, a gene ontology (GO) analysis using the top 100 DEGs of each cluster confirmed the aforementioned speculations over the identity of the identified cluster. All three clusters 2, 7, and 8 expressed genes that indicated their Mφ fate while still exhibiting different functions from each other (Figure 44).
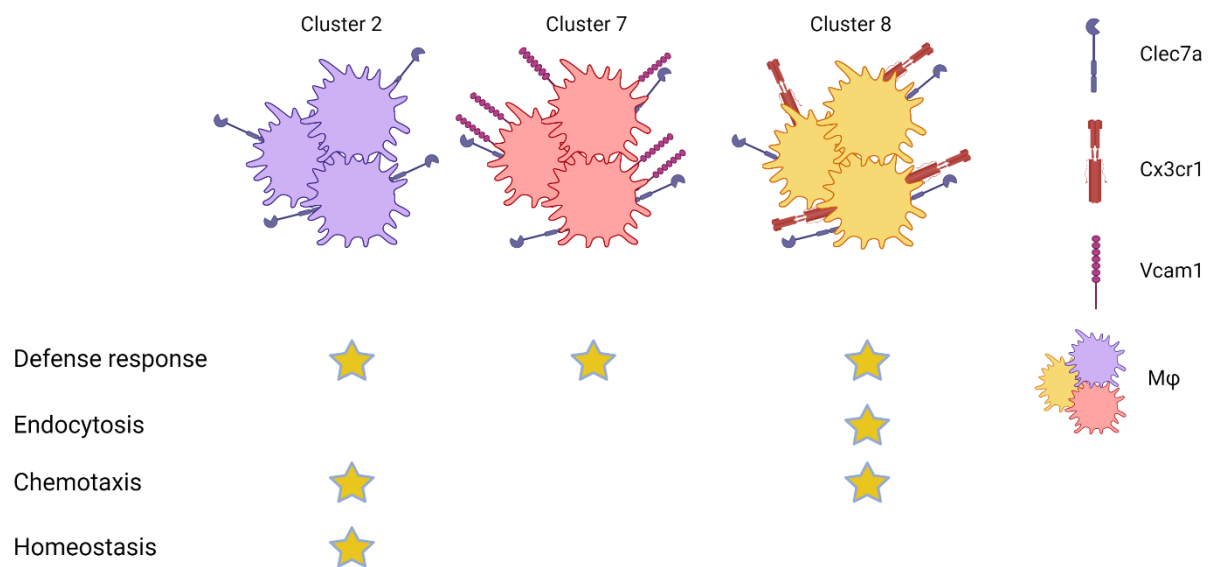


**Figure 44. Different functions of three main identified Mφ clusters based on the GO analysis.**

(Figure was created using biorender.com)

In the next step, a psuedotime analysis using the Partition-based graph abstraction (PAGA) method (Wolf, Hamey et al. 2019) was performed to analyze the trajectory of these groups. The PAGA algorithm allows a reconstructing of the lineage relations of a whole adult animal (Plass, Solana et al. 2018) mainly due to its data-driven formulation. It also has been shown that the manifold learning algorithms in PAGA can converge faster.

Cluster 1, 2, 7, 8, and 11 were analyzed for their lineage relations using this method. Cluster 9 was excluded from this analysis mainly due to two reasons; firstly, the identity of this cluster was already pretty evident secondly and most importantly, this group expressed genes related to hemoglobin such as Hba-a2 at a very high level that this high expression disturbed the initial KNN graph that is supposed to represent the high-dimensional gene expression and use it for further neighborhood relation computations.

The PAGA analysis results could show that cluster 1 relates with all other four clusters, confirming the previous conclusion that cluster 1 is not fully mature and is still differentiating. This result suggests that cluster 1 can give rise to the other clusters. The most robust relation for this cluster was observed with cluster 11, indicating a high similarity between those two clusters. Considering the expression profile and GO analysis of these two clusters, it can be concluded that cluster 11 consists of a mixture of mature/differentiated cells and is still proliferating/differentiating cells. Investigating the graph further, a close relation between clusters 7 and 8 was evident, corresponding to these two groups' gene expression. Based on this connectivity, two scenarios are probable. The first one would be that clusters 7 and 8 are at the final phase of maturation, and they would finally merge together at later time points. The other scenario would be that these two clusters are distinct populations despite their high similarity. Each of them is specialized for a function within the tissue. In addition to PAGA, a psuedotime analysis was performed on these five clusters. Its results further confirmed the inference made over the trajectory of these clusters.

Taken all the results together, the single-cell analysis of Mφ indicated heterogeneity of these cells within the FL at E14.5 with at least four distinct mature cells among the six identified clusters; however, whether these populations would persist at later time points or not require further investigation and study.

### 5.2.1. Flow-cytometry data; a complementary picture to single-cell OMICs

The single-cell RNA-Sequencing approach could show the heterogeneity of Mφ in the FL. However, there are always questions about whether the expression of genes will be translated into a protein level, making the genes a conclusive marker for the identity and function of the identified clusters or not. Hence, to answer this question and confirm the existence of the identified clusters, in the next step, using the DEG results, a set of genes that encode surface markers that could be used to detect the different identified Mφ clusters were selected and used as a staining panel (see material methods Table 1) in a flow-cytometry experiment to validate the expression of these genes at the protein level. This attempt was performed using the FL of three fate-mapper mice, namely, *Rank^{Cre}Rosa26^{eYFP}*, *Ms4a3^{Cre}Rosa26^{eYFP}*, and *Cxcr4^{Cre}Rosa26^{eYFP}*, to simultaneously also address the Mφ fate and ontogeny of the different identified Mφ clusters.

The *Rank^{Cre}Rosa26^{eYFP}* reporter mouse could be used to confirm the Mφ fate of the clusters since it has been shown that it efficiently can label YS-derived tissue-resident macrophages (Percin, Eitler et al. 2018). Using both the *Ms4a3^{Cre}Rosa26^{eYFP}* and the *Cxcr4^{Cre}Rosa26^{eYFP}* mice, the monocytic fate of these Mφ clusters was investigated. Ms4a3 has been shown to be

efficient in tracing monocytes. The *Cxcr4$^{Cre}$Rosa26$^{eYFP}$* model can permanently label HSC and distinguish HSC-derived monocytes from the other cell types (Liu, Gu et al. 2019, Werner, Mass et al. 2020).

The E14.5 FLs of these mice were prepared and stained using the generated panel and analyzed using the flow-cytometer device separately. The results were down-sampled and further imported into R and analyzed using the unsupervised clustering method to find clusters corresponding to the discovered Mφ groups from the single-cell data analysis. The first data was analyzed belonged to Ms4a3 FLs. The final clustering results of this data revealed eight clusters. Among these clusters, five groups were showing expression profiles that could be associated with the mature Mφ and the other could be differentiating/proliferating groups. In an attempt to validate the existence and the ontogeny of these clusters in the other samples, a similar analysis was performed on the E14.5 FL belonging to the Cxcr4 and the Rank fate-mapper mice. The analysis of the flow-cytometry data from the two other models could demonstrate that four out of five identified clusters, namely A, B, C, and D can be found with a relatively similar expression pattern across different samples, proving the constancy of these clusters. In contrast, cluster E showed a heterogeneous expression pattern in each of the three fate-mapper mice.

Considering that this cluster had a similar expression to clusters that were identified as not fully mature cells, it could be concluded that this cluster probably consists of heterogeneous cells regarding their maturation state, resulting in a non-consistent expressional pattern among different samples. Hence, this cluster was excluded from further downstream analysis.

The analysis of the YFP signal from the five mentioned clusters using *Rank$^{Cre}$Rosa26$^{eYFP}$* could should that all of the mentioned clusters have been labeled. Among them cluster B had the highest labeling rate with around 90% while clusters A and D were labeled around 50%. Interestingly, the YFP signal from the *Ms4a3$^{Cre}$Rosa26$^{eYFP}$* embryos indicated less than 5% labeling in these clusters while the signal from *Cxcr4$^{Cre}$Rosa26$^{eYFP}$ showed* labeling around 10% in cluster B. Considering the importance of the Rank for the development and proliferation of Mφ, these results could confirm the Mφ identity of these clusters. Furthermore, from the Ms4a3 and *Cxcr4* labeling it can be concluded that these Mφ are YS derived and not HSC derived.

In contrast, cluster C had the least labeling with Rank, 10% and the highest labeling with the *Cxcr4*. As mentioned before, since in the erythroblastic islands, an Mφ can be surrounded by multiple erythroblasts, a low percentage of Rank and a high percentage of *Cxcr4* labeling in cluster C could be justified.

Exploring the heatmap of the generated clusters, three clusters had a very similar expression to the three mature Mφ clusters identified in the single-cell analysis. These were clusters A, B, and D, and their markers expression could correspond to clusters 7, 8, and 2 from the single-cell data. Interestingly, the erythroblastic islands, cluster C, were evident among these eight clusters due to their expression of Ter119, an erythroid-specific marker expressed on cells at all stages of erythropoiesis. Similar to the single-cell data, this cluster was located further from the rest of the clusters in the UMAP visualization. Cluster C corresponded to cluster 9 from the single-cell data. The correlation analysis, which was performed to assess the similarity between the identified clusters from the single-cell and the flow-cytometry analysis, confirmed the previous conclusion regarding their correspondence.

## 5.3. The heterogeneity of Mφ can be found in the human dataset

The integration result from the mouse and human dataset could provide an insight to the possibility of the existence of different sub-population of Mφ in the human FL. The integration and merging of these two datasets were done using BBKNN (batch balanced k nearest neighbors) (Polanski, Young et al. 2020). This is a fast and straightforward method for batch alignment which also performs batch correction at the neighborhood graph inference step.

The results from the integration could show that the three clusters from the mouse that were identified as mature cells together with the erythroblastic islands can be in principle found in the human dataset. The erythroblastic island from the mouse, for example, has a complete overlap with the human cells that have been identified as erythroblastic island. However, the ingest algorithm has performed an over-clustering, meaning it also has identified part of the human cells that originally belonged to the mono-mac group as erythroblastic islands. This issue can be related to the unbalanced number of the cells between the two datasets making it hard to have enough reference cells to cover the wide range of expression that might exist in the reference dataset as the reference dataset consists of only 1363 cells while the query dataset has more than 30k cells. Furthermore, clusters 2, 7, and 8 were also evident in the human data.

Interestingly, clusters 7 and 8 were primarily projected on the cells that have been identified as the Kupffer cells in the human data. In contrast, cluster 2 was projected on the cells belonging to the mono-mac and Kupffer cell groups. Clusters 1 and 11 were spread and overlaid on a mixture of different cells, unlike the other groups which could be found in locally formed clusters. Also, these results could imply the three identified mature Mφ populations in the mouse can correspond to human data indicating the heterogeneity among Mφ populations in the human FL but, investigating the individual marker expression from the mouse data showed that the human Mφ differ in their marker expression and further analysis are required to identify new markers for defining the heterogeneity of the Mφ in human.

# 6.    References

Ajami, B., J. L. Bennett, C. Krieger, W. Tetzlaff and F. M. Rossi (2007). "Local self-renewal can sustain CNS microglia maintenance and function throughout adult life." Nat Neurosci **10**(12): 1538-1543.

Anderson, K. L., K. A. Smith, K. Conners, S. R. McKercher, R. A. Maki and B. E. Torbett (1998). "Myeloid development is selectively disrupted in PU. 1 null mice." Blood, The Journal of the American Society of Hematology **91**(10): 3702-3710.

Anghelina, M., P. Krishnan, L. Moldovan and N. I. Moldovan (2006). "Monocytes/macrophages cooperate with progenitor cells during neovascularization and tissue repair: conversion of cell columns into fibrovascular bundles." Am J Pathol **168**(2): 529-541.

Antonchuk, J., C. D. Hyland, D. J. Hilton and W. S. Alexander (2004). "Synergistic effects on erythropoiesis, thrombopoiesis, and stem cell competitiveness in mice deficient in thrombopoietin and steel factor receptors." Blood **104**(5): 1306-1313.

Areschoug, T. and S. Gordon (2009). "Scavenger receptors: role in innate immunity and microbial pathogenesis." Cell Microbiol **11**(8): 1160-1169.

Austyn, J. M. and S. Gordon (1981). "F4/80, a monoclonal antibody directed specifically against the mouse macrophage." Eur J Immunol **11**(10): 805-815.

Balkwill, F. (2003). "Chemokine biology in cancer." Semin Immunol **15**(1): 49-55.

Barker, J. E. (1968). "Development of the mouse hematopoietic system. I. Types of hemoglobin produced in embryonic yolk sac and liver." Dev Biol **18**(1): 14-29.

Beaudin, A. E., S. W. Boyer, J. Perez-Cunningham, G. E. Hernandez, S. C. Derderian, C. Jujjavarapu, E. Aaserude, T. MacKenzie and E. C. Forsberg (2016). "A Transient Developmental Hematopoietic Stem Cell Gives Rise to Innate-like B and T Cells." Cell Stem Cell **19**(6): 768-783.

Benezra, R., R. L. Davis, D. Lockshon, D. L. Turner and H. Weintraub (1990). "The protein Id: a negative regulator of helix-loop-helix DNA binding proteins." Cell **61**(1): 49-59.

Bernstein, A., L. Forrester, A. D. Reith, P. Dubreuil and R. Rottapel (1991). "The murine W/c-kit and Steel loci and the control of hematopoiesis." Semin Hematol **28**(2): 138-142.

Bertrand, J. Y., G. E. Desanti, R. Lo-Man, C. Leclerc, A. Cumano and R. Golub (2006). "Fetal spleen stroma drives macrophage commitment." Development **133**(18): 3619-3628.

Bertrand, J. Y., A. Jalil, M. Klaine, S. Jung, A. Cumano and I. Godin (2005). "Three pathways to mature macrophages in the early mouse yolk sac." Blood **106**(9): 3004-3011.

Bessis, M. (1958). "[Erythroblastic island, functional unity of bone marrow]." Rev Hematol **13**(1): 8-11.

Bessis, M. C. and J. Breton-Gorius (1962). "Iron metabolism in the bone marrow as seen by electron microscopy: a critical review." Blood **19**: 635-663.

Bleriot, C., E. Barreby, G. Dunsmore, R. Ballaire, S. Chakarov, X. Ficht, G. De Simone, F. Andreata, V. Fumagalli, W. Guo, G. Wan, G. Gessain, A. Khalilnezhad, X. M. Zhang, N. Ang, P. Chen, C. Morgantini, V. Azzimato, W. T. Kong, Z. Liu, R. Pai, J. Lum, F. Shihui, I. Low, C. Xu, B. Malleret, M. F. M. Kairi, A. Balachander, O. Cexus, A. Larbi, B. Lee, E. W. Newell, L. G. Ng, W. W. Phoo, R. M. Sobota, A. Sharma, S. W. Howland, J. Chen, M. Bajenoff, L. Yvan-Charvet, N. Venteclef, M. Iannacone, M. Aouadi and F. Ginhoux (2021). "A subset of Kupffer cells regulates metabolism through the expression of CD36." Immunity **54**(9): 2101-2116 e2106.

Bleriot, C., S. Chakarov and F. Ginhoux (2020). "Determinants of Resident Tissue Macrophage Identity and Function." Immunity **52**(6): 957-970.

Bleriot, C., T. Dupuis, G. Jouvion, G. Eberl, O. Disson and M. Lecuit (2015). "Liver-resident macrophage necroptosis orchestrates type 1 microbicidal inflammation and type-2-mediated tissue repair during bacterial infection." Immunity **42**(1): 145-158.

Boiers, C., J. Carrelha, M. Lutteropp, S. Luc, J. C. Green, E. Azzoni, P. S. Woll, A. J. Mead, A. Hultquist, G. Swiers, E. G. Perdiguero, I. C. Macaulay, L. Melchiori, T. C. Luis, S. Kharazi, T. Bouriez-Jones, Q. Deng, A. Ponten, D. Atkinson, C. T. Jensen, E. Sitnicka, F. Geissmann, I. Godin, R. Sandberg, M. F. de Bruijn and S. E. Jacobsen (2013). "Lymphomyeloid contribution of an immune-restricted progenitor emerging prior to definitive hematopoietic stem cells." Cell Stem Cell **13**(5): 535-548.

Bonnardel, J., W. T'Jonck, D. Gaublomme, R. Browaeys, C. L. Scott, L. Martens, B. Vanneste, S. De Prijck, S. A. Nedospasov, A. Kremer, E. Van Hamme, P. Borghgraef, W. Toussaint, P. De Bleser, I. Mannaerts, A. Beschin, L. A. van Grunsven, B. N. Lambrecht, T. Taghon, S. Lippens, D. Elewaut, Y. Saeys and M. Guilliams (2019). "Stellate Cells, Hepatocytes, and Endothelial Cells Imprint the Kupffer Cell Identity on Monocytes Colonizing the Liver Macrophage Niche." Immunity **51**(4): 638-654 e639.

Bosbach, B., S. Deshpande, F. Rossi, J. H. Shieh, G. Sommer, E. de Stanchina, D. R. Veach, J. M. Scandura, K. Manova-Todorova, M. A. Moore, C. R. Antonescu and P. Besmer (2012). "Imatinib resistance and microcytic

erythrocytosis in a KitV558Delta;T669I/+ gatekeeper-mutant mouse model of gastrointestinal stromal tumor." Proc Natl Acad Sci U S A **109**(34): E2276-2283.

Brotherton, T. W., D. H. Chui, J. Gauldie and M. Patterson (1979). "Hemoglobin ontogeny during normal mouse fetal development." Proc Natl Acad Sci U S A **76**(6): 2853-2857.

Burgess, M., K. Wicks, M. Gardasevic and K. A. Mace (2019). "Cx3CR1 Expression Identifies Distinct Macrophage Populations That Contribute Differentially to Inflammation and Repair." Immunohorizons **3**(7): 262-273.

Busch, K., K. Klapproth, M. Barile, M. Flossdorf, T. Holland-Letz, S. M. Schlenner, M. Reth, T. Hofer and H. R. Rodewald (2015). "Fundamental properties of unperturbed haematopoiesis from stem cells in vivo." Nature **518**(7540): 542-546.

Celada, A., F. E. Borràs, C. Soler, J. Lloberas, M. Klemsz, C. van Beveren, S. McKercher and R. A. Maki (1996). "The transcription factor PU. 1 is involved in macrophage proliferation." The Journal of experimental medicine **184**(1): 61-69.

Charbord, P., M. Tavian, L. Humeau and B. Peault (1996). "Early ontogeny of the human marrow from long bones: an immunohistochemical study of hematopoiesis and its microenvironment." Blood **87**(10): 4109-4119.

Chen, K., J. Liu, S. Heck, J. A. Chasis, X. An and N. Mohandas (2009). "Resolving the distinct stages in erythroid differentiation based on dynamic changes in membrane protein expression during erythropoiesis." Proc Natl Acad Sci U S A **106**(41): 17413-17418.

Chen, M. J., Y. Li, M. E. De Obaldia, Q. Yang, A. D. Yzaguirre, T. Yamada-Inagawa, C. S. Vink, A. Bhandoola, E. Dzierzak and N. A. Speck (2011). "Erythroid/myeloid progenitors and hematopoietic stem cells originate from distinct populations of endothelial cells." Cell Stem Cell **9**(6): 541-552.

Chou, S., J. Flygare and H. F. Lodish (2013). "Fetal hepatic progenitors support long-term expansion of hematopoietic stem cells." Exp Hematol **41**(5): 479-490 e474.

Chou, S. and H. F. Lodish (2010). "Fetal liver hepatic progenitors are supportive stromal cells for hematopoietic stem cells." Proc Natl Acad Sci U S A **107**(17): 7799-7804.

Chow, A., M. Huggins, J. Ahmed, D. Hashimoto, D. Lucas, Y. Kunisaki, S. Pinho, M. Leboeuf, C. Noizat, N. van Rooijen, M. Tanaka, Z. J. Zhao, A. Bergman, M. Merad and P. S. Frenette (2013). "CD169(+) macrophages provide a niche promoting erythropoiesis under homeostasis and stress." Nat Med **19**(4): 429-436.

Christensen, J. L., D. E. Wright, A. J. Wagers and I. L. Weissman (2004). "Circulation and chemotaxis of fetal hematopoietic stem cells." PLoS Biol **2**(3): E75.

Christy, B. A., L. K. Sanders, L. F. Lau, N. G. Copeland, N. A. Jenkins and D. Nathans (1991). "An Id-related helix-loop-helix protein encoded by a growth factor-inducible gene." Proc Natl Acad Sci U S A **88**(5): 1815-1819.

Ciriza, J., H. Thompson, R. Petrosian, J. O. Manilay and M. E. Garcia-Ojeda (2013). "The migration of hematopoietic progenitors from the fetal liver to the fetal bone marrow: lessons learned and possible clinical applications." Exp Hematol **41**(5): 411-423.

Clarke, A. R., E. R. Maandag, M. van Roon, N. M. van der Lugt, M. van der Valk, M. L. Hooper, A. Berns and H. te Riele (1992). "Requirement for a functional Rb-1 gene in murine development." Nature **359**(6393): 328-330.

Coskun, S., H. Chao, H. Vasavada, K. Heydari, N. Gonzales, X. Zhou, B. de Crombrugghe and K. K. Hirschi (2014). "Development of the fetal bone marrow niche and regulation of HSC quiescence and homing ability by emerging osteolineage cells." Cell Rep **9**(2): 581-590.

Cox, N., L. Crozet, I. R. Holtman, P. L. Loyher, T. Lazarov, J. B. White, E. Mass, E. R. Stanley, O. Elemento, C. K. Glass and F. Geissmann (2021). "Diet-regulated production of PDGFcc by macrophages controls energy storage." Science **373**(6550).

Crowell H, Z. V., Chevrier S, Robinson M (2022). CATALYST: Cytometry dATa anALYSis Tools. R package version 1.18.1.

Cumano, A., F. Dieterlen-Lievre and I. Godin (1996). "Lymphoid potential, probed before circulation in mouse, is restricted to caudal intraembryonic splanchnopleura." Cell **86**(6): 907-916.

Cumano, A., J. C. Ferraz, M. Klaine, J. P. Di Santo and I. Godin (2001). "Intraembryonic, but not yolk sac hematopoietic precursors, isolated before circulation, provide long-term multilineage reconstitution." Immunity **15**(3): 477-485.

Dai, X. M., G. R. Ryan, A. J. Hapel, M. G. Dominguez, R. G. Russell, S. Kapp, V. Sylvestre and E. R. Stanley (2002). "Targeted disruption of the mouse colony-stimulating factor 1 receptor gene results in osteopetrosis, mononuclear phagocyte deficiency, increased primitive progenitor cell frequencies, and reproductive defects." Blood **99**(1): 111-120.

Dambuza, I. M. and G. D. Brown (2015). "C-type lectins in immunity: recent developments." Curr Opin Immunol **32**: 21-27.

de Back, D. Z., E. B. Kostova, M. van Kraaij, T. K. van den Berg and R. van Bruggen (2014). "Of macrophages and red blood cells; a complex love story." Front Physiol **5**: 9.

Deem, T. L., H. Abdala-Valencia and J. M. Cook-Mills (2007). "VCAM-1 activation of endothelial cell protein tyrosine phosphatase 1B." J Immunol **178**(6): 3865-3873.

DeKoter, R. P. and H. Singh (2000). "Regulation of B lymphocyte and macrophage development by graded expression of PU. 1." Science **288**(5470): 1439-1441.

den Haan, J. M. and G. Kraal (2012). "Innate immune functions of macrophage subpopulations in the spleen." J Innate Immun **4**(5-6): 437-445.

Dieterlen-Lievre, F. (1975). "On the origin of haemopoietic stem cells in the avian embryo: an experimental approach." J Embryol Exp Morphol **33**(3): 607-619.

Dieterlen-Lievre, F., D. Beaupain and C. Martin (1976). "Origin of erythropoietic stem cells in avian development: shift from the yolk sac to an intraembryonic site." Ann Immunol (Paris) **127**(6): 857-863.

Dong, R., J. Russell, S. Malloy, K. Hall, S. E. Smith, H. Li, Y. Wang, A. Perera, S. McKinney and B. Slaughter (2021). "Using Spatial Transcriptomics to Reveal Fetal Liver Hematopoietic Stem Cell-Niche Interactions." Blood **138**: 3284.

Dzierzak, E. and N. A. Speck (2008). "Of lineage and legacy: the development of mammalian hematopoietic stem cells." Nat Immunol **9**(2): 129-136.

Evren, E., E. Ringqvist and T. Willinger (2020). "Origin and ontogeny of lung macrophages: from mice to humans." Immunology **160**(2): 126-138.

Fabriek, B. O., M. M. Polfliet, R. P. Vloet, R. C. van der Schors, A. J. Ligtenberg, L. K. Weaver, C. Geest, K. Matsuno, S. K. Moestrup, C. D. Dijkstra and T. K. van den Berg (2007). "The macrophage CD163 surface glycoprotein is an erythroblast adhesion receptor." Blood **109**(12): 5223-5229.

Fitch, S. R., G. M. Kimber, N. K. Wilson, A. Parker, B. Mirshekar-Syahkal, B. Gottgens, A. Medvinsky, E. Dzierzak and K. Ottersbach (2012). "Signaling from the sympathetic nervous system regulates hematopoietic stem cell emergence during embryogenesis." Cell Stem Cell **11**(4): 554-566.

Frelin, C., R. Herrington, S. Janmohamed, M. Barbara, G. Tran, C. J. Paige, P. Benveniste, J. C. Zuniga-Pflucker, A. Souabni, M. Busslinger and N. N. Iscove (2013). "GATA-3 regulates the self-renewal of long-term hematopoietic stem cells." Nat Immunol **14**(10): 1037-1044.

Garceau, V., J. Smith, I. R. Paton, M. Davey, M. A. Fares, D. P. Sester, D. W. Burt and D. A. Hume (2010). "Pivotal Advance: Avian colony-stimulating factor 1 (CSF-1), interleukin-34 (IL-34), and CSF-1 receptor genes and gene products." J Leukoc Biol **87**(5): 753-764.

Gautier, E. L., A. Chow, R. Spanbroek, G. Marcelin, M. Greter, C. Jakubzick, M. Bogunovic, M. Leboeuf, N. van Rooijen, A. J. Habenicht, M. Merad and G. J. Randolph (2012). "Systemic analysis of PPARgamma in mouse macrophage populations reveals marked diversity in expression with critical roles in resolution of inflammation and airway immunity." J Immunol **189**(5): 2614-2624.

Gierahn, T. M., M. H. Wadsworth, 2nd, T. K. Hughes, B. D. Bryson, A. Butler, R. Satija, S. Fortune, J. C. Love and A. K. Shalek (2017). "Seq-Well: portable, low-cost RNA sequencing of single cells at high throughput." Nat Methods **14**(4): 395-398.

Ginhoux, F., M. Greter, M. Leboeuf, S. Nandi, P. See, S. Gokhan, M. F. Mehler, S. J. Conway, L. G. Ng, E. R. Stanley, I. M. Samokhvalov and M. Merad (2010). "Fate mapping analysis reveals that adult microglia derive from primitive macrophages." Science **330**(6005): 841-845.

Godin, I. E., J. A. Garcia-Porrero, A. Coutinho, F. Dieterlen-Lievre and M. A. Marcos (1993). "Para-aortic splanchnopleura from early mouse embryos contains B1a cell progenitors." Nature **364**(6432): 67-70.

Gomez Perdiguero, E., K. Klapproth, C. Schulz, K. Busch, E. Azzoni, L. Crozet, H. Garner, C. Trouillet, M. F. de Bruijn, F. Geissmann and H. R. Rodewald (2015). "Tissue-resident macrophages originate from yolk-sac-derived erythro-myeloid progenitors." Nature **518**(7540): 547-551.

Gordon, S. and A. Pluddemann (2017). "Tissue macrophages: heterogeneity and functions." BMC Biol **15**(1): 53.

Gregory, C. J. and A. C. Eaves (1978). "Three stages of erythropoietic progenitor cell differentiation distinguished by a number of physical and biologic properties." Blood **51**(3): 527-537.

Gritz, E. and K. K. Hirschi (2016). "Specification and function of hemogenic endothelium during embryogenesis." Cell Mol Life Sci **73**(8): 1547-1567.

Guilliams, M., I. De Kleer, S. Henri, S. Post, L. Vanhoutte, S. De Prijck, K. Deswarte, B. Malissen, H. Hammad and B. N. Lambrecht (2013). "Alveolar macrophages develop from fetal monocytes that differentiate into long-lived cells in the first week of life via GM-CSF." J Exp Med **210**(10): 1977-1992.

Guilliams, M., G. R. Thierry, J. Bonnardel and M. Bajenoff (2020). "Establishment and maintenance of the macrophage niche." Immunity **52**(3): 434-451.

Guiu, J., R. Shimizu, T. D'Altri, S. T. Fraser, J. Hatakeyama, E. H. Bresnick, R. Kageyama, E. Dzierzak, M. Yamamoto, L. Espinosa and A. Bigas (2013). "Hes repressors are essential regulators of hematopoietic stem cell development downstream of Notch signaling." J Exp Med **210**(1): 71-84.

Haddad-Tovolli, R., N. R. V. Dragano, A. F. S. Ramalho and L. A. Velloso (2017). "Development and Function of the Blood-Brain Barrier in the Context of Metabolic Control." Front Neurosci **11**: 224.

Haldar, M., M. Kohyama, A. Y. So, W. Kc, X. Wu, C. G. Briseno, A. T. Satpathy, N. M. Kretzer, H. Arase, N. S. Rajasekaran, L. Wang, T. Egawa, K. Igarashi, D. Baltimore, T. L. Murphy and K. M. Murphy (2014). "Heme-mediated SPI-C induction promotes monocyte differentiation into iron-recycling macrophages." Cell **156**(6): 1223-1234.

Han, J., R. A. Harris and X. M. Zhang (2017). "An updated assessment of microglia depletion: current concepts and future directions." Mol Brain **10**(1): 25.

Hanspal, M. and J. S. Hanspal (1994). "The association of erythroblasts with macrophages promotes erythroid proliferation and maturation: a 30-kD heparin-binding protein is involved in this contact." Blood **84**(10): 3494-3504.

Hanspal, M., Y. Smockova and Q. Uong (1998). "Molecular identification and functional characterization of a novel protein that mediates the attachment of erythroblasts to macrophages." Blood **92**(8): 2940-2950.

Hata, M., M. Nanno, H. Doi, S. Satomi, T. Sakata, R. Suzuki and T. Itoh (1993). "Establishment of a hepatocytic epithelial cell line from the murine fetal liver capable of promoting hemopoietic cell proliferation." J Cell Physiol **154**(2): 381-392.

Hayashi, Y., M. Sezaki and H. Takizawa (2019). "Development of the hematopoietic system: Role of inflammatory factors." Wiley Interdiscip Rev Dev Biol **8**(4): e341.

Heider, D. (2021). Heterogeneity of tissue-resident macrophages in the fetal liver and their impact on hematopoietic stem cell development during embryogenesis. B.Sc., Rheinischen Friedrich-Wilhelms-Universität Bonn.

Hoeffel, G., J. Chen, Y. Lavin, D. Low, F. F. Almeida, P. See, A. E. Beaudin, J. Lum, I. Low, E. C. Forsberg, M. Poidinger, F. Zolezzi, A. Larbi, L. G. Ng, J. K. Chan, M. Greter, B. Becher, I. M. Samokhvalov, M. Merad and F. Ginhoux (2015). "C-Myb(+) erythro-myeloid progenitor-derived fetal monocytes give rise to adult tissue-resident macrophages." Immunity **42**(4): 665-678.

Hoeffel, G. and F. Ginhoux (2018). "Fetal monocytes and the origins of tissue-resident macrophages." Cell Immunol **330**: 5-15.

Hoeffel, G., Y. Wang, M. Greter, P. See, P. Teo, B. Malleret, M. Leboeuf, D. Low, G. Oller, F. Almeida, S. H. Choy, M. Grisotto, L. Renia, S. J. Conway, E. R. Stanley, J. K. Chan, L. G. Ng, I. M. Samokhvalov, M. Merad and F. Ginhoux (2012). "Adult Langerhans cells derive predominantly from embryonic fetal liver monocytes with a minor contribution of yolk sac-derived macrophages." J Exp Med **209**(6): 1167-1181.

Huang, K., J. Du, N. Ma, J. Liu, P. Wu, X. Dong, M. Meng, W. Wang, X. Chen, X. Shi, Q. Chen, Z. Yang, S. Chen, J. Zhang, Y. Li, W. Li, Y. Zheng, J. Cai, P. Li, X. Sun, J. Wang, D. Pei and G. Pan (2015). "GATA2(-/-) human ESCs undergo attenuated endothelial to hematopoietic transition and thereafter granulocyte commitment." Cell Regen **4**(1): 4.

Huber, C. and G. Stingl (1981). "Macrophages in the regulation of immunity." Haematol Blood Transfus **27**: 31-37.

Hughes, T. K., M. H. Wadsworth, 2nd, T. M. Gierahn, T. Do, D. Weiss, P. R. Andrade, F. Ma, B. J. de Andrade Silva, S. Shao, L. C. Tsoi, J. Ordovas-Montanes, J. E. Gudjonsson, R. L. Modlin, J. C. Love and A. K. Shalek (2020). "Second-Strand Synthesis-Based Massively Parallel scRNA-Seq Reveals Cellular States and Molecular Features of Human Inflammatory Skin Pathologies." Immunity **53**(4): 878-894 e877.

Imai, Y., I. Ibata, D. Ito, K. Ohsawa and S. Kohsaka (1996). "A novel gene iba1 in the major histocompatibility complex class III region encoding an EF hand protein expressed in a monocytic lineage." Biochem Biophys Res Commun **224**(3): 855-862.

Ivanovs, A., S. Rybtsov, L. Welch, R. A. Anderson, M. L. Turner and A. Medvinsky (2011). "Highly potent human hematopoietic stem cells first emerge in the intraembryonic aorta-gonad-mesonephros region." J Exp Med **208**(12): 2417-2427.

Jacks, T., A. Fazeli, E. M. Schmitt, R. T. Bronson, M. A. Goodell and R. A. Weinberg (1992). "Effects of an Rb mutation in the mouse." Nature **359**(6393): 295-300.

Jappinen, N., I. Felix, E. Lokka, S. Tyystjarvi, A. Pynttari, T. Lahtela, H. Gerke, K. Elima, P. Rantakari and M. Salmi (2019). "Fetal-derived macrophages dominate in adult mammary glands." Nat Commun **10**(1): 281.

Jen, Y., K. Manova and R. Benezra (1996). "Expression patterns of Id1, Id2, and Id3 are highly related but distinct from that of Id4 during mouse embryogenesis." Dev Dyn **207**(3): 235-252.

Jordan, C. T., J. P. McKearn and I. R. Lemischka (1990). "Cellular and developmental properties of fetal hematopoietic stem cells." Cell **61**(6): 953-963.

Julia, V. (2012). "CX3CL1 in allergic diseases: not just a chemotactic molecule." Allergy **67**(9): 1106-1110.

Kamiya, A., T. Kinoshita, Y. Ito, T. Matsui, Y. Morikawa, E. Senba, K. Nakashima, T. Taga, K. Yoshida, T. Kishimoto and A. Miyajima (1999). "Fetal liver development requires a paracrine action of oncostatin M through the gp130 signal transducer." EMBO J **18**(8): 2127-2136.

Kassambara, A. and M. A. Kassambara (2020). "Package 'ggpubr'." R package version 0.1 **6**.

Katayama, Y., M. Battista, W. M. Kao, A. Hidalgo, A. J. Peired, S. A. Thomas and P. S. Frenette (2006). "Signals from the sympathetic nervous system regulate hematopoietic stem cell egress from bone marrow." Cell **124**(2): 407-421.

Kaufman, M. H. (1992). Atlas of mouse development, Academic press.

Kelley, J. L., T. R. Ozment, C. Li, J. B. Schweitzer and D. L. Williams (2014). "Scavenger receptor-A (CD204): a two-edged sword in health and disease." Crit Rev Immunol **34**(3): 241-261.

Khan, J. A., A. Mendelson, Y. Kunisaki, A. Birbrair, Y. Kou, A. Arnal-Estape, S. Pinho, P. Ciero, F. Nakahara, A. Ma'ayan, A. Bergman, M. Merad and P. S. Frenette (2016). "Fetal liver hematopoietic stem cell niches associate with portal vessels." Science **351**(6269): 176-180.

Kiel, M. J., O. H. Yilmaz, T. Iwashita, O. H. Yilmaz, C. Terhorst and S. J. Morrison (2005). "SLAM family receptors distinguish hematopoietic stem and progenitor cells and reveal endothelial niches for stem cells." Cell **121**(7): 1109-1121.

Kierdorf, K., D. Erny, T. Goldmann, V. Sander, C. Schulz, E. G. Perdiguero, P. Wieghofer, A. Heinrich, P. Riemke, C. Holscher, D. N. Muller, B. Luckow, T. Brocker, K. Debowski, G. Fritz, G. Opdenakker, A. Diefenbach, K. Biber, M. Heikenwalder, F. Geissmann, F. Rosenbauer and M. Prinz (2013). "Microglia emerge from erythromyeloid precursors via Pu.1- and Irf8-dependent pathways." Nat Neurosci **16**(3): 273-280.

Kieusseian, A., P. Brunet de la Grange, O. Burlen-Defranoux, I. Godin and A. Cumano (2012). "Immature hematopoietic stem cells undergo maturation in the fetal liver." Development **139**(19): 3521-3530.

Kim, I., S. He, O. H. Yilmaz, M. J. Kiel and S. J. Morrison (2006). "Enhanced purification of fetal liver hematopoietic stem cells using SLAM family receptors." Blood **108**(2): 737-744.

Kingsley, P. D., J. Malik, K. A. Fantauzzo and J. Palis (2004). "Yolk sac-derived primitive erythroblasts enucleate during mammalian embryogenesis." Blood **104**(1): 19-25.

Kobayashi, H., J. M. Butler, R. O'Donnell, M. Kobayashi, B. S. Ding, B. Bonner, V. K. Chiu, D. J. Nolan, K. Shido, L. Benjamin and S. Rafii (2010). "Angiocrine factors from Akt-activated endothelial cells balance self-renewal and differentiation of haematopoietic stem cells." Nat Cell Biol **12**(11): 1046-1056.

Kolde, R. and M. R. Kolde (2015). "Package 'pheatmap'." R package **1**(7): 790.

Kraal, G. (1992). "Cells in the marginal zone of the spleen." Int Rev Cytol **132**: 31-74.

Krishnaraju, K., B. Hoffman and D. A. Liebermann (2001). "Early growth response gene 1 stimulates development of hematopoietic progenitor cells along the macrophage lineage at the expense of the granulocyte and erythroid lineages." Blood **97**(5): 1298-1305.

Ku, C. J., T. Hosoya, I. Maillard and J. D. Engel (2012). "GATA-3 regulates hematopoietic stem cell maintenance and cell-cycle entry." Blood **119**(10): 2242-2251.

Kumaravelu, P., L. Hook, A. M. Morrison, J. Ure, S. Zhao, S. Zuyev, J. Ansell and A. Medvinsky (2002). "Quantitative developmental anatomy of definitive haematopoietic stem cells/long-term repopulating units (HSC/RUs): role of the aorta-gonad-mesonephros (AGM) region and the yolk sac in colonisation of the mouse embryonic liver." Development **129**(21): 4891-4899.

Kunisaki, Y., I. Bruns, C. Scheiermann, J. Ahmed, S. Pinho, D. Zhang, T. Mizoguchi, Q. Wei, D. Lucas, K. Ito, J. C. Mar, A. Bergman and P. S. Frenette (2013). "Arteriolar niches maintain haematopoietic stem cell quiescence." Nature **502**(7473): 637-643.

Kusumbe, A. P., S. K. Ramasamy, T. Itkin, M. A. Mae, U. H. Langen, C. Betsholtz, T. Lapidot and R. H. Adams (2016). "Age-dependent modulation of vascular niches for haematopoietic stem cells." Nature **532**(7599): 380-384.

Lai, S. M., J. Sheng, P. Gupta, L. Renia, K. Duan, F. Zolezzi, K. Karjalainen, E. W. Newell and C. Ruedl (2018). "Organ-Specific Fate, Recruitment, and Refilling Dynamics of Tissue-Resident Macrophages during Blood-Stage Malaria." Cell Rep **25**(11): 3099-3109 e3093.

Landsman, L., L. Bar-On, A. Zernecke, K. W. Kim, R. Krauthgamer, E. Shagdarsuren, S. A. Lira, I. L. Weissman, C. Weber and S. Jung (2009). "CX3CR1 is required for monocyte homeostasis and atherogenesis by promoting cell survival." Blood **113**(4): 963-972.

Lee, E. Y., C. Y. Chang, N. Hu, Y. C. Wang, C. C. Lai, K. Herrup, W. H. Lee and A. Bradley (1992). "Mice deficient for Rb are nonviable and show defects in neurogenesis and haematopoiesis." Nature **359**(6393): 288-294.

Lee, G., A. Lo, S. A. Short, T. J. Mankelow, F. Spring, S. F. Parsons, K. Yazdanbakhsh, N. Mohandas, D. J. Anstee and J. A. Chasis (2006). "Targeted gene deletion demonstrates that the cell adhesion molecule ICAM-4 is critical for erythroblastic island formation." Blood **108**(6): 2064-2071.

Lee, G., F. A. Spring, S. F. Parsons, T. J. Mankelow, L. L. Peters, M. J. Koury, N. Mohandas, D. J. Anstee and J. A. Chasis (2003). "Novel secreted isoform of adhesion molecule ICAM-4: potential regulator of membrane-associated ICAM-4 interactions." Blood **101**(5): 1790-1797.

Lee, S. H., P. R. Crocker, S. Westaby, N. Key, D. Y. Mason, S. Gordon and D. J. Weatherall (1988). "Isolation and immunocytochemical characterization of human bone marrow stromal macrophages in hemopoietic clusters." J Exp Med **168**(3): 1193-1198.

Lee, Y. S., M. H. Kim, H. S. Yi, S. Y. Kim, H. H. Kim, J. H. Kim, J. E. Yeon, K. S. Byun, J. S. Byun and W. I. Jeong (2018). "CX3CR1 differentiates F4/80(low) monocytes into pro-inflammatory F4/80(high) macrophages in the liver." Sci Rep **8**(1): 15076.

Lefevre, L., A. Gales, D. Olagnier, J. Bernad, L. Perez, R. Burcelin, A. Valentin, J. Auwerx, B. Pipy and A. Coste (2010). "PPARgamma ligands switched high fat diet-induced macrophage M2b polarization toward M2a thereby improving intestinal Candida elimination." PLoS One **5**(9): e12828.

Lemischka, I. R., D. H. Raulet and R. C. Mulligan (1986). "Developmental potential and dynamic behavior of hematopoietic stem cells." Cell **45**(6): 917-927.

Lewis, K., M. Yoshimoto and T. Takebe (2021). "Fetal liver hematopoiesis: from development to delivery." Stem Cell Res Ther **12**(1): 139.

Li, D., W. Xue, M. Li, M. Dong, J. Wang, X. Wang, X. Li, K. Chen, W. Zhang, S. Wu, Y. Zhang, L. Gao, Y. Chen, J. Chen, B. O. Zhou, Y. Zhou, X. Yao, L. Li, D. Wu and W. Pan (2018). "VCAM-1(+) macrophages guide the homing of HSPCs to a vascular niche." Nature **564**(7734): 119-124.

Li, Y., A. Kovach, K. Suino-Powell, D. Martynowski and H. E. Xu (2008). "Structural and biochemical basis for the binding selectivity of peroxisome proliferator-activated receptor gamma to PGC-1alpha." J Biol Chem **283**(27): 19132-19139.

Liu, Z., Y. Gu, S. Chakarov, C. Bleriot, I. Kwok, X. Chen, A. Shin, W. Huang, R. J. Dress, C. A. Dutertre, A. Schlitzer, J. Chen, L. G. Ng, H. Wang, Z. Liu, B. Su and F. Ginhoux (2019). "Fate Mapping via Ms4a3-Expression History Traces Monocyte-Derived Cells." Cell **178**(6): 1509-1525 e1519.

Love, M. I., W. Huber and S. Anders (2014). "Moderated estimation of fold change and dispersion for RNA-seq data with DESeq2." Genome Biol **15**(12): 550.

Lu, Y., M. Liu, J. Yang, S. M. Weissman, X. Pan, S. G. Katz and S. Wang (2021). "Spatial transcriptome profiling by MERFISH reveals fetal liver hematopoietic stem cell niche architecture." Cell Discov **7**(1): 47.

Lund, H., M. Pieber, R. Parsa, J. Han, D. Grommisch, E. Ewing, L. Kular, M. Needhamsen, A. Espinosa, E. Nilsson, A. K. Overby, O. Butovsky, M. Jagodic, X. M. Zhang and R. A. Harris (2018). "Competitive repopulation of an empty microglial niche yields functionally distinct subsets of microglia-like cells." Nat Commun **9**(1): 4845.

Lyden, D., A. Z. Young, D. Zagzag, W. Yan, W. Gerald, R. O'Reilly, B. L. Bader, R. O. Hynes, Y. Zhuang, K. Manova and R. Benezra (1999). "Id1 and Id3 are required for neurogenesis, angiogenesis and vascularization of tumour xenografts." Nature **401**(6754): 670-677.

Macosko, E. Z., A. Basu, R. Satija, J. Nemesh, K. Shekhar, M. Goldman, I. Tirosh, A. R. Bialas, N. Kamitaki, E. M. Martersteck, J. J. Trombetta, D. A. Weitz, J. R. Sanes, A. K. Shalek, A. Regev and S. A. McCarroll (2015). "Highly Parallel Genome-wide Expression Profiling of Individual Cells Using Nanoliter Droplets." Cell **161**(5): 1202-1214.

Manwani, D. and J. J. Bieker (2008). "The erythroblastic island." Curr Top Dev Biol **82**: 23-53.

Mass, E., I. Ballesteros, M. Farlik, F. Halbritter, P. Günther, L. Crozet, C. E. Jacome-Galarza, K. Händler, J. Klughammer and Y. Kobayashi (2016). "Specification of tissue-resident macrophages during organogenesis." Science **353**(6304).

McCusker, K. and J. Hoidal (1989). "Characterization of scavenger receptor activity in resident human lung macrophages." Exp Lung Res **15**(4): 651-661.

McGrath, K. E., J. M. Frame, K. H. Fegan, J. R. Bowen, S. J. Conway, S. C. Catherman, P. D. Kingsley, A. D. Koniski and J. Palis (2015). "Distinct Sources of Hematopoietic Progenitors Emerge before HSCs and Provide Functional Blood Cells in the Mammalian Embryo." Cell Rep **11**(12): 1892-1904.

McGrath, K. E., J. M. Frame and J. Palis (2015). "Early hematopoiesis and macrophage development." Semin Immunol **27**(6): 379-387.

McInnes, L., J. Healy and J. Melville (2018). "Umap: Uniform manifold approximation and projection for dimension reduction." arXiv preprint arXiv:1802.03426.

McKercher, S., B. E. Torbett, K. L. Anderson, G. W. Henkel, D. J. Vestal, H. Baribault, M. Klemsz, A. J. Feeney, G. E. Wu and C. J. Paige (1996). "Targeted disruption of the PU. 1 gene results in multiple hematopoietic abnormalities." The EMBO journal **15**(20): 5647-5658.

McQuattie-Pimentel, A. C., G. R. S. Budinger and M. N. Ballinger (2018). "Monocyte-derived Alveolar Macrophages: The Dark Side of Lung Repair?" Am J Respir Cell Mol Biol **58**(1): 5-6.

Mebius, R. E. and G. Kraal (2005). "Structure and function of the spleen." Nat Rev Immunol **5**(8): 606-616.

Medvinsky, A. and E. Dzierzak (1996). "Definitive hematopoiesis is autonomously initiated by the AGM region." Cell **86**(6): 897-906.

Medvinsky, A. L., N. L. Samoylina, A. M. Muller and E. A. Dzierzak (1993). "An early pre-liver intraembryonic source of CFU-S in the developing mouse." Nature **364**(6432): 64-67.

Mendez-Ferrer, S., D. Lucas, M. Battista and P. S. Frenette (2008). "Haematopoietic stem cell release is regulated by circadian oscillations." Nature **452**(7186): 442-447.

Merad, M., M. G. Manz, H. Karsunky, A. Wagers, W. Peters, I. Charo, I. L. Weissman, J. G. Cyster and E. G. Engleman (2002). "Langerhans cells renew in the skin throughout life under steady-state conditions." Nat Immunol **3**(12): 1135-1141.

Miller, C. L., V. I. Rebel, M. E. Lemieux, C. D. Helgason, P. M. Lansdorp and C. J. Eaves (1996). "Studies of W mutant mice provide evidence for alternate mechanisms capable of activating hematopoietic stem cells." Exp Hematol **24**(2): 185-194.

Morris, L., C. F. Graham and S. Gordon (1991). "Macrophages in haemopoietic and other tissues of the developing mouse detected by the monoclonal antibody F4/80." Development **112**(2): 517-526.

Morrison, S. J., H. D. Hemmati, A. M. Wandycz and I. L. Weissman (1995). "The purification and characterization of fetal liver hematopoietic stem cells." Proc Natl Acad Sci U S A **92**(22): 10302-10306.

Mukherjee, K., L. Xue, A. Planutis, M. N. Gnanapragasam, A. Chess and J. J. Bieker (2021). "EKLF/KLF1 expression defines a unique macrophage subset during mouse erythropoiesis." Elife **10**.

Muller, A. M., A. Medvinsky, J. Strouboulis, F. Grosveld and E. Dzierzak (1994). "Development of hematopoietic stem cell activity in the mouse embryo." Immunity **1**(4): 291-301.

Naito, M., F. Yamamura, S. Nishikawa and K. Takahashi (1989). "Development, differentiation, and maturation of fetal mouse yolk sac macrophages in cultures." J Leukoc Biol **46**(1): 1-10.

Nakano, H., X. Liu, A. Arshi, Y. Nakashima, B. van Handel, R. Sasidharan, A. W. Harmon, J. H. Shin, R. J. Schwartz, S. J. Conway, R. P. Harvey, M. Pashmforoush, H. K. Mikkola and A. Nakano (2013). "Haemogenic endocardium contributes to transient definitive haematopoiesis." Nat Commun **4**: 1564.

Neo, W. H., C. A. G. Booth, E. Azzoni, L. Chi, P. Delgado-Olguin, M. de Bruijn, S. E. W. Jacobsen and A. J. Mead (2018). "Cell-extrinsic hematopoietic impact of Ezh2 inactivation in fetal liver endothelial cells." Blood **131**(20): 2223-2234.

Nguyen, H. Q., B. Hoffman-Liebermann and D. A. Liebermann (1993). "The zinc finger transcription factor Egr-1 is essential for and restricts differentiation along the macrophage lineage." Cell **72**(2): 197-209.

Nosaka, T., J. M. van Deursen, R. A. Tripp, W. E. Thierfelder, B. A. Witthuhn, A. P. McMickle, P. C. Doherty, G. C. Grosveld and J. N. Ihle (1995). "Defective lymphoid development in mice lacking Jak3." Science **270**(5237): 800-802.

Ogawa, M., S. Nishikawa, K. Yoshinaga, S. Hayashi, T. Kunisada, J. Nakao, T. Kina, T. Sudo, H. Kodama and S. Nishikawa (1993). "Expression and function of c-Kit in fetal hemopoietic progenitor cells: transition from the early c-Kit-independent to the late c-Kit-dependent wave of hemopoiesis in the murine embryo." Development **117**(3): 1089-1098.

Orkin, S. H. (1995). "Hematopoiesis: how does it happen?" Curr Opin Cell Biol **7**(6): 870-877.

Orkin, S. H. (1995). "Hematopoiesis: how does it happen?" Current opinion in cell biology **7**(6): 870-877.

Orkin, S. H. (2000). "Diversification of haematopoietic stem cells to specific lineages." Nat Rev Genet **1**(1): 57-64.

Palecanda, A., J. Paulauskis, E. Al-Mutairi, A. Imrich, G. Qin, H. Suzuki, T. Kodama, K. Tryggvason, H. Koziel and L. Kobzik (1999). "Role of the scavenger receptor MARCO in alveolar macrophage binding of unopsonized environmental particles." J Exp Med **189**(9): 1497-1506.

Palis, J. (2014). "Primitive and definitive erythropoiesis in mammals." Front Physiol **5**: 3.

Palis, J. (2016). "Hematopoietic stem cell-independent hematopoiesis: emergence of erythroid, megakaryocyte, and myeloid potential in the mammalian embryo." FEBS Lett **590**(22): 3965-3974.

Palis, J., R. J. Chan, A. Koniski, R. Patel, M. Starr and M. C. Yoder (2001). "Spatial and temporal emergence of high proliferative potential hematopoietic precursors during murine embryogenesis." Proc Natl Acad Sci U S A **98**(8): 4528-4533.

Palis, J., S. Robertson, M. Kennedy, C. Wall and G. Keller (1999). "Development of erythroid and myeloid progenitors in the yolk sac and embryo proper of the mouse." Development **126**(22): 5073-5084.

Park, S. Y., K. Saijo, T. Takahashi, M. Osawa, H. Arase, N. Hirayama, K. Miyake, H. Nakauchi, T. Shirasawa and T. Saito (1995). "Developmental defects of lymphoid cells in Jak3 kinase-deficient mice." Immunity **3**(6): 771-782.

Pei, W., T. B. Feyerabend, J. Rossler, X. Wang, D. Postrach, K. Busch, I. Rode, K. Klapproth, N. Dietlein, C. Quedenau, W. Chen, S. Sauer, S. Wolf, T. Hofer and H. R. Rodewald (2017). "Polylox barcoding reveals haematopoietic stem cell fates realized in vivo." Nature **548**(7668): 456-460.

Percin, G. I., J. Eitler, A. Kranz, J. Fu, J. W. Pollard, R. Naumann and C. Waskow (2018). "CSF1R regulates the dendritic cell pool size in adult mice via embryo-derived tissue-resident macrophages." Nat Commun **9**(1): 5279.

Pietras, E. M., D. Reynaud, Y. A. Kang, D. Carlin, F. J. Calero-Nieto, A. D. Leavitt, J. M. Stuart, B. Gottgens and E. Passegue (2015). "Functionally Distinct Subsets of Lineage-Biased Multipotent Progenitors Control Blood Production in Normal and Regenerative Conditions." Cell Stem Cell **17**(1): 35-46.

Plass, M., J. Solana, F. A. Wolf, S. Ayoub, A. Misios, P. Glazar, B. Obermayer, F. J. Theis, C. Kocks and N. Rajewsky (2018). "Cell type atlas and lineage tree of a whole complex animal by single-cell transcriptomics." Science **360**(6391).

Polanski, K., M. D. Young, Z. Miao, K. B. Meyer, S. A. Teichmann and J. E. Park (2020). "BBKNN: fast batch alignment of single cell transcriptomes." Bioinformatics **36**(3): 964-965.

Popescu, D. M., R. A. Botting, E. Stephenson, K. Green, S. Webb, L. Jardine, E. F. Calderbank, K. Polanski, I. Goh, M. Efremova, M. Acres, D. Maunder, P. Vegh, Y. Gitton, J. E. Park, R. Vento-Tormo, Z. Miao, D. Dixon, R. Rowell, D. McDonald, J. Fletcher, E. Poyner, G. Reynolds, M. Mather, C. Moldovan, L. Mamanova, F. Greig, M. D. Young, K. B. Meyer, S. Lisgo, J. Bacardit, A. Fuller, B. Millar, B. Innes, S. Lindsay, M. J. T. Stubbington, M. S. Kowalczyk, B. Li, O. Ashenberg, M. Tabaka, D. Dionne, T. L. Tickle, M. Slyper, O. Rozenblatt-Rosen, A. Filby, P. Carey, A. C. Villani, A. Roy, A. Regev, A. Chedotal, I. Roberts, B. Gottgens, S. Behjati, E. Laurenti, S. A. Teichmann and M. Haniffa (2019). "Decoding human fetal liver haematopoiesis." Nature **574**(7778): 365-371.

Poulos, M. G., P. Guo, N. M. Kofler, S. Pinho, M. C. Gutkin, A. Tikhonova, I. Aifantis, P. S. Frenette, J. Kitajewski, S. Rafii and J. M. Butler (2013). "Endothelial Jagged-1 is necessary for homeostatic and regenerative hematopoiesis." Cell Rep **4**(5): 1022-1034.

Ramond, C., C. Berthault, O. Burlen-Defranoux, A. P. de Sousa, D. Guy-Grand, P. Vieira, P. Pereira and A. Cumano (2014). "Two waves of distinct hematopoietic progenitor cells colonize the fetal thymus." Nat Immunol **15**(1): 27-35.

Rane, S. G., J. K. Mangan, A. Amanullah, B. C. Wong, R. K. Vora, D. A. Liebermann, B. Hoffman, X. Grana and E. P. Reddy (2002). "Activation of the Jak3 pathway is associated with granulocytic differentiation of myeloid precursor cells." Blood **100**(8): 2753-2762.

Ratliff, M. L., T. D. Templeton, J. M. Ward and C. F. Webb (2014). "The Bright Side of Hematopoiesis: Regulatory Roles of ARID3a/Bright in Human and Mouse Hematopoiesis." Front Immunol **5**: 113.

Rey, D. and M. Neuhäuser (2011). Wilcoxon-Signed-Rank Test. International Encyclopedia of Statistical Science. M. Lovric. Berlin, Heidelberg, Springer Berlin Heidelberg**:** 1658-1659.

Riechmann, V., I. van Cruchten and F. Sablitzky (1994). "The expression pattern of Id4, a novel dominant negative helix-loop-helix protein, is distinct from Id1, Id2 and Id3." Nucleic Acids Res **22**(5): 749-755.

Rodrigues, N. P., A. S. Boyd, C. Fugazza, G. E. May, Y. Guo, A. J. Tipping, D. T. Scadden, P. Vyas and T. Enver (2008). "GATA-2 regulates granulocyte-macrophage progenitor cell function." Blood **112**(13): 4862-4873.

Rodrigues, N. P., A. J. Tipping, Z. Wang and T. Enver (2012). "GATA-2 mediated regulation of normal hematopoietic stem/progenitor cell function, myelodysplasia and myeloid leukemia." Int J Biochem Cell Biol **44**(3): 457-460.

Rodriguez-Fraticelli, A. E., S. L. Wolock, C. S. Weinreb, R. Panero, S. H. Patel, M. Jankovic, J. Sun, R. A. Calogero, A. M. Klein and F. D. Camargo (2018). "Clonal analysis of lineage fate in native haematopoiesis." Nature **553**(7687): 212-216.

Rugh, R. (1968). "The mouse. Its reproduction and development." The mouse. Its reproduction and development.

Russell, E. S. (1979). "Hereditary anemias of the mouse: a review for geneticists." Adv Genet **20**: 357-459.

Sadahira, Y., T. Yoshino and Y. Monobe (1995). "Very late activation antigen 4-vascular cell adhesion molecule 1 interaction is involved in the formation of erythroblastic islands." J Exp Med **181**(1): 411-415.

Saito, Y., T. Fujiwara, K. Ohashi, Y. Okitsu, N. Fukuhara, Y. Onishi, K. Ishizawa and H. Harigae (2015). "High-Throughput siRNA Screening to Reveal GATA-2 Upstream Transcriptional Mechanisms in Hematopoietic Cells." PLoS One **10**(9): e0137079.

Sawai, C. M., S. Babovic, S. Upadhaya, D. Knapp, Y. Lavin, C. M. Lau, A. Goloborodko, J. Feng, J. Fujisaki, L. Ding, L. A. Mirny, M. Merad, C. J. Eaves and B. Reizis (2016). "Hematopoietic Stem Cells Are the Major Source of Multilineage Hematopoiesis in Adult Animals." Immunity **45**(3): 597-609.

Scadden, D. T. (2014). "Nice neighborhood: emerging concepts of the stem cell niche." Cell **157**(1): 41-50.

Schofield, R. (1978). "The relationship between the spleen colony-forming cell and the haemopoietic stem cell." Blood Cells **4**(1-2): 7-25.

Schulz, C., E. Gomez Perdiguero, L. Chorro, H. Szabo-Rogers, N. Cagnard, K. Kierdorf, M. Prinz, B. Wu, S. E. Jacobsen, J. W. Pollard, J. Frampton, K. J. Liu and F. Geissmann (2012). "A lineage of myeloid cells independent of Myb and hematopoietic stem cells." Science **336**(6077): 86-90.

Scott, C. L., W. T'Jonck, L. Martens, H. Todorov, D. Sichien, B. Soen, J. Bonnardel, S. De Prijck, N. Vandamme and R. Cannoodt (2018). "The transcription factor ZEB2 is required to maintain the tissue-specific identities of macrophages." Immunity **49**(2): 312-325. e315.

Scott, C. L., F. Zheng, P. De Baetselier, L. Martens, Y. Saeys, S. De Prijck, S. Lippens, C. Abels, S. Schoonooghe, G. Raes, N. Devoogdt, B. N. Lambrecht, A. Beschin and M. Guilliams (2016). "Bone marrow-derived monocytes give rise to self-renewing and fully differentiated Kupffer cells." Nat Commun **7**: 10321.

Seki, M. and H. Shirasawa (1965). "Role of the reticular cells during maturation process of the erythroblast. 3. The fate of phagocytized nucleus." Acta Pathol Jpn **15**(4): 387-405.

Sharma, R., R. Sharma, T. P. Khaket, C. Dutta, B. Chakraborty and T. K. Mukherjee (2017). "Breast cancer metastasis: Putative therapeutic role of vascular cell adhesion molecule-1." Cell Oncol (Dordr) **40**(3): 199-208.

Sheng, J., C. Ruedl and K. Karjalainen (2015). "Most Tissue-Resident Macrophages Except Microglia Are Derived from Fetal Hematopoietic Stem Cells." Immunity **43**(2): 382-393.

Sherr, C. J., C. W. Rettenmier, R. Sacca, M. F. Roussel, A. T. Look and E. R. Stanley (1985). "The c-fms proto-oncogene product is related to the receptor for the mononuclear phagocyte growth factor, CSF-1." Cell **41**(3): 665-676.

Shi, Y., M. Hon and R. M. Evans (2002). "The peroxisome proliferator-activated receptor delta, an integrator of transcriptional repression and nuclear receptor signaling." Proc Natl Acad Sci U S A **99**(5): 2613-2618.

Shuai, K. and B. Liu (2003). "Regulation of JAK-STAT signalling in the immune system." Nat Rev Immunol **3**(11): 900-911.

Skutelsky, E. and D. Danon (1972). "On the expulsion of the erythroid nucleus and its phagocytosis." Anat Rec **173**(1): 123-126.

Smith, M. R., T. J. Standiford and R. C. Reddy (2007). "PPARs in alveolar macrophage biology." PPAR Res **2007**: 23812.

Soares-da-Silva, F., M. Peixoto, A. Cumano and O. P. Pinto-do (2020). "Crosstalk Between the Hepatic and Hematopoietic Systems During Embryonic Development." Front Cell Dev Biol **8**: 612.

Soares, M. P. and I. Hamza (2016). "Macrophages and Iron Metabolism." Immunity **44**(3): 492-504.

Sontheimer, R. D., E. Racila and D. M. Racila (2005). "C1q: its functions within the innate and adaptive immune responses and its role in lupus autoimmunity." J Invest Dermatol **125**(1): 14-23.

Squarzoni, P., G. Oller, G. Hoeffel, L. Pont-Lezica, P. Rostaing, D. Low, A. Bessis, F. Ginhoux and S. Garel (2014). "Microglia modulate wiring of the embryonic forebrain." Cell Rep **8**(5): 1271-1279.

Stanley, E. R. and V. Chitu (2014). "CSF-1 receptor signaling in myeloid cells." Cold Spring Harb Perspect Biol **6**(6).

STEMCELL "MethoCult™ GF M3434 Manual."

Sugiyama, D., K. Kulkeaw, C. Mizuochi, Y. Horio and S. Okayama (2011). "Hepatoblasts comprise a niche for fetal liver erythropoiesis through cytokine production." Biochem Biophys Res Commun **410**(2): 301-306.

Sun, J., A. Ramos, B. Chapman, J. B. Johnnidis, L. Le, Y. J. Ho, A. Klein, O. Hofmann and F. D. Camargo (2014). "Clonal dynamics of native haematopoiesis." Nature **514**(7522): 322-327.

Sun, X. H., N. G. Copeland, N. A. Jenkins and D. Baltimore (1991). "Id proteins Id1 and Id2 selectively inhibit DNA binding by one class of helix-loop-helix proteins." Mol Cell Biol **11**(11): 5603-5611.

Taichman, R. S., M. J. Reilly and S. G. Emerson (2000). "The Hematopoietic Microenvironment: Osteoblasts and The Hematopoietic Microenvironment." Hematology **4**(5): 421-426.

Takahashi, K., F. Yamamura and M. Naito (1989). "Differentiation, maturation, and proliferation of macrophages in the mouse yolk sac: a light-microscopic, enzyme-cytochemical, immunohistochemical, and ultrastructural study." J Leukoc Biol **45**(2): 87-96.

Taoudi, S., C. Gonneau, K. Moore, J. M. Sheridan, C. C. Blackburn, E. Taylor and A. Medvinsky (2008). "Extensive hematopoietic stem cell generation in the AGM region via maturation of VE-cadherin+CD45+ pre-definitive HSCs." Cell Stem Cell **3**(1): 99-108.

Taylor, P. R., G. D. Brown, D. M. Reid, J. A. Willment, L. Martinez-Pomares, S. Gordon and S. Y. Wong (2002). "The beta-glucan receptor, dectin-1, is predominantly expressed on the surface of cells of the monocyte/macrophage and neutrophil lineages." J Immunol **169**(7): 3876-3882.

Team, T. (2014). "BSgenome. Mmusculus. UCSC. mm10: Full genome sequences for Mus musculus (UCSC version mm10)."

Theodore, L. N., E. J. Hagedorn, M. Cortes, K. Natsuhara, S. Y. Liu, J. R. Perlin, S. Yang, M. L. Daily, L. I. Zon and T. E. North (2017). "Distinct Roles for Matrix Metalloproteinases 2 and 9 in Embryonic Hematopoietic Stem Cell Emergence, Migration, and Niche Colonization." Stem Cell Reports **8**(5): 1226-1241.

Thomis, D. C., C. B. Gurniak, E. Tivol, A. H. Sharpe and L. J. Berg (1995). "Defects in B lymphocyte maturation and T lymphocyte activation in mice lacking Jak3." Science **270**(5237): 794-797.

Tober, J., A. Koniski, K. E. McGrath, R. Vemishetti, R. Emerson, K. K. de Mesy-Bentley, R. Waugh and J. Palis (2007). "The megakaryocyte lineage originates from hemangioblast precursors and is an integral component both of primitive and of definitive hematopoiesis." Blood **109**(4): 1433-1441.

Toobian, D., P. Ghosh and G. D. Katkar (2021). "Parsing the Role of PPARs in Macrophage Processes." Front Immunol **12**: 783780.

Traag, V. A., L. Waltman and N. J. van Eck (2019). "From Louvain to Leiden: guaranteeing well-connected communities." Sci Rep **9**(1): 5233.

Trompouki, E., T. V. Bowman, L. N. Lawton, Z. P. Fan, D. C. Wu, A. DiBiase, C. S. Martin, J. N. Cech, A. K. Sessa, J. L. Leblanc, P. Li, E. M. Durand, C. Mosimann, G. C. Heffner, G. Q. Daley, R. F. Paulson, R. A. Young and L. I. Zon (2011). "Lineage regulators direct BMP and Wnt pathways to cell-specific programs during differentiation and regeneration." Cell **147**(3): 577-589.

Tsai, F. Y., G. Keller, F. C. Kuo, M. Weiss, J. Chen, M. Rosenblatt, F. W. Alt and S. H. Orkin (1994). "An early haematopoietic defect in mice lacking the transcription factor GATA-2." Nature **371**(6494): 221-226.

Tsai, F. Y. and S. H. Orkin (1997). "Transcription factor GATA-2 is required for proliferation/survival of early hematopoietic cells and mast cell formation, but not for erythroid and myeloid terminal differentiation." Blood **89**(10): 3636-3643.

Tsai, S., S. G. Emerson, C. A. Sieff and D. G. Nathan (1986). "Isolation of a human stromal cell strain secreting hemopoietic growth factors." J Cell Physiol **127**(1): 137-145.

Ulyanova, T., Y. Jiang, S. Padilla, B. Nakamoto and T. Papayannopoulou (2011). "Combinatorial and distinct roles of alpha(5) and alpha(4) integrins in stress erythropoiesis in mice." Blood **117**(3): 975-985.

van Furth, R. and Z. A. Cohn (1968). "The origin and kinetics of mononuclear phagocytes." J Exp Med **128**(3): 415-435.

Van Gassen, S., B. Callebaut, M. J. Van Helden, B. N. Lambrecht, P. Demeester, T. Dhaene and Y. Saeys (2015). "FlowSOM: Using self-organizing maps for visualization and interpretation of cytometry data." Cytometry A **87**(7): 636-645.

Van Rossum, G. and F. L. Drake Jr (1995). Python tutorial, Centrum voor Wiskunde en Informatica Amsterdam, The Netherlands.

Wang, L. D. and A. J. Wagers (2011). "Dynamic niches in the origination and differentiation of haematopoietic stem cells." Nat Rev Mol Cell Biol **12**(10): 643-655.

Wang, T., T. Kono, M. M. Monte, H. Kuse, M. M. Costa, H. Korenaga, T. Maehr, M. Husain, M. Sakai and C. J. Secombes (2013). "Identification of IL-34 in teleost fish: differential expression of rainbow trout IL-34, MCSF1 and MCSF2, ligands of the MCSF receptor." Mol Immunol **53**(4): 398-409.

Weissman, I., V. Papaioannou and R. Gardner (1977). Fetal hematopoietic origins of the adult hematolymphoid system (Clarkson B ed), Cold Spring Harbor Laboratory Press, Cold Spring Harbor.

Werner, Y., E. Mass, P. Ashok Kumar, T. Ulas, K. Handler, A. Horne, K. Klee, A. Lupp, D. Schutz, F. Saaber, C. Redecker, J. L. Schultze, F. Geissmann and R. Stumm (2020). "Cxcr4 distinguishes HSC-derived monocytes from microglia and reveals monocyte immune responses to experimental stroke." Nat Neurosci **23**(3): 351-362.

White, G. E. and D. R. Greaves (2012). "Fractalkine: a survivor's guide: chemokines as antiapoptotic mediators." Arterioscler Thromb Vasc Biol **32**(3): 589-594.

Wickham, H., W. Chang and M. H. Wickham (2016). "Package 'ggplot2'." Create elegant data visualisations using the grammar of graphics. Version **2**(1): 1-189.

Wilkerson, M. D. and D. N. Hayes (2010). "ConsensusClusterPlus: a class discovery tool with confidence assessments and item tracking." Bioinformatics **26**(12): 1572-1573.

Wilson, A., E. Laurenti, G. Oser, R. C. van der Wath, W. Blanco-Bose, M. Jaworski, S. Offner, C. F. Dunant, L. Eshkind, E. Bockamp, P. Lio, H. R. Macdonald and A. Trumpp (2008). "Hematopoietic stem cells reversibly switch from dormancy to self-renewal during homeostasis and repair." Cell **135**(6): 1118-1129.

Wolf, F. A., P. Angerer and F. J. Theis (2018). "SCANPY: large-scale single-cell gene expression data analysis." Genome Biol **19**(1): 15.

Wolf, F. A., F. K. Hamey, M. Plass, J. Solana, J. S. Dahlin, B. Gottgens, N. Rajewsky, L. Simon and F. J. Theis (2019). "PAGA: graph abstraction reconciles clustering with trajectory inference through a topology preserving map of single cells." Genome Biol **20**(1): 59.

Wong, K., P. A. Valdez, C. Tan, S. Yeh, J. A. Hongo and W. Ouyang (2010). "Phosphatidylserine receptor Tim-4 is essential for the maintenance of the homeostatic state of resident peritoneal macrophages." Proc Natl Acad Sci U S A **107**(19): 8712-8717.

Wu, Y. and K. K. Hirschi (2020). "Tissue-Resident Macrophage Development and Function." Front Cell Dev Biol **8**: 617879.

Xue, L., J. Y. Cai, J. Ma, Z. Huang, M. X. Guo, L. Z. Fu, Y. B. Shi and W. X. Li (2013). "Global expression profiling reveals genetic programs underlying the developmental divergence between mouse and human embryogenesis." BMC Genomics **14**: 568.

Yap, J., H. A. Cabrera-Fuentes, J. Irei, D. J. Hausenloy and W. A. Boisvert (2019). "Role of Macrophages in Cardioprotection." Int J Mol Sci **20**(10).

Yee, N. S., I. Paek and P. Besmer (1994). "Role of kit-ligand in proliferation and suppression of apoptosis in mast cells: basis for radiosensitivity of white spotting and steel mutant mice." J Exp Med **179**(6): 1777-1787.

Yokoyama, T., H. Kitagawa, T. Takeuchi, S. Tsukahara and Y. Kannan (2002). "No apoptotic cell death of erythroid cells of erythroblastic islands in bone marrow of healthy rats." J Vet Med Sci **64**(10): 913-919.

Yona, S., K. W. Kim, Y. Wolf, A. Mildner, D. Varol, M. Breker, D. Strauss-Ayali, S. Viukov, M. Guilliams, A. Misharin, D. A. Hume, H. Perlman, B. Malissen, E. Zelzer and S. Jung (2013). "Fate mapping reveals origins and dynamics of monocytes and tissue macrophages under homeostasis." Immunity **38**(1): 79-91.

Yong, K. S., C. T. Keng, S. Q. Tan, E. Loh, K. T. Chang, T. C. Tan, W. Hong and Q. Chen (2016). "Human CD34(lo)CD133(lo) fetal liver cells support the expansion of human CD34(hi)CD133(hi) hematopoietic stem cells." Cell Mol Immunol **13**(5): 605-614.

Yoshida, T. and K. Georgopoulos (2013). "GATA-3 controls self-renewal in stressed HSCs." Nat Immunol **14**(10): 1032-1033.

Yu, G., L. G. Wang, Y. Han and Q. Y. He (2012). "clusterProfiler: an R package for comparing biological themes among gene clusters." OMICS **16**(5): 284-287.

Yvernogeau, L., R. Gautier, L. Petit, H. Khoury, F. Relaix, V. Ribes, H. Sang, P. Charbord, M. Souyri, C. Robin and T. Jaffredo (2019). "In vivo generation of haematopoietic stem/progenitor cells from bone marrow-derived haemogenic endothelium." Nat Cell Biol **21**(11): 1334-1345.

Zhang, C. C., M. Kaba, G. Ge, K. Xie, W. Tong, C. Hug and H. F. Lodish (2006). "Angiopoietin-like proteins stimulate ex vivo expansion of hematopoietic stem cells." Nat Med **12**(2): 240-245.

Zhang, D.-E., C. J. Hetherington, H.-M. Chen and D. G. Tenen (1994). "The macrophage transcription factor PU. 1 directs tissue-specific expression of the macrophage colony-stimulating factor receptor." Molecular and cellular biology **14**(1): 373-381.

Zhu, J. and S. G. Emerson (2002). "Hematopoietic cytokines, transcription factors and lineage commitment." Oncogene **21**(21): 3295-3313.

Zong, Y. and J. R. Friedman (2014). "Liver development." Liver Disease in Children: 1-813.